vol. 4, no. 4

april, 1958

THE SOVIET JOURNAL OF

ATOMIC ENERGY

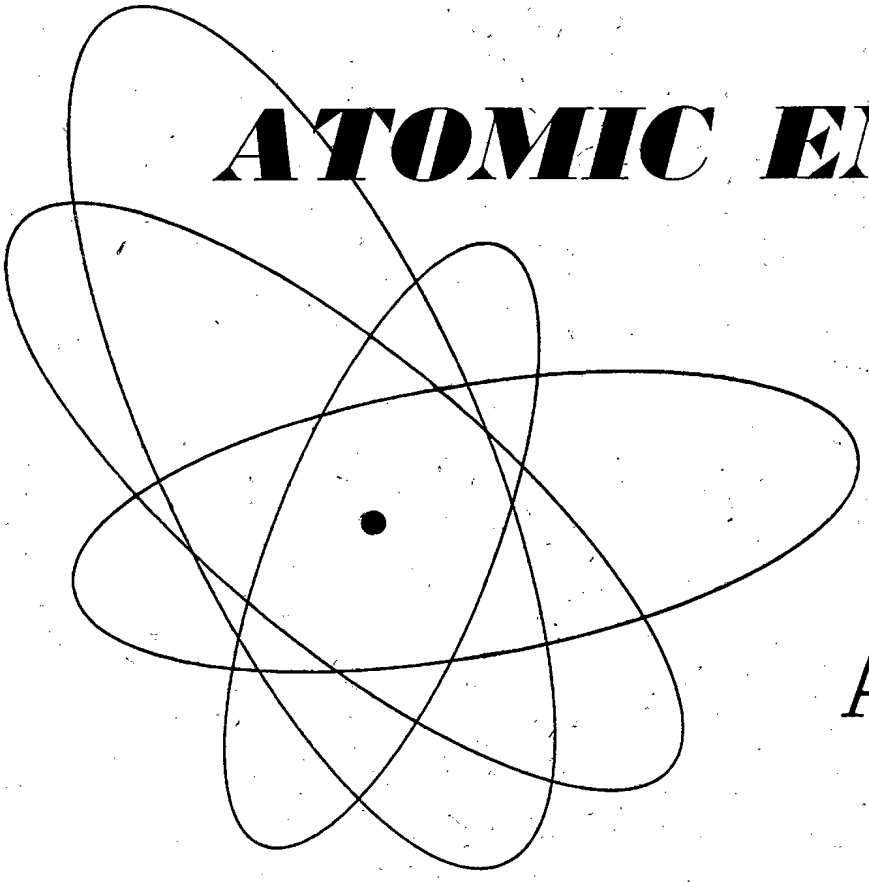

Атомная энергия

TRANSLATED FROM RUSSIAN

CONSULTANTS BUREAU, INC.

Three new translations from C B

a journal . . . a supplement . . . and a monograph

THE CZECHOSLOVAK JOURNAL OF PHYSICS

REGARDED throughout the world as one of the most important journals in its field, THE CZECHOSLOVAK JOURNAL OF PHYSICS is originally published in an edition containing *English, Russian, German* and *French* articles. Unfortunately, those who cannot read *all* these languages have been deprived of the bulk of this invaluable information.

To overcome this language barrier, *Consultants Bureau* is now undertaking the translation of *all non-English* articles appearing in each issue. This will be done on a subscription basis, starting with the January, 1959 issue. Thus, every English-speaking scientist will now have these up-to-the-minute advances readily available for use in his own investigative work. (Articles *originally* published in English are obtainable from the Czechoslovak edition of the journal.)

Annual Subscription to English Edition $50.00

PHYSICS AND HEAT TECHNOLOGY OF REACTORS

Supplement No. 1, to the 1958 Soviet Journal of Atomic Energy
in complete English translation

THE NINETEEN original papers in this important volume may conveniently be divided into two sections: The first deals mainly with *reactor physics—mathematical calculations; specialized experiments; reactor safety;* and a variety of related problems. (These papers will be of special value to the Western scientist, because they encompass a wide circle of problems *which have not been studied or treated in the literature to any great extent.*) The second group is more concerned with *engineering aspects: heat problems; obtaining the highest efficiency of heat removal and the greatest utilization of the heat generated in the core of a reactor.* The intimately related problems of *radioactive loading of the reactor heat removal systems* is also considered at length.

cloth bound; 178 pages, profusely illustrated, $22.50

DENDRITIC CRYSTALLIZATION

2nd Edition, Revised and Enlarged

by D. D. SARATOVKIN

translated from Russian

IN THE LIGHT of recent data, the author has brought the 1953 edition of his work completely up to date: *fresh material derived from observations under the stereoscopic microscope* has been incorporated; *the section on steel casting* has been extensively revised, and presents a lucid explanation of how the various structures found in real castings can be fit into the author's theory of dendritic crystallization. The approach is *concrete, pragmatic and nonmathematical,* and includes copious use of experimental observations on many crystals——all of which provides a highly useful volume of interest to the *crystal-physics or chemical crystallography worker concerned with handling and producing real crystals.*

cloth bound; 126 pp., illustrated; $6.00

C.B. translations by bilingual scientists include all tabular, diagrammatic and photographic material integral with the text.

At your bookstore, or order directly from:

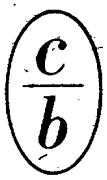

CONSULTANTS BUREAU, INC.
227 W. 17th St., NEW YORK 11, N.Y.

vol. 4, no. 4

april, 1958

THE SOVIET JOURNAL OF

ATOMIC ENERGY

ATOMNAIA ENERGIIA

A publication of the Academy of Sciences of the USSR

Annual Subscription $75.00
Single Issue 20.00

Year and issue of first translation:
volume 1, number 1 january 1956

TRANSLATED FROM RUSSIAN

Printed in the United States

SOVIET JOURNAL OF ATOMIC ENERGY

Volume 4, Number 4 April 1958

CONTENTS

CONTENTS (continued)

SPECTRA OF NEUTRONS PRODUCED BY 14-Mev NEUTRONS IN FISSILE MATERIALS

Iu. S. Zamiatnin, I. N. Safina, E. K. Gutnikova and N. I. Ivanova

Measurements have been made of the energy distribution of neutrons produced in the passage of 14-Mev neutrons through layers of Th^{232}, U^{233}, U^{235}, U^{238} and Pu^{239}. It is shown for all nuclides which were investigated that the secondary-neutron spectrum consists of two components: fission neutrons and evaporation neutrons. The dependence of the coefficients in the secondary neutron spectrum on the nuclear constants of the corresponding nuclides are determined, thus making it possible to find these coefficients without an experimental investigation of the neutron spectra.

The following can occur when 14-Mev neutrons interact with heavy fissile nuclei:

a) processes involving the loss of neutrons (radiative capture, reactions with the production of charged particles);

b) elastic scattering of neutrons, in which there is no essential change of the energy of the primary neutrons;

c) processes involving the evaporation of neutrons from an intermediate nucleus in an excited state—inelastic scattering, (n, n'γ) reactions, (n, 2n) reactions etc.;

d) nuclear fission, which leads to the production of secondary fission neutrons.

Thus, the spectrum associated with neutrons which pass through a layer of fissile material should exhibit secondary neutrons associated with the inelastic interactions given in (c) and (d) in addition to the primary neutrons and elastically scattered neutrons.

A great deal of work [1]-[4] has been devoted to investigations of the spectrum of secondary neutrons produced in the interaction of 14-Mev neutrons with nonfissile elements.

These investigations show that the spectrum of secondary neutrons is essentially in agreement with that to be expected for statistical evaporation of neutrons from an excited intermediate nucleus:

$$F(E) = C_1 E e^{-E/T}, \quad (1)$$

where T is a parameter which characterizes the temperature of the residual nucleus* and C_1 is a normalizing factor.

In a number of other papers [5], [6] it has been shown that the neutron spectrum for fission in heavy elements induced by thermal neutrons is of the following form:

* Strictly speaking, the (n, 2n) process should exhibit a more complicated neutron distribution because the temperature is different in the evaporation of the first neutron and the second neutron; however, because of the weak dependence of T on excitation energy of the intermediate nucleus, the change in T is small and cannot be observed experimentally.

$$F(E)\, C_2 \sinh \frac{2\sqrt{\omega E}}{T_f}\, e^{-E/T_f}, \qquad (2)$$

where T_f is the temperature of the fragment after neutron evaporation, $\underline{w}$ is the mean kinetic energy of the nucleon in the fragment and C_2 is a normalizing factor.

On the basis of these results one would expect that the passage of 14-Mev neutrons through a layer of fissile material should result in a complicated secondary-neutron spectrum, consisting of two components: fission neutrons and evaporation neutrons.

In the present work we present results which tend to verify this interpretation; these results were obtained by the authors in 1950-1956.

Method of Measurement and Results

The secondary-neutron energy distribution was studied using Ilford C-2 and NIKFI-K photographic plates with an emulsion thickness of 100μ. The energy of the neutrons was determined from the recoil protons which were emitted in the forward direction within the angular limits ±15°.

The source of 14-Mev neutrons was a tritium-zirconium target which was bombarded by 150-kev deuterons.

The neutron source was surrounded by a layer of the material being investigated. The measurements were performed with the following fissile nuclides: Th^{232}, U^{233}, U^{235}, U^{238}, and Pu^{239}, and with a mixture of the U^{235} and U^{238} isotopes with different concentrations. The thickness of the layer of fissile material was chosen so that the attenuation of the 14-Mev neutron flux would be less than 30% in passage through the layer. In practice the layer thickness was varied from 0.15 λ to 0.4 λ (λ is the neutron-free path length for inelastic interactions, cf. Table). Under these conditions the contribution of multiple inelastic processes was small.

To compute the background of primary neutrons the plates were exposed without the layer of fissile material. In subtracting of the background, it was assumed that the number of background tracks was proportional to the primary neutron flux.

The microscope scanning of the plates was carried out by several observers. The total number of measured recoil-proton tracks for each material investigated is given in the Table.*

The recoil-proton distribution was used in determining the neutron spectrum, and corrections for the finite thickness of the emulsion and the variation of the neutron-scattering cross section in hydrogen were introduced.

To analyze the neutron distribution which was obtained, F(E), a plot was made of the energy dependence of the ratio F(E)/E in semilogarithmic coordinates, in which the distribution in (1) is a straight line; this procedure makes it possible to separate the two components of the neutron spectrum since $T_f > T$ and the hard part of the spectrum ($E_n > 3$ Mev) is essentially determined completely by the fission neutrons. Extrapolation of the fission neutron spectrum into the energy region $E_n < 3$ Mev then makes it possible to determine the excess of low-energy neutrons; these are taken as evaporation neutrons. As a rule, the difference between the experimental curve and the fission neutron spectrum is in good agreement with the distribution given in (1). The values of the parameter T obtained in this way are given in the Table.

In extrapolating the fission-neutron spectrum one usually uses the distribution given in (2). The values of the parameter T_f (cf. Table) are determined from the hard part of the spectrum, while the quantity $\underline{w}$ is taken as 0.5 Mev in all cases. In this connection it is interesting to note that in the energy region $E_n > 3$ Mev the slope of the curves, and consequently, the values of T_f obtained for U^{233}, U^{235} and Pu^{239}, are in good agreement with the corresponding quantities for the fission-neutron spectrum for these isotopes in fission induced by thermal neutrons. This correspondence means that the fission neutron spectrum is a weak function of the energy of the fission-inducing neutrons; thus the fission spectrum for thermal-neutron fission can be used for extrapolation.

The experimental results, the results of the graphical analysis, and the coefficients for the two components of the neutron spectrum [α_f (the fission-neutron fraction) and α_n (the evaporation-neutron spectrum)] are shown

*To increase the statistical accuracy of the measurements, additional areas of the plates were scanned in the energy region above 2.5 Mev.

TABLE 1

Investigated nuclide	Thickness of the layer in mean free path lengths, λ	Number of tracks measured	Fission-neutron fraction (experimental values), α_f	Correction for inelastic interactions of secondary neutrons	Fission-neutron spectrum (corrected values), α_f	Temperature of residual nucleus T, Mev	Temperature of fragment T_f, Mev
Th^{232}	0,4	2000	0,20±0,05	0,03	0,23±0,06	0,54±0,05	1,2*)
U^{233}	0,15	4400	0,75±0,1	0,01	0,76±0,1	0,55±0,1	1,2±0,08
U^{235}	0,36	6700	0,65±0,05	0,03	0,68±0,06	0,4±0,05	1,05±0,06
U^{238}	0,24 0,34	4700 4400	0,44±0,05 0,42±0,06	0,05 0,08 Average	0,49±0,06 0,5 ±0,08 0,49±0,05	0,52±0,07 0,43±0,06 0,48±0,05	1,2 ±0,1 1,25±0,15 —
Pu^{239}	0,29	4600	0,7±0,09	0,02	0,72±0,1	0,53±0,06	1,25±0,08

*) The value taken for the extrapolated fission-neutron spectrum.

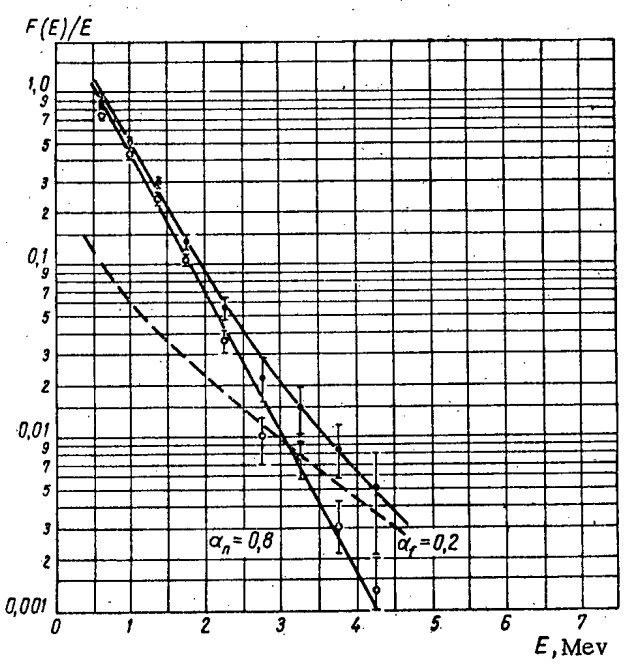

Fig. 1. Spectrum of secondary neutrons produced in the passage of 14-Mev neutrons through Th^{232} (thickness of the layer is 0.4 λ).

I
●) experimental results; – – – –) extrapolated fission-neutron
I

spectrum; I ○) evaporation-neutron spectrum.
I

in Figs. 1-6 for the single-isotope samples which were investigated.

The experimental results contain corrections which take into account the distortion of α_f and α_n due to inelastic interactions of the secondary neutrons with the material in the layer. This effect is due to the reduction in the fission cross section in going from a neutron energy of 14 Mev to secondary-neutron energies and results

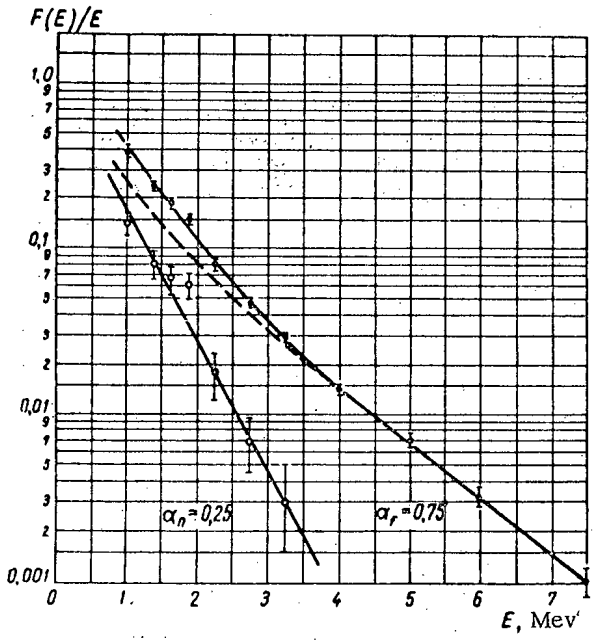

Fig. 2. Spectrum of secondary neutrons produced in the passage of 14-Mev neutrons through U^{233} (thickness of the layer is 0.15 λ).

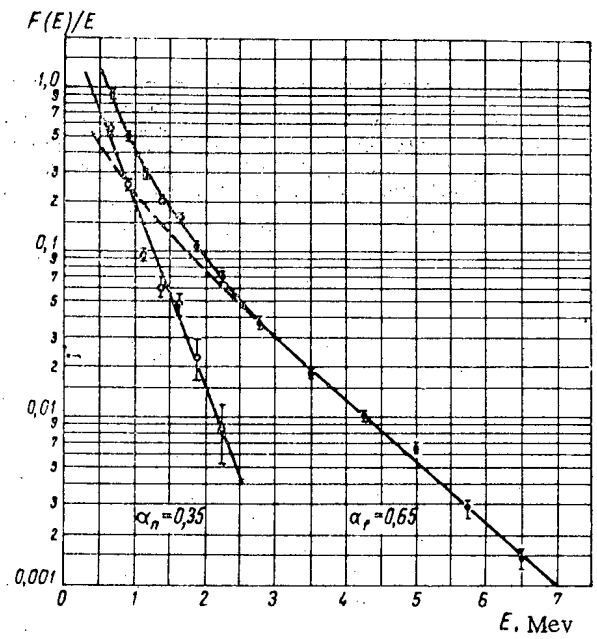

Fig. 3. Spectrum of secondary neutrons produced in the passage of 14-Mev neutrons through U^{235} (thickness of the layer is 0.36 λ).

I
●)Experimental results; – – – –) extrapolated fission-neutron spectrum; I ○) evaporation-neutron spectrum.

from the fact that the probability for inelastic scattering of secondary neutrons is larger than that for primary neutrons; hence the fission-neutron fraction of the spectrum is reduced to some extent. An estimate of this effect shows that it must be taken into account even when small layer thicknesses are used.* The magnitude of the correction which is introduced and the corrected values of α_f are given in Table 1.

DISCUSSION OF THE RESULTS

It is apparent from the Table that the fission neutrons predominate in a material which is highly fissile (U^{233}, U^{235}, Pu^{239}) while in a material which is not very fissile (Th^{232} and U^{238}) the fission-neutron fraction is considerably smaller, i.e., the experimental results indicate a qualitatively correct dependence between the coefficients α_f and α_n and the fission capabilities of the nuclei being investigated.

We now find a quantitative relation between the spectrum coefficients for the two components and the values of the nuclear constants of the corresponding fissile elements. The total cross section for the production of secondary neutrons is given in the form of a sum:

$$\nu_{\text{eff}}\,\sigma_c = \nu\sigma_f + \sigma_{n,\,n'\gamma} + 2\sigma_{n,\,2n}. \qquad (3)$$

The last two terms in this sum are to be associated with the formation of evaporation neutrons.** The fission neutrons are to be associated with the first term; however, this term also contains a certain fraction of the evaporation neutrons. This is due to the fact that at neutron energies of 14 Mev fission can occur after

*The magnitude of the correction is found as the difference of the effects due to inelastic scattering of fission neutrons and fission induced by evaporation neutrons, taking account of the corresponding cross sections and the mean paths of the secondary neutrons in the layer.

**If the (n, 3n) reaction is energetically possible, Eq. (3) should contain an additional term. The cross section for radiative capture of 14-Mev neutrons can be neglected.

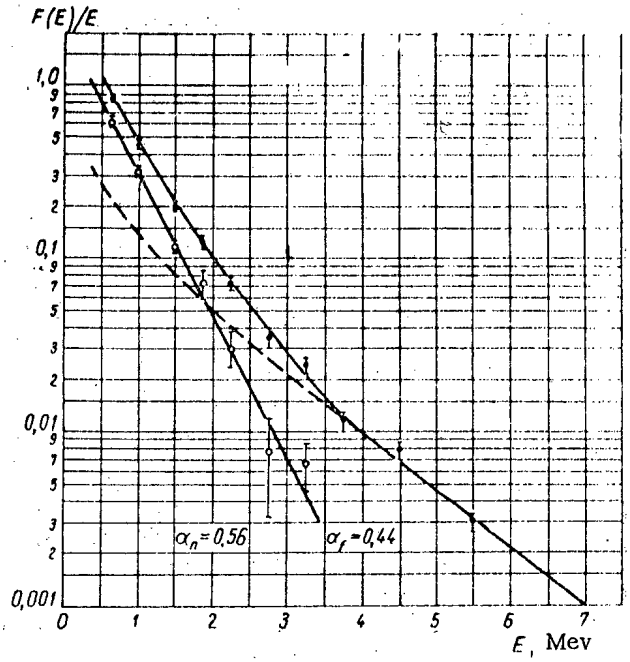

Fig. 4. Spectrum of secondary neutrons produced in the passage of 14-Mev neutrons through U^{238} (thickness of the layer is 0.24 λ).

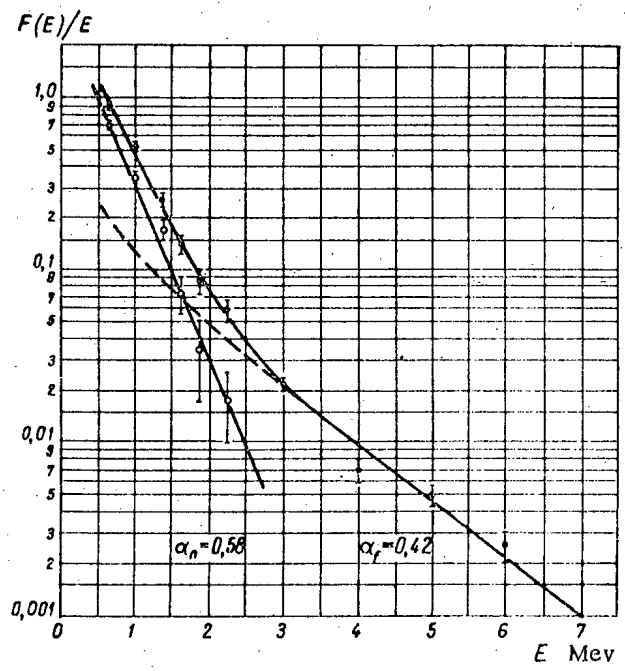

Fig. 5. Spectrum of secondary neutrons produced in the passage of 14-Mev neutrons through U^{238} (thickness of the layer is 0.34 λ).

I ● I) Experimental results; – – – –) extrapolated fission-neutron spectrum; T ○ ⊥) evaporation-neutron spectrum.

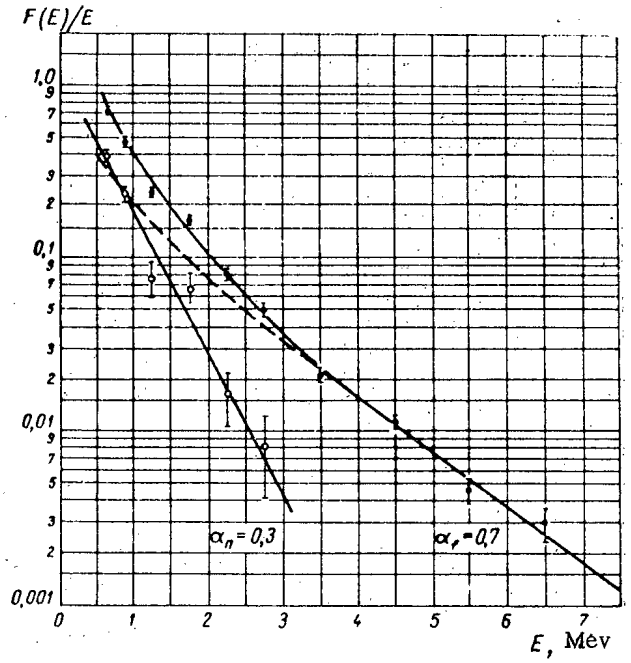

Fig. 6. Spectrum of secondary neutrons produced in the passage of 14-Mev neutrons through Pu^{239} (thickness of the layer is 0.29 λ).

●) Experimental results; – – – –) extrapolated fission-neutron spectrum; ○) evaporation-neutron spectrum.

preliminary evaporation of neutrons from the excited intermediate nucleus – the (n, n'f) process.* In this case the fission cross section σ_f must be considered as the sum of the cross sections for two processes: fission without preliminary evaporation of neutrons σ_{f_0} and fission after evaporation of neutrons σ_{fn} [7]. Then the term $\nu\sigma_f$ in Eq. (3) is replaced by the sum $\nu_0\sigma_{f_0} + (\nu_1 + 1)\,\sigma_{fn}$, in which the fission neutrons and evaporation neutrons can be separated easily. Thus, the fission-neutron fraction α_f and the evaporation-neutron fraction α_n can be given as

$$\alpha_f = \frac{\nu_0\sigma_{f_0} + \nu_1\sigma_{fn}}{\nu_{\text{eff}}\sigma_c} \quad \text{and} \quad \alpha_n = \frac{\sigma_{fn} + \sigma_{n,n\gamma} + 2\sigma_{n,2n}}{\nu_{\text{eff}}\sigma_c}.$$

In practice, in place of ν_0, ν_1 and σ_{fn} it is more convenient to use the quantities ν, σ_f and σ_{f_0} which can be obtained directly from an experiment.** Then the expressions for α_f and α_n assume the form

$$\alpha_f = \frac{\nu\sigma_f - (\sigma_f - \sigma_{f_0})\ *)}{\nu_{\text{eff}}\sigma_c},$$
$$\alpha_n = \frac{(\sigma_f - \sigma_{f_0}) + \sigma_{n,n\gamma} + 2\sigma_{n,2n}}{\nu_{\text{eff}}\sigma_c} \ldots \qquad (4)$$

In the case in which 14-Mev neutrons pass through material consisting of two different isotopes the contributions of the fission neutrons and evaporation neutrons can be found from the coefficients α_f and α_n known for

*For simplicity the treatment here does not take account of the possible (n, 2nf) reaction since the probability for this reaction is small.

** α_f can be given as $\alpha_f = \frac{\nu_f\sigma_f}{\nu_{\text{eff}}\sigma_c}$, where ν_f is the actual number of neutrons produced in the fission process without taking account of preliminary emission of neutrons. In this case $\nu_f\sigma_f = \nu\sigma_f - (\sigma_f - \sigma_{f_0})$, i.e., $\nu_f = \nu - \frac{\sigma_f - \sigma_{f_0}}{\sigma_f} = \nu - \frac{\sigma_{fn}}{\sigma_f}$.

each isotope individually: α_{f_1}, α_{f_2} and α_{n_1}, α_{n_2}. In this case the total cross section for the production of secondary neutrons is

$$\beta_1 \nu_{eff\,1} \sigma_{c_1} + \beta_2 \nu_{eff\,2} \sigma_{c_2},$$

where β_1 and β_2 are the individual isotopic contents. The fission-neutron fraction is

$$\alpha_f = \frac{\gamma_1 \alpha_f + \gamma_2 \alpha_{f_2}}{\gamma_1 + \gamma_2} \ldots, \tag{5}$$

where $\gamma = \beta_1 \nu_{eff\,1} \sigma_{c_1}$ and $\gamma_2 = \beta_2 \nu_{eff\,2} \sigma_{c_2}$ are the contributions for each isotope to the total number of secondary neutrons. Similarly the evaporation-neutron fraction is

$$\alpha_n = \frac{\gamma_1 \alpha_{n_1} + \gamma_2 \alpha_{n_2}}{\gamma_1 + \gamma_2}. \tag{5a}$$

The values of α_f and α_n calculated using Eqs. (4) and (5) generally agree with α_f and α_n within the limits of the experimental errors, where the latter quantities are obtained from an analysis of the neutron spectra for the pure isotopes and for isotopic mixtures. The exceptions are U^{233} and Pu^{239}, for which experimental values of α_f are somewhat lower than the calculated values.

The authors wish to express their thanks to V. A. Davidenko for his interest in the work and discussion of the results, to A. G. Shlygin for taking part in the initial stages in the work, to Iu. A. Vasil'ev, G. S. Malkiel' and E. I. Sirotinin for exposing the plates in the accelerator, and to L. S. Andreev, L. V. Evseev, N. F. Nikolaev and V. A. Chernyshov for scanning the plates.

Received September 7, 1957

LITERATURE CITED

[1] Iu. S. Zamiatnin, E. K. Gutnikova, N. I. Ivanova and I. N. Safina, J. Atomic Energy 3, 540 (1957).*

[2] P. H. Stelson, C. Goodman, Phys. Rev. 82, 69 (1951).

[3] E. R. Graves, L. Rosen, Phys. Rev. 89, 343 (1953).

[4] G. K. O'Neill, Phys. Rev. 95, 1235 (1955).

[5] I. I. Gurevich and K. N. Mukhin, unpublished work (1951). B. G. Erozlimskii, Supplement No. 1, J. Atomic Energy (1957) p. 74.*

[6] B. E. Watt, Phys. Rev. 87, 1037 (1952).

[7] Iu. S. Zamiatnin, Supplement No. 1, J. Atomic Energy (1957) p. 27.*

* Original Russian pagination. See C. B. Translation.

RADIATION OXIDATION OF TETRAVALENT URANIUM SOLUTIONS

V. G. Firsov and B. V. Ershler

Treatment of a sulfuric acid solution of tetravalent uranium, containing 0.8 N H_2SO_4, in the absence of O_2 and at a concentration of U^{+4} ~100 mg-equiv/liter, with Co^{60} γ-radiation gave an oxidation yield of U^{+4} close to 5.0. U^{+4} was not oxidized by the molecular ion H_2^+ even with greatly increased acidity of the solution and a decreased U^{+4} concentration. A decrease in U^{+4} concentration resulted in a lower yield mainly due to recombination of the H and OH radicals. An equation for the relation of G to $[U^{+4}]$ is put forward which agrees with experimental data, and a ratio involving the rate constants of the three reactions H + OH, H + H and U^{+4} + OH was found. A decrease in the yield G was observed on increasing the U^{+4} concentration above 110 mg-equiv/liter. This phenomenon is apparently explained by the reduction of U^{+4} radicals by H. We considered some mechanism by which uranyl ions may retard U^{+4} oxidation. As a result of this consideration we were able to calculate the ratio of the rate constants of the reactions UO_2^{+2} + H and H + H and a ratio involving the rate constants of the reactions UO_2^{+2} + OH, H + OH and H + H.

An equation based on the mechanism suggested for the oxidation of tetravalent uranium in dilute solution in the presence of uranyl ion has been deduced for the relation of G to $[U^{+4}]$ and $[UO_2^{+2}]$ and this agrees with the experimental data for a wide range of concentrations.

The chemical processes occurring in solutions of tetravalent uranium salts when treated with γ-radiation are of practical interest but have been studied little. Besides the old papers on photochemical reduction of hexavalent uranium, there is only the paper by Boyle et al., published in 1955 [1], in which they reported that U^{+4} is oxidized to UO_2^{+2} when irradiated with mixed α-, β- and γ-radiation and fission fragments. Haissinsky and Duflo, [2] and [3], found that the oxidation yield of U^{+4}, in the absence of oxygen, had a value of $G^* = 2\text{-}4$ equiv/100 ev; in addition they determined the yield in the presence of oxygen in relation to a series of factors. We considered it advantageous to investigate these processes more thoroughly and to try to elucidate their mechanism, using the quantitative data compiled by Allen [4] from the analysis of a series of papers on water radiolysis.

Experimental Conditions

Sulfuric acid solutions, containing tetravalent uranium sulfate and mixtures with uranyl sulfate, were placed in quartz ampules with a ground capillary stopper and were treated with Co^{60} γ-radiation in a source with a dose strength $1.28 \cdot 10^{21}$ ev/liter · min [5]. The concentration was determined by titration with potassium dichromate by the usual method. Deaerated solutions as well as those saturated with air or hydrogen were studied. The accuracy of the measurement was 3-4%.

*From here on G refers to U^{+4} ions.

Measurement Results

Figure 1 shows the relation of the oxidation yield G to U^{+4} concentration in the absence of uranyl ions. All the solutions were deaerated and contained 0.8 N H_2SO_4. As can be seen from the Figure, with increasing $[U^{+4}]$ the magnitude G increases and approaches a limit but then decreases. A considerable increase in the acidity of the solution at $[U^{+4}]$ = 5.33 mg-equiv/liter (Fig. 2) and saturation of the solution with hydrogen hardly affect the yield G. In the presence of oxygen the value of G increases to 16.0 ± 1.0 equiv/100 ev; i.e., within the accuracy of the experimental data, it was found to be equal to the radiation oxidation yield of divalent iron under the same conditions.

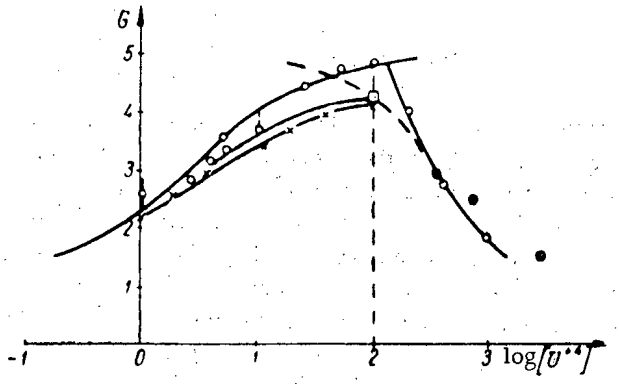

Fig. 1. The relation of the oxidation yield of U^{+4} to the concentration (without UO_2^{+2}).
O) Our data ($1.09 \cdot 10^{21}$ ev/liter · min); □) our data ($1.29 \cdot 10^{20}$ ev/liter · min); ×) Haissinsky and Dulfo's data (0.055-$1.07 \cdot 10^{20}$ ev/liter · min); ●) data of Boyle et al. (fission fragments); – – – –) data calculated by equation (II).

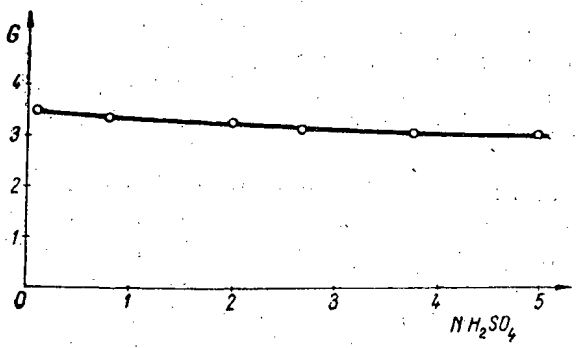

Fig. 2. The effect of H_2SO_4 concentration on the oxidation yield of U^{+4} (ΣU = 5.33 mg-equiv/liter, U^{+4} fraction = = 80.0 ± 1.6%).

The value of G decreases noticeably with an increase in the uranyl ion concentration in the absence of O_2 (Fig. 3). The total concentration of U^{+4} and UO_2^{+2}, which we shall denote as ΣU, remains constant along the curves in Fig. 3, but the fraction of each of these components changes.

Figure 4 gives the curves for the relation of G to $[UO_2^{+2}]$ at a constant value of $[U^{+4}]$.

DISCUSSION

For analyzing the results obtained, we used the data given in Allen's summary [4] of the yields of various components in water radiolysis. These data may be summarized by the equation

$$(n+2k)\,H_2O = (m+2l)\,H_2O \rightarrow nH + mOH + kH_2 + lH_2O_2, \qquad (1)$$

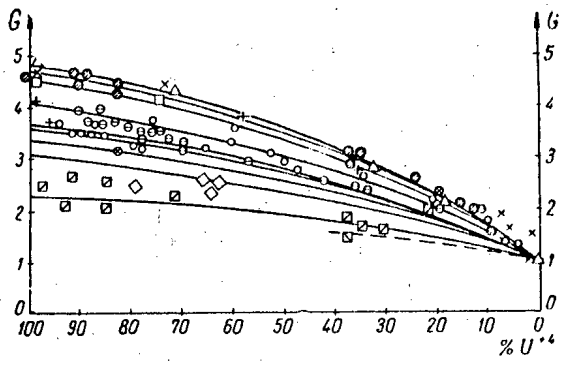

Fig. 3. The relation of the oxidation yield of tetravalent uranium to the ratio of U^{+4} and UO_2^{+2} at ΣU = const. Δ) 110 mg-equiv/liter, Θ) 6.35 mg-equiv/liter, ⊠) 1.065 mg-equiv/liter, ×) 53.2 mg-equiv/liter, O) 5.33 mg-equiv/liter, ⊠) 0.53 mg-equiv/liter, □) 25.9 mg-equiv/liter, ⊗) 4.26 mg-equiv/liter, ⊘) 5.33 mg-equiv/liter, +) 10.65 mg-equiv/liter, ◇) 2.85 mg-equiv/liter, U^{+6} + + 0.1 M glucose.

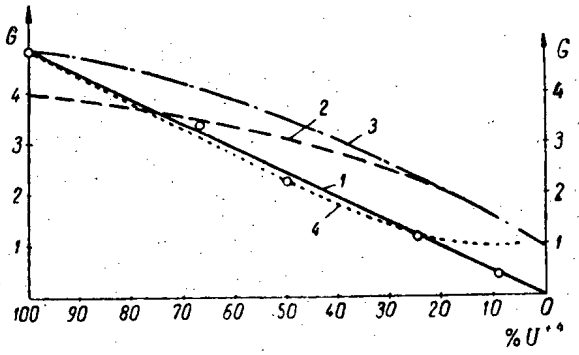

Fig. 4. The relation of the uranium oxidation yield to uranyl ion concentration.
Curve 1) at $[U^{+4}]$ = 106.5 mg-equiv/liter, curve 2) at $[U^{+4}]$ = 10.0 mg-equiv/liter, curve 3) calculated by equation (III), curve 4) calculated by equation (IV).

in which the alphabetical coefficients denote the amount of the corresponding component formed when 100 ev is absorbed in water. According to Allen, n = 3.64, m = 2.86, k = 0.48, l = 0.87.

The value G is quite close to the value of the maximum in the range 26-110 mg-equiv/liter U^{+4} (Fig. 1) and agrees, within the accuracy of the measurements, with the magnitude m + 2l = 4.60 given by Allen, i.e., with the sum of the oxidizing components formed in water on absorbing 100 ev. Apparently, this is explained by the occurrence of the reactions

$$U^{+4} + OH \rightarrow U(V) + OH^-, \quad (2)$$
$$U^{+4} + H_2O_2 \rightarrow U(V) + OH + OH^-, \quad (3)$$

in which all the oxidizing components are consumed.

The elimination of U(V) ions is probably due to disproportionation which, as is known, proceeds at quite a high rate [6], [7].

TABLE 1

The Values of $\left(\frac{100\,n}{I}\right)^{1/2} \frac{K_2 K_4^{1/2}}{K_5}$ at Various $[U^{+4}]$ Concentrations

$[U^{+4}]$, g-equiv/liter · 10^3	2,85	4,26	5,33	26,0	53,25	110	Average 363±13
$\left(\frac{100n}{I}\right)^{1/2} \frac{K_2 K_4^{1/2}}{K_5}$	277	300	382*)	320	357*)	350*)	

*) The most reliable data.

The fact that the maximum yield coincides with the value $m + 2l$ shows that the H_2^+ complex does not have oxidative properties in the radiolysis of U^{+4} solutions, contrary to what is assumed in the case of Fe^{+2} [8], [9]. A considerable rise in acidity, which helps to increase the concentration of H_2^+ ions and, consequently, their participation in the oxidation, also does not increase G (Fig. 2). Thus, in the upper part of the curve in Fig. 1, the H radicals may be eliminated from the solution only by recombination to form H_2^+:

$$H + H \longrightarrow H_2. \qquad (4)$$

However, in the presence of oxygen they participate in U^{+4} oxidation apparently by the same mechanisms as in the radiation oxidation of Fe^{+2}, i.e., through the formation of the HO_2 radical; at least the oxidation yields of both reactions coincide quantitatively.

Saturation of the solutions with hydrogen does not decrease the G yield, which seems to indicate the absence of the reaction $H_2 + OH \longrightarrow H_2O + H$ even in dilute solutions. We therefore assumed that under our experimental conditions, molecular hydrogen remains chemically inert.

Competition between the H and U^{+4} radicals is small in comparison with the oxidizing components of water radiolysis products in the range $[U^{+4}]$ = 26-110 mg-equiv/liter. Apparently, competition is possible at a quite low U^{+4} concentration, as the fall in the curve on the left side of Fig. 1 indicates. The reaction

$$H + OH \longrightarrow H_2O \qquad (5)$$

is the only reaction we will consider as competing with reactions (2) and (3).

This approximation is justified somewhat by the fact that more than 80% of the oxidizing components, obtained during water radiolysis, is accounted for by OH radicals formed directly from water and from H_2O_2 as a result of subsequent reactions, for example reaction (3). The accuracy of this hypothesis is further confirmed by the agreement between the equations obtained and the experimental data.

An examination of the mechanism of U^{+4} oxidation using the stationary state method for reactions (1)-(5) gave the following relation of G to the $[U^{+4}]$ ion concentration:

$$\left(\frac{100n}{I}\right)^{1/2} \frac{K_2 K_4^{1/2}}{K_5} = \frac{G-l}{n+2k-G} (1/2G-k)^{1/2} \frac{1}{[U^{+4}]}, \qquad (I)$$

where K_2, K_4 and K_5 are the formal rate constants of the corresponding reactions, I is the intensity of irradiation in ev/liter · min, n is Avogadro's constant, $[U^{+4}]$ is the concentration of tetravalent uranium in g-equiv/liter. Table 1 gives the value of $\left(\frac{100\,n}{I}\right)^{1/2} \frac{K_2 K_4^{1/2}}{K_5}$, calculated from Equation (I) by substituting the experimental values of G and $[U^{+4}]$ and the values of m, n, k, l found by Allen. We had to correct Allen's coefficients for our case, as there was some difference in the value $m + 2l$ found in our experiments and in Allen's data (5.0 and 4.60, respectively). $m + 2l$ was taken as 5.0; the values for m, n, k and l were multiplied by a factor of 1.087.

If one considers that the separate factors in the right side of Equation (I) change 20-30 fold in the $[U^{+4}]$ range being examined, then the constancy of the value $\left(\frac{100\,n}{I}\right)^{1/2} \frac{K_2 K_4^{1/2}}{K_5}$ found in the experiment should be

considered satisfactory. The left branch of the curve in Fig. 1 is plotted from Equation (I) using the value $3.63 \cdot 10^2$ from Table 1 for the constant. The calculated curve agrees well with the experimental data up to the maximum region.

The fall in G after the maximum is naturally explained by the reaction

$$U^{+4} + H \rightarrow U^{+3} + H^{+} \qquad (6)$$

competing with reaction (4), as apparently reaction (5) does not occur. Allowing for reaction (6) leads to the equation

$$\left(\frac{I}{100n}\right)^{1/2} \frac{K_6}{K_4^{1/2}} = \frac{n + 2k - G}{(1/2G - k)^{1/2}} \frac{1}{[U^{+4}]} . \qquad (II)$$

The curve of the relation of G to $[U^{+4}]$ plotted from this equation is shown in Fig. 1 by a dotted line; it does not coincide so well with experimental data. One should, however, take into account the fact that to the right of the maximum the total concentration of ions in the solution increases noticeably with an increase in $[U^{+4}]$. If one assumes that some kind of complexes of U^{+4} ions with sulfate ions participate in reaction (6), then there is considerably greater agreement with the experiment.

The mechanism of the processes occurring in U^{+4} solutions at

$$[U^{+4}] > 110 \text{ mg-equiv/liter}$$

should be studied In the future we propose to study the relation of the falling slope of the curve (right branch in Fig. 1) to anion concentration and intensity of radiation.

The fall in G with the accumulation of uranyl ions in the solution (see Fig. 3) indicates the interaction of the ions with H or OH radicals. However, it is difficult to analyze the mechanism of this reaction as at $[U^{+4}] < 110$-25 mg-equiv/liter the reactions of uranyl ions with the radicals must compete with reaction (5). We will try to take this phenomenon into account.

The U^{+4} concentration remains above 25 mg-equiv/liter for a considerable time along the top curve in Fig. 3, and therefore the observed decrease in G is not due to the effect of reaction (5). We can then assume that the decrease in yield is due only to reactions of UO_2^{+2} with radicals. These reactions are usually considered as the reaction

$$UO_2^{+2} + H \rightarrow UO_2^{+} + H^{+}, \qquad (7)$$

which is accompanied by the process

$$UO_2^{+} + OH \rightarrow UO_2^{+2} + OH^{-}.$$

Allowing for reaction (7), we obtain equation

$$\left(\frac{I}{100n}\right)^{1/2} \frac{K_7}{K_4^{1/2}} = \frac{n + 2k - G}{(1/2G - k)^{1/2}} \frac{1}{[UO_2^{+2}]} , \qquad (III)$$

according to which the yield depends only on $[UO_2^{+2}]$, as all the other terms are constant. This result does not agree well, even qualitatively, with the fact that the curves in Fig. 3 for ΣU equal to 25.96; 53.25 and 110 mg-equiv/liter almost run into each other. In fact, the ratio of U^{+4} and UO_2^{+2} concentrations is plotted on the abscissa in Fig. 3, and therefore the proximity of the three upper curves indicates that, in the ΣU range indicated above, the value of G should only be a function of this ratio. This assumption might have been possible if U^{+4} competed with UO_2^{+2} for the same oxidizing component, formed during water radiolysis. The reaction

$$UO_2^{+2} + OH \rightarrow UO_2OH^{++}. \qquad (8)$$

may be considered as the UO_2^{+2} ion competing with U^{+4} oxidation.

TABLE 2

The Values of the Constants $\left(\frac{I}{100\,n}\right)^{1/2}\frac{K_7}{K_4^{1/2}}$ and $\frac{K_8}{K_2}$ in Relation to the Magnitude of the Ratio $\frac{[U^{+4}]}{[UO_2^{+2}]}$ and $[UO_2^{+2}]$ for ΣU = 110 mg-equiv/liter

G	4,32	3,55	2,81	2,20	
$[U^{+4}]/[UO_2^{+2}]$	2,51	1,0	0,49	0,22	
$[UO_2^{+2}]$ g-equiv/liter · 10^3	30,3	53,3	71,0	87,3	Average 0,54±0,03
$\frac{K_8}{K_2}$	0,51	0,55	0,58	0,50	
$\left(\frac{I}{100n}\right)^{1/2}\frac{K_7}{K_4^{1/2}}$	17,4	24,1	33,2	42,0	

TABLE 3

The Magnitudes $\left(\frac{I}{100\,n}\right)^{1/2}\frac{K_7}{K_4^{1/2}}$ and $\frac{K_8}{K_2}$ at $[U^{+4}]$ = = 106.5 mg-equiv/liter, Calculated by Equations (III) and (IV)

G	3,42	2,24	1,19	
$[U^{+4}]/[UO_2^{+2}]$	2,0	1,0	0,33	
$[UO_2^{+2}]$ g-equiv/liter · 10^3	53,25	106,5	319,5	Average 34,1±5,2
$\left(\frac{I}{100n}\right)^{1/2}\frac{K_7}{K_4^{1/2}}$	27,2	33,2	42,0	
$\frac{K_8}{K_2}$	1,28	2,14	5,16	

The unstable complex thus formed reacts much more slowly with U^{+4} than with the H radical. From this hypothesis we get the equation

$$\frac{K_8}{K_2} = \frac{n+2k-G}{G-l}\,\frac{[U^{+4}]}{[UO_2^{+2}]}, \qquad \text{(IV)}$$

in which G depends only on the ratio $[U^{+4}]/[UO_2^{+2}]$. The results of calculating the constants, determined by Equations (III) and (IV), are given below.

As Table 2 shows, the constant of Equation (IV) agrees well with experimental data, differing only by ± 7% from the average value when the ratio $[U^{+4}]/[UO_2^{+2}]$ is changed by a factor of more than 10; the constant of Equation (III), however, increases by a factor of 2.5 in the same range.

One may assume that both reactions (7) and (8) affect the decrease in the yield G. In this case, with equal values for the ratio $[U^{+4}]/[UO_2^{+2}]$, as the UO_2^{+2} concentration decreases, reaction (8) will predominate and as it increases, reaction (7) will predominate. In order to check this hypothesis G was measured at a constant U^{+4} concentration equal to 106.5 mg-equiv/liter and an increasing concentration of UO_2^{+2} ions. As is seen, reactions (5) and (6) were excluded from this experiment. The divergence of the curves in Fig. 4, calculated by Equations (III) and (IV), shows that at high UO_2^{+2} concentrations the value G is no longer only a function of the ratio

$$[U^{+4}]/[UO_2^{+2}].$$

This is also confirmed by data in Table 3 which indicate that the constant for the curve calculated by Equation (III) is more invariable.

At UO_2^{+2} concentrations below 110 mg-equiv/liter retardation may be best explained by taking into account the reaction UO_2^{+2} + OH; apparently at higher concentrations the reaction UO_2^{+2} + H starts to play a large role in the decrease of G.

Figure 3 gives the results (of up to 180 series of experiments, 7-10 points in each series) for G at $[U^{+4}]$ and $[UO_2^{+2}] < 26$ mg-equiv/liter. It follows from the above that under these conditions the decrease of G must be caused only by reactions (8) and (5) and not by (7). Taking this into account, we get the equation

$$\frac{K_8}{K_2}\frac{[UO_2^{+2}]}{[U^{+4}]} + \left(\frac{I}{100n}\right)^{1/2}\frac{K_5}{K_2K_4^{1/2}}\frac{(1/2\,G-k)^{1/2}}{[U^{+4}]} = \frac{n+2k-G}{G-l}. \qquad (V)$$

The series of curves in Fig. 3 were plotted from this equation at $\frac{K_8}{K_2} = 0.54$ and

$$\left(\frac{I}{100n}\right)^{1/2}\frac{K_5}{K_2K_4^{1/2}} = 1.363$$

(see Tables 1 and 2) for the values of ΣU given under the figure. As can be seen, it agrees well with experimental data and may thus be used as an argument for the mechanism proposed by us for the oxidation of tetravalent uranium under these conditions.

Received May 20, 1957

LITERATURE CITED

[1] J. W. Boyle, W. F. Kieffer, C. J. Hochanadel, T. J. Sworski, J. A. Ghormley, Proc. Intern. Conf. Peaceful Uses Atomic Energy, Geneva, 1955, U. N. (New York, 1956) v. 7, p. 576.

[2] M. Haissinsky, J. chim. phys. et phys.-chim. biol. 53, 542 (1956).

[3] M. Haissinsky, M. Duflo, J. chim. phys. et phys.-chim. biol. 53, 970 (1956).

[4] A. O. Allen, Radiation Res. I, 85 (1954).

[5] V. G. Firsov, J. Atomic Energy 2, 182 (1957).*

[6] H. G. Heal, Nature 157, 225 (1946).

[7] H. G. Heal, G. N. Thomas, Trans. Faraday Soc. 45, 11 (1949).

[8] T. Rigg, G. Stein, J. Weiss, Proc. Roy. Soc. A211, 375 (1952).

[9] T. Rigg, G. Stein, J. Weiss, J. Amer. Chem. Soc. 77, No. 17, 4526 (1955).

*Original Russian pagination. See C. B. Translation.

STUDY OF THE VELOCITY OF THE MAGNESIUM REDUCTION PROCESS OF ZIRCONIUM PRODUCTION

F. G. Reshetnikov and E. N. Oblomeev

An apparatus is described for studying the velocity of the magnesium reduction process of zirconium production by the "floating-crucible" method, in which the rise in level of the molten $MgCl_2$ + KCl, due to the increase in weight of the reaction crucible immersed in the melt, was measured by means of a Co^{60} γ-level gauge. The pressure of the zirconium vapor in the reduction apparatus was measured by means of an ordinary pressure gauge, connected by a molten tin seal to the space within the reduction apparatus.

Measurements showed that when the vaporizer was heated to 450°C, the temperature of the zirconium chloride during magnesium reduction did not exceed 330°C.

The mean velocity of the magnesium process for the reduction of zirconium chloride increases with increase in the temperature of the reaction crucible from 760 to 850°C more slowly than with increase in the temperature of the vaporizer from 460 to 490°C. The deciding factors determining the velocity of the magnesium reduction process of zirconium production are the temperature of the vaporizer and the rate of sublimation and pressure of the zirconium chloride vapor, which are dependent on it.

Unlike most thermal metallurgical processes, the reduction of zirconium chloride by magnesium does not proceed at a very high rate. For instance, in our experiments, the reduction of 4-5 kg of chloride took 3-4 hours. In [1] it is stated that for the reduction of 240 kg of zirconium chloride working temperatures must be maintained for 14 hours, and the entire process, including auxiliary operations, takes more than 32 hours.

There is little information in the literature [1], [2] regarding the influence of the various factors on the velocity of the process or regarding the methods of studying this question.

Application of the method described in [2] was found to be unsuccessful, particularly for the reason that a pressure of approximately 1 atm had to be maintained in the apparatus. This made it impossible to carry out the process under any given conditions. An apparatus and method (conditionally called the floating-crucible method) were developed, in which the reaction velocity of the process was determined directly from the weight of the reacted zirconium chloride. The latter was measured by means of a Co^{60} γ-pressure gauge from the level of the molten salt displaced by the floating reaction crucible.

Apparatus

Figure 1 is a general view of the apparatus for studying the velocity of the magnesium process of zirconium reduction. It consists of an upper furnace with a thermally insulating cover 3, for the volatilization of the zirconium chloride; this cover is set on a thermally insulating ring, supported on the lower furnace 6, in which the reaction crucible 8 is heated. The furnace accommodates the hermetic reaction apparatus 15 (preserving the vacuum and withstanding excess pressure), fitted with a two-way vacuum cock 11. The latter is intended for flushing and filling the apparatus with argon, and for releasing excess gas in the initial heating period of the apparatus.

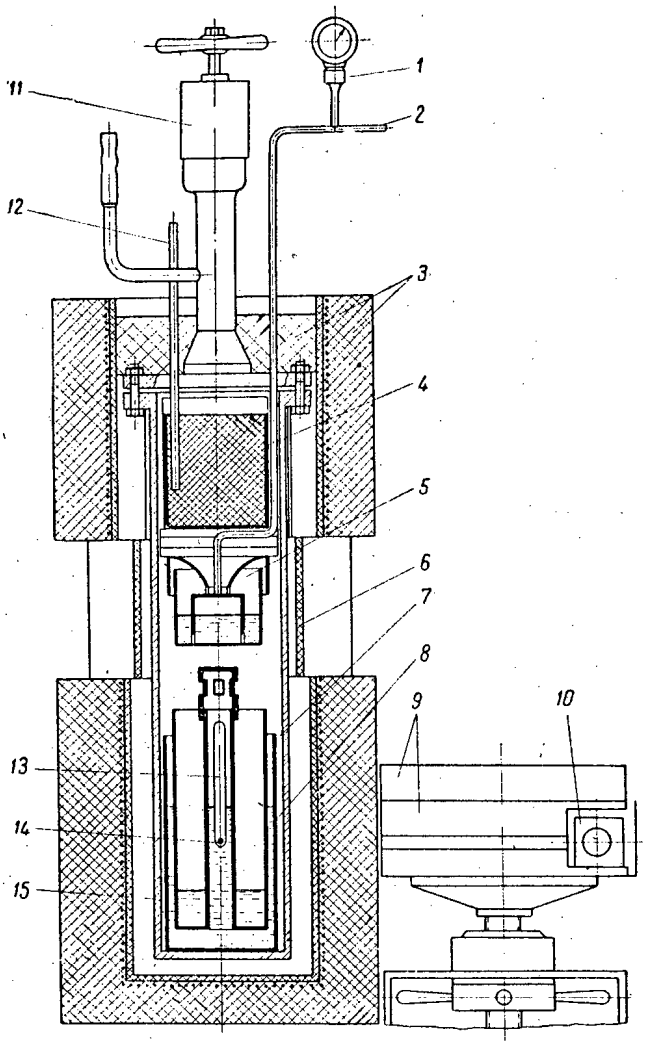

Fig. 1. General view of the apparatus for determining the reduction velocity.
1) Spring pressure gauge; 2) to mercury manometer; 3) upper furnace with thermally insulating cover; 4) vaporizer with chloride; 5) seal; 6) thermally insulating ring and lower furnace; 7) pot; 8) reaction crucible; 9) lead collimator; 10) γ-counter pickup; 11) two-way cock; 12) sheath for thermocouple; 13) ampoule float; 14) Co^{60}; 15) reaction apparatus.

The reaction crucible is the pot 8, charged with magnesium and having a central tube (floating crucible). It is placed within another pot 7, partly filled with the eutectic mixture $MgCl_2$ + KCl. In the central tube is a thin-walled quartz or metal ampoule 13, with the cobalt source 14, sealed in a case of stainless steel. The dimensions and weight of the ampoule were selected so that it floated freely in the molten mixture of $MgCl_2$ + + KCl. The pot containing the reaction crucible was placed in the reduction apparatus. At first, the lower part of the apparatus was heated until the mixture of $MgCl_2$ + KCl was melted, the reaction crucible with the magnesium and the ampoule with the Co^{60} floating up at the same time. The position of the ampoule was noted from the maximum γ-radiation, by means of the γ-counter 10, to an accuracy of ± 1 mm. The vaporizer with the chloride 4 was then heated, and the reduction of zirconium chloride by magnesium commenced. The weight of the reaction crucible increased; it sank deeper in the melt, raising the Co^{60} ampoule. The height of ascent of the ampoule, proportional to the amount of reacted zirconium chloride, was determined from the vertical displacement of maximum γ-activity. The dimensions of the pot and reaction crucible were such as to ensure maximum ascent of the Co^{60} ampoule.

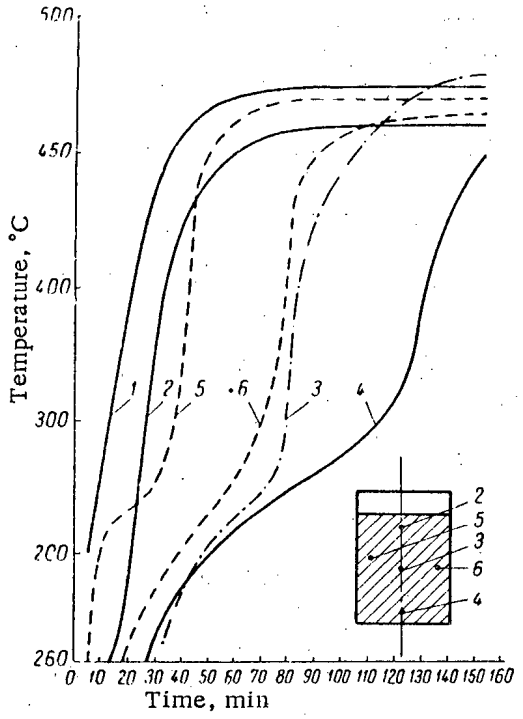

Fig. 2. Temperature of zirconium chloride at different points of the vaporizer as a function of time.
1) Indication of the control thermocouple; 2-6) indications of thermocouples sited in the vaporizer as shown diagrammatically in the graph.

The pressure of zirconium chloride vapor at 437°C is 25 atm, which had to be taken into account. The measurement of the partial pressure of chloride vapor and inert gas was also of considerable interest. The reduction apparatus was therefore fitted with a pressure gauge for measuring the chloride pressure at high temperature (Fig. 1), comprising a molten tin seal 5, situated inside the reduction apparatus, and a mercury manometer or spring pressure gauge 1, situated outside the apparatus and hermetically connected to the seal. The pressure acting on the molten tin seal was transmitted from the latter through an argon-filled tube to the external pressure gauge. The accuracy of pressure measurement increased with decrease in the volume of the connections between the seal and the pressure gauge, and with decrease in the difference in level of the molten tin in the pot and in the internal chamber of the seal. In our experiments the error in the readings of the pressure gauge did not exceed 10 mm Hg.

For diminishing the reaction of the tin with the chloride-containing volatile matter ($COCl_2$, C_2Cl_6, etc.) in the zirconium chloride, the surface of the tin should be protected by a very fusible mixture of chlorides, for example $MgCl_2$ + KCl + NaCl.

The pressure of the zirconium chloride vapor during the reduction process could be ascertained from the difference in pressure during and after the reduction process.

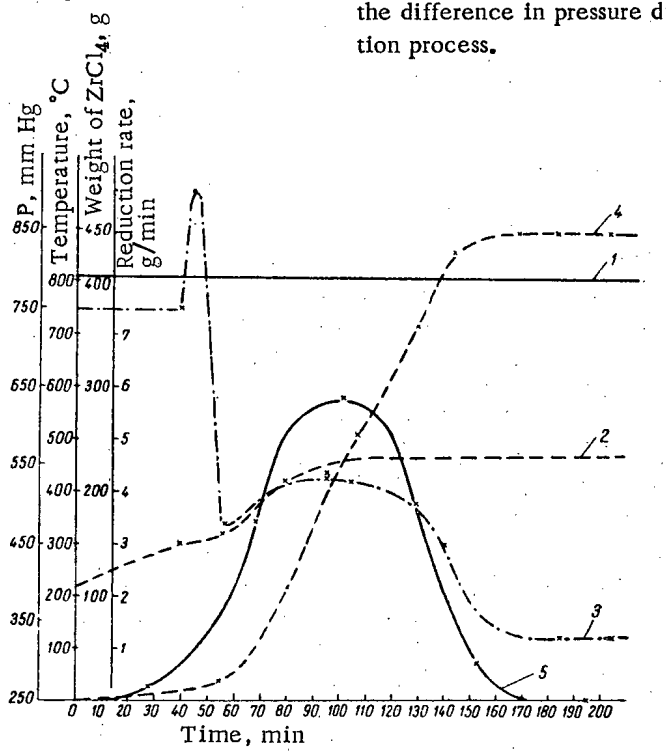

Fig. 3. Variation in operating conditions in the process of the reduction of zirconium chloride by magnesium.
1) Temperature of the reaction crucible; 2) temperature of the vaporizer; 3) variation of pressure P in the apparatus; 4) variation of weight of reaction crucible; 5) rate of reduction.

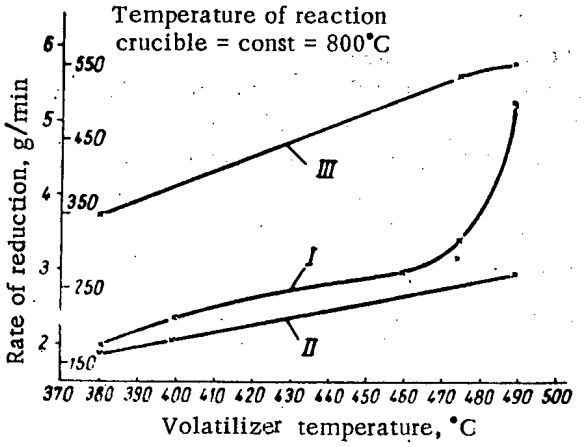

Fig. 4. Mean rate of reduction (I), pressure of zirconium chloride (II) and argon pressure (III) as function of volatilizer temperature.

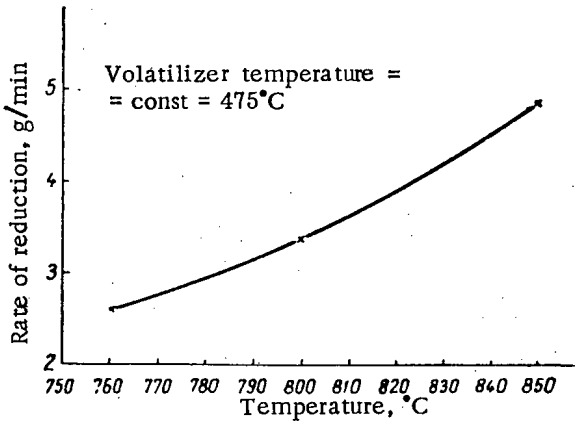

Fig. 5. Mean rate of reduction as function of the temperature of the reaction crucible.

Measurement of the Temperature of Zirconium Chloride in the Vaporizer.

Supervision of the vaporizer heating temperature was effected by means of a thermocouple 12 (Fig. 1). Actually, this thermocouple indicated the temperature of the furnace zone in which the vaporizer was situated, but not the temperature of the zirconium chloride. In production, the temperature of the vaporizer zone is also supervised.

In our experiments, for a temperature of the vaporizer zone of 450-500°C, the pressure in the apparatus did not exceed 3 atm, indicating the existence of a considerable temperature gradient between the zirconium chloride and the peripheral zone of the vaporizer.

For measuring the actual temperature of the zirconium chloride, five additional thermocouples were introduced into the vaporizer, the readings and positions of which are shown graphically in Fig. 2. As will be seen from the graph, the temperature in the upper part of the pot vaporizer and close to its wall, indicated by thermocouple 1, increases much sooner than at the positions of the other thermocouples. A noteworthy feature is the presence of deflections on the curves of thermocouples 3, 4, 5 and 6 in the range ~310-330°C, i.e., approximately at the sublimation temperature of the chloride at atmospheric pressure. From the relation between the time of appearance of the deflection and the position of the thermocouples, it follows that, while a thermocouple is situated in the chloride, its indications do not exceed 330°C. When the level of the vaporizing chloride is lower than the position of the corresponding thermocouple, the latter indicates a jump – a rapid rise in temperature. Consequently, the temperature of the chloride does not exceed ~330°C, even when the vaporizer zone is heated to 450°C. This may be utilized, in particular, for verifying the termination of the volatilization of the whole of the zirconium chloride.

Measurement of the Velocity of the Magnesium Process of Zirconium Production

Figure 3 shows a typical record of the working conditions of an experiment to determine the velocity of the process for constant temperature of the reaction crucible. The first maximum on the pressure curve corresponds to the desorption of volatile matter contained in the zirconium chloride, and the second, flatter maximum characterizes the maximum pressure in the apparatus, composed of the argon pressure and the pressure of zirconium chloride vapor. The volatile matter, liberated when the zirconium chloride is heated, reacts comparatively rapidly with the magnesium and partly also with the material of the apparatus, and subsequently does not produce pressure in the apparatus. After completion of the reduction, the pressure in the apparatus is equal to the argon pressure. The difference between the pressure during the reduction process and the pressure of the argon (except during the period of desorption of volatile matter) is equal to the pressure of zirconium chloride vapor.

Figure 4 shows that the mean rate of reduction increases rapidly with increase in temperature of the vaporizer (curve I), while the partial pressure of the zirconium chloride varies little (curve II). This points to the fact that the deciding factors in the mean velocity of the process are the heating temperature of the vaporizer of given construction and the rate of volatilization and the partial pressure of zirconium chloride vapor, which depend upon the vaporizer temperature.

Excessive increase in the rate of sublimation of the zirconium chloride may result in an inacceptable increase in temperature of the reaction crucible and in contamination of the metallic zirconium produced, due to the reaction of the latter with the material of the crucible. In the case of forced reduction of zirconium chloride, diminution in the heating of the reaction zone of the apparatus may be recommended for lowering the temperature of the reaction crucible, or according to the scale of reduction, complete switching off of the furnace and even cooling of the apparatus.

An increase in the rate of sublimation of the chloride may be obtained not only by increasing the temperature, but also by increasing the sublimation surface, i.e., by modifying the form and dimensions of the vaporizer. The velocity of the actual reaction of zirconium chloride vapor with the molten magnesium is evidently quite high.

From the dependence of the mean velocity of the magnesium process on the temperature of the reaction crucible (Fig. 5), it is clear that within the limits of 760-850°C, the mean velocity varies more slowly than in the case of increase in the vaporizer temperature from 460-490°C (Fig. 4). This is due to the fact that the limiting factor in the reduction rate is, as was pointed out above, the rate of sublimation of the zirconium chloride. For constant and higher concentration of chloride vapor in the apparatus, the influence of the reaction crucible temperature on the velocity of the process may be greater.

The data which have been given on the velocity of the process (in g/min) were obtained with an 80 mm diameter floating reaction crucible. The absolute value of these data vary with variation in the dimensions of the crucible, but the dependence of the velocity of the process upon the temperature of vaporizer and reaction crucible will obviously remain the same. It does not appear possible to express the velocity of the reaction in g/min per unit volume of crucible or of the surface on which the reaction proceeds, due to the variation in volume of the reaction surface during the course of the experiment.

Received May 29, 1957

LITERATURE CITED

[1] S. M. Shelton and E. D. Dilling, The Manufacture of Zirconium Sponge, Zirconium and Zirconium Alloys (A. S. M. Cleveland, Ohio, 1953) p. 82.

[2] F. E. Block and A. D. Abraham, J. Electrochem. Soc. 102, No. 6, 311 (1955).

DETERMINATION OF THE SOLUBILITY OF DIFFICULTLY SOLUBLE COMPOUNDS USING NONISOTOPIC RADIOACTIVE INDICATORS

N. B. Nikheev

We established the rules governing the transfer into solution of a microelement, truly isomorphous with the compound of a macroelement, with partial solution of the solid phase containing the microelement. A method was developed for determining the solubility of difficultly soluble compounds using nonisotopic radioactive indicators, truly isomorphous with the given compound. The effect of the degree to which thermodynamic equilibrium was attained between the whole precipitate and the saturated solution on the character of the curves used for determining solubility was elucidated. We propose a method for determining the solubility of difficultly soluble compounds in solutions containing similar ions. The relations found were confirmed by determining the solubility of $BaSO_4$ with Sr^{90} and of K_2PtCl_6 with Cs^{134}.

In their article, Korenman et al. [1] proposed a new method for determining the solubility of difficultly soluble compounds using nonisotopic radioactive indicators (that were truly isomorphous with the given compound). This paper does not give sufficiently convincing data in support of the applicability of this method. On the contrary, on determining the solubility of cadmium tetrathiocyanomercurate using Cd^{115} as the radioactive indicator (isotopic indicator) and Zn^{65} (nonisotopic indicator), the authors obtained solubility data which differed by a factor of almost four, and this cannot be considered satisfactory. The authors of the article based their investigations on the following assumptions: 1) when the solution reaches saturation, the thermodynamic equilibrium between all the precipitate and the saturated solution is not yet established; 2) the ratio between the macro- and microelements is the same in both phases. If the first assumption is accepted, then the second would be true only in the case where the macro- and microelements were isotopes.

In the choice of components of a system of different elements capable of forming truly isomorphous solid solutions, the thermodynamic equilibrium state is characterized by the following equation [2]:

$$\frac{x}{y} = D\frac{(1-x)}{(1-y)}, \qquad (1)$$

where x, y and $(1-x)$, $(1-y)$ are the micro- and macroelement contents of the precipitate and of the solution, respectively, and D is the crystallization coefficient.

Let us examine the case when a solution is saturated with a compound containing a radioactive indicator that is truly isomorphous with the given compound. B will denote the amount of the macroelement taken for saturating the solution so that the microelement content of the sample would be $A = kB$, where k is a proportionality coefficient.

Using Equation (1), we get

$$\frac{A-a}{B-b} = D\frac{a}{b}, \qquad (2)$$

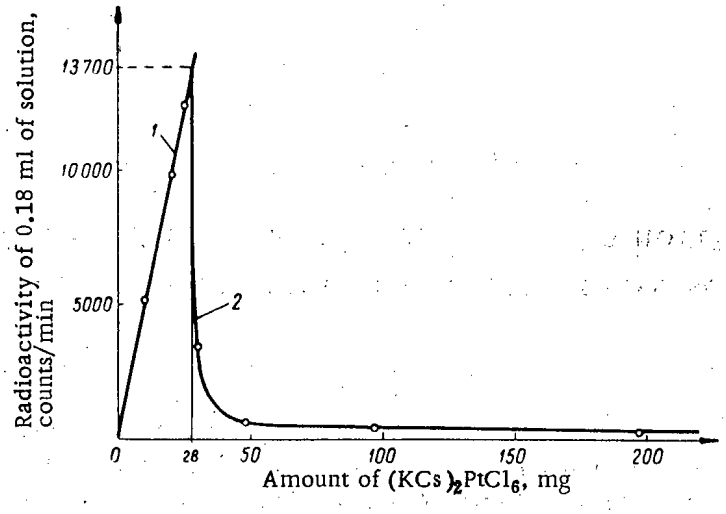

Fig. 1. Determination of the solubility of potassium chloroplatinate in water, using radio-cesium.

where a and b are the micro- and macroelement contents of the solution. Assuming that B = nb, upon solving Equation (2) for a, we find

$$a = \frac{knb}{D(n-1)+1}, \tag{3}$$

where $n \geq 1$.

It follows from Equation (3) that the microelement content of the solution, a, depends on n and D. By analyzing Equation (3) we establish the following: 1) at $D > 1$, $n > 1$ $a/b < A/B$; 2) when $D < 1$, $n > 1$, $a/b > A/B$; 3) if $D \neq 1$, $n = 1$, $a/b = A/B$; 4) in the particular case when the micro- and macroelements are isotopes and $D = 1$, when $n \geq 1$, $a/b = A/B$. This means that the calculated value of the solubility will be correct only in cases 3 and 4. Case 3 is of special interest as the curve $a = f(n)$, extrapolated to the value $n = 1$, will give the magnitude a and the true solubility of the compound may be calculated from it.

First of all we must decide whether a linear extrapolation is acceptable for the curve, expressed by Equation (3), in the region where the value of n is close to unity. Substituting $m = n - 1$ in (3), we find

$$a = \frac{kb(m+1)}{Dm+1}, \tag{4}$$

where $m \geq 0$.

It is readily seen that at $Dm \ll 1$

$$a \approx kb[m(1-D)+1]. \tag{5}$$

It follows from this that the absolute error

$$[\Delta a]_{abs} = \frac{kb(m+1)}{Dm+1} - kb[m(1-D)+1].$$

By effecting the simplest transpositions we get

$$[\Delta a]_{abs} = kb\left[\frac{Dm^2(D-1)}{Dm+1}\right], \tag{6}$$

from which the relative error

$$[\Delta a]_{rel} = \frac{Dm^2(D-1)}{m+1}. \quad (7)$$

This shows that on maintaining the condition Dm << 1, we may neglect the error arising in (5) in the approximation of the curve expressed by Equation (4). In addition it is clear that the region of linear approximation increases at values of D approaching unity.

In order to check the equations found, we determined the solubility of potassium chloroplatinate in water, using radio-cesium.

Determination of the solubility of potassium chloroplatinate in water, using radio-cesium

According to literature data, the chloroplatinates of potassium and cesium are isomorphous [3], [4]. The solubility of K_2PtCl_6 in 100 g of water at 20 and 30°C is 0.7742 and 1 g, while the solubility of Cs_2PtCl_6 under the same conditions is 0.0086 and 0.0119 g, respectively [5]. One can conclude from this that the crystallization coefficient of cesium in the $K_2PtCl_6-Cs_2PtCl_6$ system is considerably greater than unity. We prepared the potassium chloroplatinate with Cs^{134} as indicator by treating KNO_3 solution containing radio-cesium with a H_2PtCl_6 solution. The precipitate formed was recrystallized with mixing for 1 hour, after which it was separated from the mother liquors by filtration through a funnel with a filter bottom and washed. The washed precipitate was dried at 90°C. To determine the solubility of K_2PtCl_6, small amounts of the salt prepared were placed in ampules, a definite amount of water, the same in each case (3 ml), was added and the ampules were sealed. Preliminary experiments established that with small ratios of solid and liquid, saturated solutions were obtained after shaking the mixture on a vibrator for 1-2 hours. In order to saturate the solutions, all the ampules were shaken at the same time at a temperature of 28°C for 6 hours, after which samples were removed for measuring the radioactivity.

The results obtained are shown graphically in Fig. 1. As the graph shows, in the region of unsaturated solutions (when the solid phase dissolved completely) there is a linear increase in activity (curve 1). When the solid phase was present, the activity decreased in accordance with Equation (3) for D > 1 (curve 2).

Taking the above into consideration, we extrapolated curve 2 until it intersected curve 1. The intersection point corresponds to the value of a when n = 1, from which we can readily calculate the solubility of potassium chloroplatinate, knowing the specific activity of the salt.

The solubility of potassium chloroplatinate at 28°C, which we found, was 0.93 g per 100 ml, which agrees with the literature data.

It should be noted that in these experiments thermodynamic equilibrium was not attained between the solid phase and the solution. In connection with this, it is necessary to examine the effect of the degree of equilibrium attained on the character of the curve for calculating solubility.

The effect of the degree of equilibrium attained between all the precipitate and the solution on the character of the curve for calculating solubility.

As indicated above, Equation (3) was derived on the assumption that a state of equilibrium had been reached between all the precipitate and the solution. In the case where there is equilibrium only between a part of the precipitate and the solution, Equation (3) becomes

$$a = \frac{kbin}{D(in-1)+1}, \quad (8)$$

where the coefficient i indicates the degree of reaction of the precipitate with the solution. It follows from Equation (8) that the approach to equilibrium should be indicated by a steeper slope of the curve of activity of the solution against the amount of the solid phase.

To check this we carried out experiments on the determination of the solubility of $BaSO_4$ in water, using Sr^{90} with various reaction times for the phases.

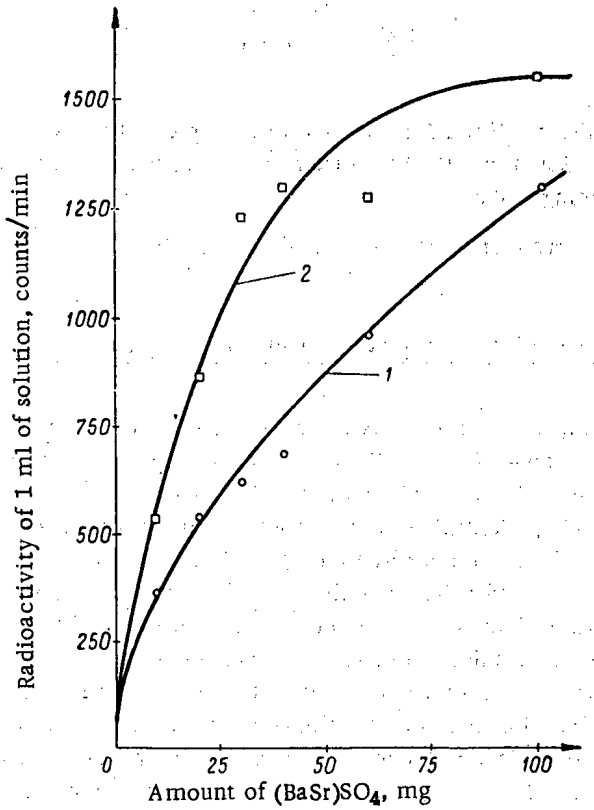

Fig. 2. The effect of the degree to which $(BaSr)SO_4$ reacted with the solution on the character of the curve for determining solubility.

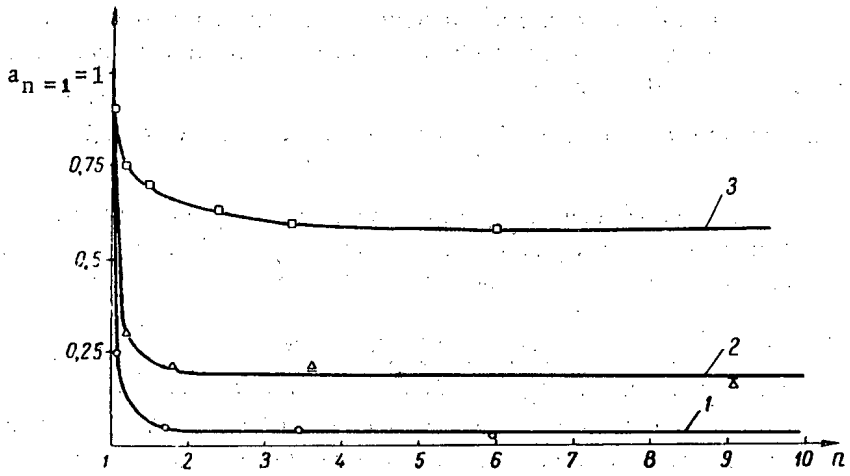

Fig. 3. The changes in the character of curves $a = f(n)$ in relation to the increase in the concentration of similar isotopes in the solution.

According to the literature data [3], $BaSO_4$ and $SrSO_4$ are isomorphous. However, the solubility of $BaSO_4$ is considerably less than that of $SrSO_4$. At a temperature of 25°C, 1 liter of a saturated solution contains 0.00246 g of $BaSO_4$, while at 30°C, the $SrSO_4$ content is 0.114 g/liter [6].

One would expect from these data that the crystallization coefficient of strontium in the $BaSO_4$–$SrSO_4$ system would be considerably less than unity.

The precipitate of $(BaSr)SO_4$ was prepared by reacting a $BaCl_2$ solution containing Sr^{90} with excess sulfuric acid, while it was stirred. For recrystallization the precipitate was left overnight in the mother liquors and then carefully washed with water. The washed precipitate was dried at 100°C and used in the experiments on the solubility determination. The specific activity of the precipitate was determined by measuring the radioactivity of a small sample (0.23 mg) under the same conditions as those used for measuring the samples of saturated solution. The amount of $(BaSr)SO_4$ used for saturating the solution was changed from experiment to experiment, while the volume of water was 50 ml in each case. The suspensions prepared were shaken on a vibrator at a temperature of 28°C. Samples were removed from the solutions after 12 and 24 hours of shaking, but the radioactivity was measured only after 15 days, i.e., after the radioactive equilibrium had been reached between Sr^{90} and Y^{90}. The results obtained are shown graphically in Fig. 2 and they show that when curve 1 (12 hour saturation) is extrapolated to the beginning of the coordinate, it converges with curve 2 (24 hour reaction of solid phase and solution). From this one can conclude that in both cases the solution had reached saturation. The steeper slope of curve 2 is due to the more complete reaction of the phases and, consequently, to the greater value of the coefficient i.

The value of a at $n \approx 1$ may be determined from the data obtained, and then the solubility of $BaSO_4$ may be calculated, knowing the specific radioactivity of $(BaSr)SO_4$. The solubility of $BaSO_4$ at 28°C which we found was 2.6 mg/liter ±25%, which agrees with literature data.

Determination of the solubility of a salt in the presence of similar ions

As shown by the calculations, the method of nonisotopic radioactive indicators may be used for determining the solubility of a salt in the presence of similar ions. In a state of thermodynamic equilibrium between the precipitate and the solution, the following relation is maintained:

$$\frac{A-a}{B-b} = D\frac{a}{b(q+1)}, \tag{9}$$

where qb is the macroelement content of the solution due to foreign salts.

Ratner [7] and Polesitskii [8] established that

$$D = D_0\left(\frac{\gamma}{\gamma'}\right)^{\nu}, \tag{10}$$

where D_0 is the true fractionation coefficient, γ' and γ are the activity coefficients of the macro- and microelement salts in the solution and ν is the number of ions into which the salt investigated dissociates. Considering Equations (9) and (10), we find

$$a = \frac{knb}{\frac{D_0\left(\frac{\gamma}{\gamma'}\right)^{\nu}}{q+1}(n-1)+1}. \tag{11}$$

As can be seen, Equation (11) is analogous to (3). To test (11) experimentally, we determined the solubility of K_2PtCl_6 in 0.1 and 0.2 N solutions of KCl with radio-cesium. The same $(KCs)_2PtCl_6$ precipitate was used in this work as was used in determining the solubility of this salt in water. The procedure was analogous to that used previously. The experiments were carried out at 28°C. The precipitate reacted for 6 hours with the solution, and in this respect one can assume that the coefficient i has similar values in all the experiments.

Figure 3 shows graphically $a = f(n)$ for $(KCs)_2PtCl_6$ solutions in water (curve 1), and in 0.1 and 0.2 N KCl (curves 2 and 3, respectively). For all the curves we assumed that $a_{n=1} = 1$.

As the KCl concentration of the solution increased, there was a decrease in the magnitude $D_0\left(\frac{\gamma}{\gamma'}\right)^{\nu}/q+1$ in Equation (11); this is reflected in the shape of the curves of $a = f(n)$ given in Fig. 3. In addition, Fig. 3 shows that as the value of

$$D_0\left(\frac{\gamma}{\gamma'}\right)^{\nu}/q+1$$

approaches unity, there is an increase in the accuracy of the determination of the solubility of the salt.

The values we obtained for the solubility of K_2PtCl_6 in 0.1 and 0.2 N solutions of KCl at 28°C were 110 and 33 mg per 100 ml of solution, respectively. According to literature data [5], the solubility of K_2PtCl_6 in 0.2 N KCl at 20°C is 23.6 mg per 100 ml.

The author is grateful to Corresponding Member of the Acad. Sci. USSR, V. I. Spitsyn, and his fellow scientist at the Institute of Physical Chemistry of the Acad. Sci. USSR, V. P. Smilg, for their comments on the work.

Received May 4, 1957

LITERATURE CITED

[1] I. M. Korenman, F. R. Sheianova, M. A. Potanova, J. Gen. Chem., XXVI (XXXVIII), No. 8, 2114 (1956).*

[2] L. H. Henderson, F. Kracek, J. Amer. Chem. Soc. 49, 738 (1927).

[3] B. F. Ormont, The Structure of Crystalline Substances (State Tech. Press, 1950).**

[4] O. L. Erdmann, J. f. Pract. Chem. 86, 373 (1862).

[5] A. Seidell, Solubilities of Inorganic and Metal Organic Compounds, vol. 1 (D. van Nostrand Comp. Inc. N. Y., 1940.

[6] Handbook of Chemistry and Physics, Ed. 37 (Publ. Chem. Rubb. Publishing Co., 1955-1956).

[7] A. P. Ratner, Trans. Radium Inst. Acad. Sci. USSR, II, 67 (1933).

[8] A. Polesitskii, A. Karataeva, Acta Physicochimica URSS, VIII, No. 2, 251 (1938).

* Original Russian pagination. See C. B. Translation.
** In Russian.

RESULTS OF EXPERIMENTS IN APPLICATION OF SELECTIVE GAMMA-GAMMA LOGGING

G. M. Voskoboinikov

Results of laboratory and field studies of dependence of the intensity of soft scattered γ-radiation in rocks on the content of elements with high atomic numbers are given. Tests confirm applicability of selective gamma-gamma logging to the search for heavy metals. It is shown that the anomalies caused by ore zones are of the same order of magnitude as those previously obtained by the author on theoretical grounds.

INTRODUCTION

In a previous paper [1] the author showed theoretically the possibility of using selective gamma-gamma logging by registering the intensity of very soft scattered γ-radiation for discovery and investigation of ore zones in boreholes in deposits containing elements of high atomic number when the density of the enclosing rocks is either equal to the density of the ore or is not sufficiently sharply differentiated from it. Sharp anomalies in the form of minima of intensity can be expected theoretically on the log when the sonde passes ore bodies containing as little as a few tenths of one percent of a heavy element.

In order to check the approximate theoretical conclusions and extend them to the more complex geometrical conditions of gamma-gamma logging of boreholes, the author has conducted laboratory and field tests whose main results are given below.

Laboratory Investigations

Two models of boreholes were used in laboratory investigations: No. 1, 30 mm in diameter, and No. 2, 70 mm in diameter. The enclosing rock was moist sand, the ore, the same sand with an admixture of lead acetate in amounts corresponding to the content of 0.5 to 1.5% of metallic lead. The density of the "ore" and of the "enclosing rock" was constant for each model – 1.63 g/cm^3 for model No. 1 and 1.80 g/cm^3 for model No. 2.

Measurements were made by means of a sonde consisting of a tungsten counter VS-4 in an aluminum case, a source of radiation and a screen in the form of a massive lead cylinder 30 mm in diameter, placed parallel to the axis of the borehole, so that the entire space between the source and the counter was filled by the screen. The length of the sonde was taken as the distance from the source to the center of the cathode of the counter and could be adjusted from 20 to 40 cm. The intensity of radiation was registered by counting impulses by means of the recorder "B".

Figure 1 presents results of the investigation of the relation between the intensity of scattered radiation and the content of lead in the sand. The sources of radiation were Co^{60}, Hg^{203} and Se^{75} in amounts corresponding to 0.3, 1.8 and 1.0 millicuries, respectively, having average energies of 1.25, 0.28 and 0.26 Mev (according to the data in [2]).

In model No. 1, no space was left between the screen and the walls of the borehole, and the measurements were interpreted as if made in a homogeneous medium (as if the borehole were absent). The theoretical curves calculated by the formulas given in [1] for the Co^{60} and Hg^{203} radiations are also given in Fig. 1. It will be seen that the experimental values agree well with the theoretical.

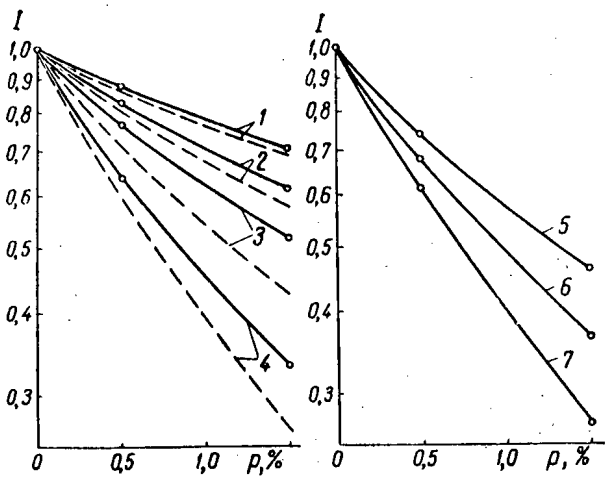

Fig. 1. Relation between intensity of scattered γ-radiation I and the amount of lead in sand p.
————) experimental data; – – – –) theoretical values;
1) radiation from Co^{60}, length of sonde r = 21.9 cm; 2) Co^{60}, r = 40.1 cm; 3) Hg^{203}, r = 23.5 cm; 4) Hg^{203}, r = 38.4 cm; 5) Se^{75}, r = 21.9 cm; 6) Se^{75}, r = 30.2 cm; 7) Se^{75}, r = 40.1 cm.

Se^{75} is the most suitable material for selective logging since, as compared with other sources of soft radiation, it has a relatively longer half-life (127 days) and a high γ-activity. It also gives a clearer record of the dependence of intensity of radiation on the content of the heavy elements in rocks than the other sources.

Figure 2 shows the results of point-by-point selective logging with the Se^{75} source and sondes of different length in a wide borehole near the bottom of an ore body.

The area of the cross section of space between the walls of the borehole and the sonde, which determines essentially the intensity of the parasitic rays spreading along the borehole ("borehole rays"), was 31 cm^2 and corresponded to that existing in actual boreholes when sondes of practicable size are used (for example, a sonde of 78 mm diameter in a 100 mm hole).

The object of the experiment was to study the dependence of the change in amplitude of an anomaly on the method of screening of borehole rays. Logging was done in a dry and in a water-filled borehole. Curves 1 and 2, Fig. 2, were obtained with the usual 30 mm sonde; curves 3 and 4, with an auxiliary absorber of borehole rays placed over the sonde and consisting of a brush of lead rods on a spring frame ("counter screen"). The average density of lead created by this screen in the space between the sonde and the borehole walls was 0.28 g/cm^3.

The arrows marked '6' on the diagram indicate limits of the level of intensity of radiation observed in case the ore and the enclosing rock had the same density; arrows marked '5' indicate analogous levels obtained in media with density of 1.63 g/cm^3 in experiments with model No. 1.

To show the results more graphically, smoothed curves based on relative values of intensities (diagram on the right) have been constructed by the side of the curves drawn on the basis of the absolute values of intensity (diagram on the left).

In all tests the ore with a moderate content of lead (1.5%) is marked by a sharp anomaly whose amplitude increases substantially with introduction of auxiliary absorbers of borehole rays, such as water and the lead brush; with sondes longer than 30 cm, the use of a lead brush in a borehole filled with water results in a perfect coincidence of the upper and lower branches of the diagram with the limiting levels '6', which indicates that the effect of the borehole rays has been completely removed.*

* A certain increase in intensity of radiation in the upper parts of the diagram is explained by the effect of the edge of the borehole as the counter nears its opening.

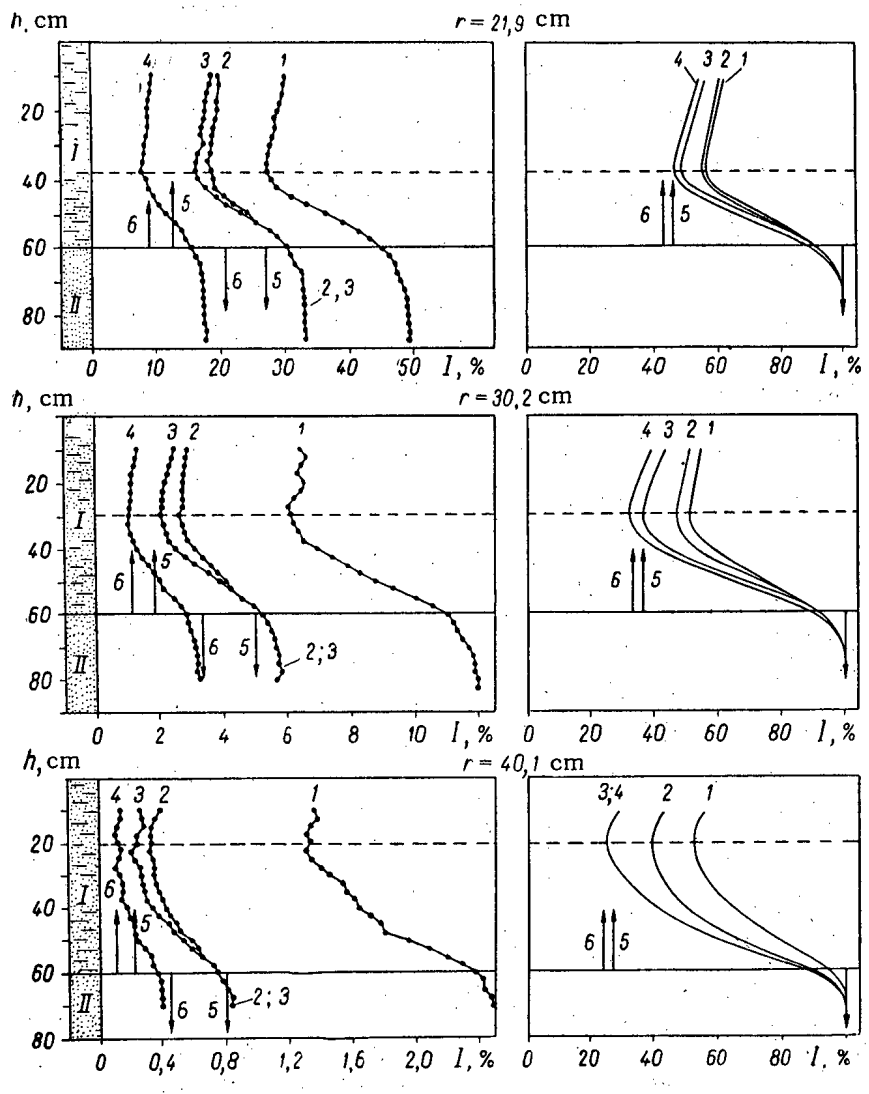

Fig. 2. Records of selective logging with Se^{75} as the source, obtained from a model borehole with 70 mm diameter in a medium with density of 1.80 g/cm^3 near the bottom of an ore body.
I) Sand containing 1.5% of lead ("ore"); II) pure sand ("enclosing rock"); h is the depth of the center of the counter; at left: I is the intensity of radiation in thousands of counts per minute; the points indicate observed values; at right: I is the relative intensity in percent of its value in the enclosing rock; r is the length of the sonde; 1) logging with a 30 mm screen in a dry hole; 2) same, in a water-filled hole; 3) logging with a lead brush screen in a dry hole; 4) same, in a water-filled hole. The arrows indicate intensity of radiation in homogeneous media of similar composition in the absence of a borehole: 5) density of the medium 1.63 g/cm^3; 6) density, 1.80 g/cm^3; ——) bottom of the ore body; – – – –) position of the center of the counter in the sonde at the moment when the source of radiation passes the boundary of the body.

Characteristics of the Sondes for Some Applications of Selective Logging

The basic elements of the sonde determining its effectiveness in work with a given complex of rocks are its length and the energy of the quanta emitted by the source, which depends on the nature of the source.

In comparing measurements in rocks of substantially different densities it is more convenient to use the product of the length of the sonde by the density of the rock, called the "adjusted length of the sonde," rather than the length of the sonde itself. Other conditions being the same, the adjusted length determines, by use of the formula given in [1], the intensity of scattered radiation and the magnitude of the anomaly.

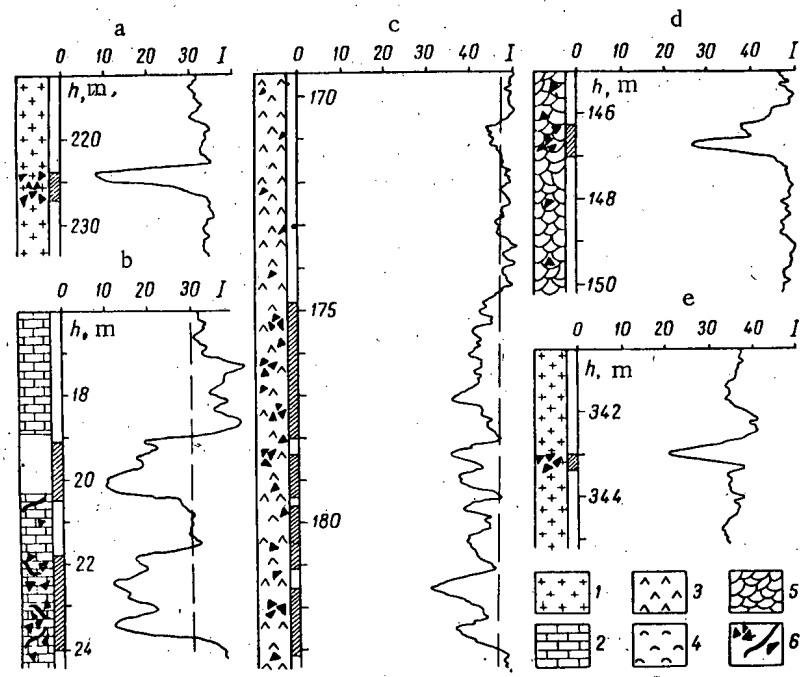

Fig. 3. Records of selective gamma-gamma logging in boreholes in ore bodies.

1) Albitized granodiorite; 2) limestone; 3) jasperoid; 4) arenaceous shale; 5) quartz-jasperoid and jasperoid-limestone shale breccia; 6) nests, veinlets and disseminations of ore minerals: a) scheelite, b) galena, c) cinnabar, d) stibnite, e) molybdenite; h is the depth, m; I is the intensity of scattered gamma-radiation in arbitrary units. Ore zones determined by logging are shaded.

The experimental data reviewed above indicate that for relatively rich ores a sonde with the adjusted length of 65 g/cm^2 and Se^{75} as the source of radiation may be recommended. The sonde gives an anomaly of about 10% of the intensity of radiation per 0.1% of lead content. If it is assumed that for a clear-cut result the anomaly should have an amplitude not lower than 20% of the intensity, the sonde with the above dimensions may be used successfully for logging deposits of metals with atomic numbers near 80(tungsten, mercury, lead, bismuth, uranium) if their content in ore is 0.2% or more, and also for metals with atomic numbers near 50 (antimony, tin) if their content in ore is 0.6% and higher.

For logging in rocks with normal radioactivity, it is sufficient to have a source of 10 millicuries. If the counter VS-4 is used, such a source guarantees an intensity of scattered radiation of about 800 mc/hour in the rock and an intensity of about 200 mc/hour in an ore containing 1.5% of metal (recalculated to the radium emanation in air) and permits logging without correction for the natural radioactivity of the rocks.

In selective logging of boreholes (for direct determination of their uranium content independently from their radium content), to diminish the confusing effect of the high background produced by the radioactivity of rocks, the intensity of the source should be increased to 1-2 curies; at the same time, the sensitivity of the counter should be reduced but with preservation of response to the soft radiation.

Results of Field Tests

The method was tested under working conditions in a number of localities in Central Asia by the author and the workers of the "Sredaztsvetmetrazvedka" trust.*

* An organization searching for colored metals in Soviet Central Asia – Publisher.

A sonde with a lead-covered cylindrical steel screen was used. The sonde was 25.5 cm long, the screen 73 mm in diameter. To reduce the effect of borehole rays, the sonde was pressed against the wall of a borehole by a spring. The source of radiation, a plexiglas vial containing 10 mc of Se^{75}, was held in an eccentric cutout in the screen on the side pressed against the wall of the borehole, and screened on the opposite side by a plate of iron 40 mm thick. The counter, VS-4, was placed in an aluminum case with 6 mm walls and screened over a 240° sector by a layer of lead 9 mm thick.

Recording was done by means of the logging recorded KRT.

Figure 3 shows characteristic portions of some of the logs obtained in boreholes 110 to 130 mm in diameter. The curves a and b are from dry upper parts of the boreholes, which had numerous cavities. The normal radiation background of the barren parts of the boreholes without cavities is marked on the logs by interrupted lines; it corresponds to the minima of intensity repeatedly recorded in those parts of the boreholes which were known to be dry and without ore and, in most cases, lay beyond the portions of the boreholes represented in the logs. Cavities are recorded on the diagrams by sharp increases in intensity of radiation, anomalies due to ore by decrease in intensity below the level of the normal background. The rest of the logs were recorded under more favorable conditions, in relatively smooth boreholes filled with water, and show an even background and sharp anomalies.

The ore zones, shown by the anomalies of the logs, are shaded and correspond to the following metal content in the ore: a) 8.3% tungsten, b) 1.7% lead (lower zone), c) 0.2-0.4% mercury, d) 2% antimony, e) 1.8% molybdenum. The upper anomaly on diagram b is from the depth of 18.9-20.3 m, an interval which did not yield a drill core. This interval is interpreted as an anomaly due to an ore zone missed during geological investigation.

Anomalies on logs a, b and c were obtained from ores with different content of metals with comparable atomic numbers giving anomalies of like magnitude. Comparison of these anomalies makes it possible to judge the resolving capacity of the method in distinguishing ores with different metal content. As can be seen from the logs, the anomaly increases from 25 to 77% of the intensity corresponding to the change in metal content from about 0.3 to 8.3%, providing a scale with 4 to 5 graduations for determining the metal content in ores; a finer differentiation is possible with lower metal content.

It should be noted that in all cases reviewed here, except for that shown in log a (Fig. 3), density logging carried out at the same time with a 40 cm sonde did not record perceptible anomalous effects. In the case of log a, recording a very high content of tungsten, the density log showed a slight anomaly with an amplitude of about 25% of the intensity of radiation.

SUMMARY

1. Experiments have confirmed the theoretical results given in [1] on the possibilities and limitations of the method of selective gamma-gamma logging.

2. Laboratory and field tests proved the applicability of this method of locating ore zones with metal content of 0.2-0.3% and more in deposits of lead, tungsten and mercury, and of ore zones with 0.6-1.0% of metal in case of antimony and molybdenum. It is recommended that experimental-production selective gamma-gamma logging be done in those deposite of the elements mentioned above and of the elements near them in atomic number, where the content of these elements in the ores of economic value is within the limits given above. In case of deposits with ore pockets, the metal content averaged over the exploitable thickness of the deposit may be far below the limits given above.

3. The necessary condition for application of selective gamma-gamma logging is careful screening of borehole rays. Some methods of screening (brush, eccentric sonde) were tested in the field and gave satisfactory results.

Received November 27, 1957

LITERATURE CITED

[1] G. M. Voskoboinikov, Izv. AN SSSR, ser. geofiz. No. 3 (1957).

[2] G. T. Seaborg, Table of Isotopes (Russian translation) (IL 1956).

LETTERS TO THE EDITOR

SAFE REACTOR START-UP FROM ZERO POWER

B. G. Dubovskii

By zero power we are to understand the power of a reactor in the subcritical state.

In this case the power of the reactor is determined by fissions induced by spontaneous neutrons or by neutrons from a source, neutron multiplication in the subcritical reactor, delayed neutrons, and β-decays of fission fragments produced as a result of prior operation of the reactor at high power levels.

As is well known, the excess reactivity of a reactor may be greater than 10%; this is significantly greater than the reactivity introduced by the delayed neutrons. After reactor shutdown the excess reactivity may be changed by factors which are as important as the delayed neutrons (large temperature effect, xenon poisoning, change in uranium loading, introduction of strong absorbers into the reactor, removal or addition of water, etc.).

Let us consider the subcritical state of the reactor at the first Soviet Atomic Power Station [1]. The large change in excess reactivity requires the total insertion of all the boron rods at shutdown. Under these conditions the reactor power, due mainly to spontaneous uranium fission, is $W \approx 10^{-7}$ watt. The monitoring instrumentation is of no use at such low power levels since the apparatus is insensitive at power levels below 200 watts. Without proper monitoring instrumentation it is dangerous to increase the reactor power in the region 10^{-7}-200 watts because even the introduction of supercriticality by an amount $\Delta k \approx 0.7\%$ can lead to a runaway situation.

It is difficult to monitor the reactor in this power region using sensitive instruments since the earlier operation of the reactor at high power levels means that the instruments will record the residual γ-radiation or be put out of operation altogether. Automatic introduction of sensitive pickup units into the core is also useless for short shutdown periods because of the strong γ-background.

For these reasons it must be assumed that the preliminary estimates of excess reactivity are very inexact and that an error in the estimate can lead to runaway in reactor start-up. The difficulty lies in the fact that in bringing the reactor up to controllable power levels, the amount by which the power is increased over the original zero power is a factor of order $\sim 2 \cdot 10^9$.

To facilitate start-up of a reactor power station (these considerations also apply for other reactors) from zero power level, a slab Sb + Be-source was placed in the reactor stack. Because of the antimony activation this slab becomes a photoneutron source with an intensity of approximately $4 \cdot 10^7$ neutrons/sec. The introduction of this source into the reactor reduces the uncontrollable power region by approximately a factor of $5 \cdot 10^5$.

The essence of the method, which provides a safe permissible rate for increasing the reactor power up to levels at which it can be controlled, lies in the uniform (step-by-step) withdrawal of sections of the boron rods which are equivalent in effectiveness.

Let us consider the uniform step-by-step removal of reactivity by an amount $\Delta k = 4.5 \cdot 10^{-4}$ in one minute. At any instant of time, because of the increase in k_{eff} the reactor becomes critical (or slightly supercritical), i.e., $\Delta k \approx 0$ (this instant is not recorded by the instruments). A further uniform increase in reactivity (due to withdrawal of the boron rods) leads to a subsequent increase in Δk and, consequently, an increase in reactor power. In the Table on page 478 are the appropriate power increments (these data are to be considered descriptive). In computing the values of the period for doubling the power T due to Δk, the neutron lifetime in the reactor lattice has been taken as $\tau \approx 3 \cdot 10^{-4}$ sec.

As is apparent from the Table, after the sixth withdrawal operation the reactor power increases by approximately a factor $5 \cdot 10^5$ (for $\Delta k = 31.5 \cdot 10^{-4} = 0.31\%$) and a controllable power level is achieved with a safe rate of rise (the doubling time is 0.1 min). Before activation of the Sb, a Po + Be-source with an intensity of $\sim 10^6$ neutrons/sec is placed in the reactor; in this case, for the sake of safety, the time between two rod withdrawal operations is increased to 1.5 min.

TABLE

Increase in Reactor Power

Rod withdrawal	$\Delta k \cdot 10^4$	Power doubling period, T (in minutes)	Power increase in one minute	Total increase in power from the instant at which criticality is achieved
1	4.5	2	$K_1 = 20.5$	$K_1 = 20.5$
2	9	1	$K_2 = 2$	$K_1K_2 = P_2K = 21.5$
3	13.5	0.5	$K_3 = 2^2$	$P_3K = 2^{3.5}$
4	18	0.33	$K_4 = 2^3$	$P_4K = 2^{6.5}$
5	22.5	0.2	$K_5 = 2^5$	$P_5K = 2^{11.5}$
6	27	0.13	$K_6 = 2^{7.5}$	$P_6K = 2^{19}$
7	31.5	0.10	$K_7 = 2^{10}$	$P_7K = 2^{29}$

The fact that a safe increase in reactivity can be obtained in passing through the uncontrollable region, using only ordinary monitoring instrumentation, means that a sub-critical reactor can be automatically brought to useful power levels. The step-by-step increase in reactivity is replaced by a continuous increase where the rate of rise of reactivity is chosen in such a way as to provide a safe rate of rise of power in coming up to controllable power levels. A similar method for automatic start-up from zero power levels is described in [2].

Experiments carried out together with S. A. Ogorodnikov on automatic start-up from zero power levels, using the reactor at the Atomic Power Station, have shown that this procedure is completely safe. It should be noted that the time required for coming up from zero power levels for a given maximum rate of rise of reactor power is determined by the intensity of the neutron source and the sensitivity of the monitoring instrumentation to neutrons and the ability to discriminate against γ-rays.

The method described here for safely increasing the power through the uncontrollable region was proposed and tried by us in 1950. The application of this method in automatic start-up of reactors was suggested together with A. K. Krasin in 1954.

The author is indebted to V. S. Fursov for suggesting this problem and for valuable comments, to E. N. Babulevich for participating in the discussions and for valuable advice, and to A. K. Krasin for his continued interest in the work.

Received October 29, 1957

LITERATURE CITED

[1] A. K. Krasin, B. G. Dubovskii, E. Ia. Doil'nitsyn, L. A. Matalin, E. Ia. Iniutin, A. V. Kamaev and M. N. Lantsov, J. Atomic Energy 1, 3 (1956).*

[2] M. A. Schultz, Control of Nuclear Reactors and Power Plants. Russian Translation, IL (1958).

* Original Russian pagination. See C. B. Translation.

USE OF A DIRECT-FLOW CYCLE IN A BOILING-WATER REACTOR

Iu. N. Alekseenko

Boiling-water reactors have received a great deal of attention in recent years. Studies carried out at the BORAX* reactor show that the experimental boiling-water reactor has a self-regulating characteristic because of the negative reactivity coefficient of the steam and that it can be operated under stable conditions with a mean steam volume of 20-25% in the core. Under these conditions the radioactivity of the steam used in the reactor is rather low and the steam can be used directly in the steam turbine. In this connection there have appeared in the literature many papers devoted to considerations of various flow schemes in boiling-water reactors.

In particular, Leyse (Nucleonics, 6, June, 1955*) has considered the possibility of a system which operates in accordance with the scheme shown in the figure (p. 480).

In the author's opinion the chief danger is the possibility of overheating of the fuel elements which are located above the level of the water and are cooled only by the steam. However, on the basis of experiments which have been carried out he indicates that there is a marked reduction in the density of thermal neutrons as a function of height in the upper part of the core as well as a reduction from the center to the periphery because of the high vapor porosity of the moderator; thus overheating of the fuel elements is not to be expected.

We have carried out a more detailed analysis of this type of reactor. In order to investigate the nature of the drop in neutron density in the upper part of the reactor and to determine the nonuniformity in heat generation through the volume of the core, a calculation has been made of the behavior of this type of reactor.

The calculation indicates the following:

1. The drop in neutron density from the center to the periphery in the upper part of the reactor, due to the low density of the moderator in this part of the core, occurs very rapidly. Because of this situation it is reasonable to expect that there will be no overheating of fuel elements which are located above the water level.

2. The nonuniformity in the neutron density over the volume of the reactor is very high (mainly because of the axial component) and reaches a value $K_v = 5.50$ for $K_z = 3.60$ in a reactor 500 mm in diameter with a core 800 mm high.

For most reactors the nonuniformity factor will be still higher because of the relatively weaker effect of the reflector.

3. The region of maximum neutron density over the height of the reactor coincides with the region in which the temperature of the water is equal to the saturation temperature, or very close to it, and in which boiling has not been initiated.

With a high nonuniformity factor, this situation presents a serious danger. In a reactor of the type being described, high water flow rates are not possible in the core since the water flow is determined by the steam capacity or power of the reactor.

Using reasonable ratios between the reactor dimensions and power, based on the practical possibilities of extracting heat from a reactor with an energy density of 50 kw/liter in the core, the water velocity is several centimeters per second. This situation sets up conditions favorable for a transition to film boiling in the region of maximum heat generation.

* The Russian text seems to be mistaken here. The references seem to be, respectively, to the SPERT reactor and to the issue of Nucleonics of July, 1956.

The literature contains no data on critical heat loading for heat removal in a liquid which moves at slow velocity in which the nucleate temperature is close to the saturation temperature. However, on the basis of experimental data concerning critical loading for required temperature conditions and water velocities for W = 0.5 m/sec and higher, obtained at the Power Institute of the Academy of Sciences, USSR, some notion of the danger involved in the above-described conditions can be gained. In this work the following values of the critical heat loading are given:

W=0,5 m/sec		W=1,0 m/sec	
p atm	q_{cr} kcal/m²·hr ($\times 10^{-6}$)	p atm	q_{cr} kcal/m²·hr ($\times 10^{-6}$)
28	0,65	28	1,2
100	1,15	100	2,4
180	1,15	180	1,5
220	0,4	220	0,7

The data obtained at other water velocities also indicate a maximum q_{cr} at $p \approx 100$ atm.

It follows from these data that the maximum critical loading falls off rapidly with reduction in water velocity; although there is no direct data on these loads at low velocities, it is reasonable to expect that these will be still lower. Hence, from the point of view of obtaining feasible power, the direct-flow boiling-water reactor is much poorer than a multiple-circulation boiling-water reactor, since the latter is characterized by higher water velocities in the core and lower nonuniformity factors, because of the smaller steam content in the water.

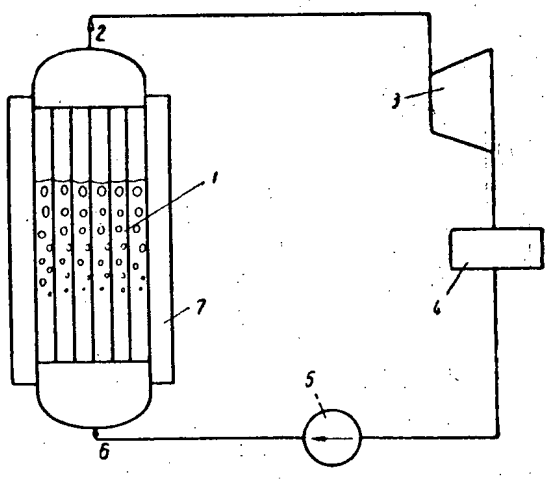

Diagram of the boiling-water reactor.
1) Reactor; 2) steam output; 3) turbine; 4) condenser; 5) pump; 6) water input; 7) reflector.

Even if the construction of a direct-flow reactor is feasible, it will still require a highly developed heat-removal surface. At the same time, this surface and the nuclear fuel will be used inefficiently because the high nonuniformity in the reactor will mean a high value for the maximum heat flux at a low average value of specific power. Any attempt to equalize the heat generation, for example by using fuel with higher enrichment in the upper part of the core, may lead to overheating of the fuel elements located above the water level. Moreover, a system of this kind would have the disadvantage that it would require continuous partial reloading of the lower part of the core and replenishing of the fuel in the upper part.

Received November 4, 1957

BINARY CYCLE IN A BOILING-WATER REACTOR

Iu. D. Arsen'ev

In heterogeneous boiling-water reactors it is possible to use a so-called binary cycle, i.e., a cycle in which the turbine receives steam directly from the reactor as well as steam, at intermediate pressure, which is generated by the heat of the water which circulates through the reactor [1]. The secondary steam generator can be either a heat exchanger or a flash tank.

These two versions of the binary cycle are shown in Fig. 1. For convenience, the analysis is carried out using the parameters described in [2] for a large boiling-water reactor with an electric power capacity of approximately 180 megawatts.

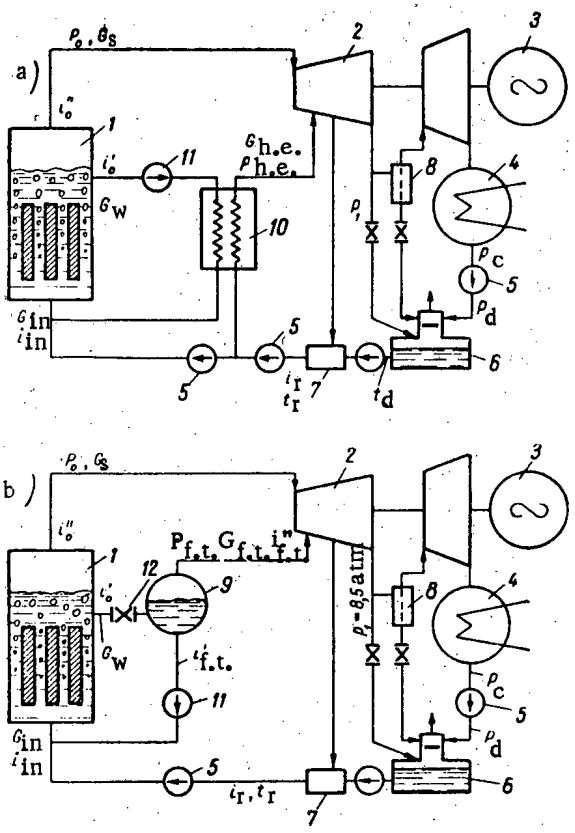

Fig. 1. a) Heat-exchanger cycle; b) flash-tank cycle.
1) Reactor; 2) turbine; 3) generator; 4) condenser; 5) pump; 6) deaerator; 7) regenerator; 8) separator; 9) flash tank; 10) secondary steam heat exchanger; 11) circulation pump; 12) throttle valve.

TABLE 1

Heat-Exchanger Cycle at Regeneration Temperatures 212 and 104°C

	t_r = 212°C	t_r = 104°C
Secondary steam pressure ($p_{h.e.}$, atm)	36	36
Steam flow in the heat exchanger ($G_{h.e.}$, ton/hr)	585	324
Pressure differential in the circulating pump ($\Delta p_{c.p.\ (h.e.)}$, atm)	6	6
Circulation pump power ($N_{c.p.(h.e.)}$, megawatts)	3.3	3.3
Electric power of the station (N_{oe}, megawatts)	185.2	178
Station efficiency (η_{oe}, %)	28.2	27
Relative pump power ($\xi_{p\ (h.e.)}$, %)	1.8	1.85
Ratio of primary and secondary flows ($G_s/G_{h.e.}$)	1.09	1.97
Improvement with regeneration ($\Delta\eta$, %)	1.2	0

TABLE 2

Flash-Tank Cycle at Regeneration Temperatures 212 and 104°C

	t_r = 212°C	t_r = 104°C
Flash-tank pressure ($p_{f.t.}$, atm)	55	61
Steam flow in flash tank ($G_{f.t.}$, ton/hr)	603	367
Pressure differential in circulation pump ($\Delta p_{c.p.\ (f.t.)}$, atm)	20	14
Circulation pump power ($N_{c.p.\ (f.t.)}$, megawatts)	10.2	7.3
Electric power of the station (N_{oe}, megawatts)	188.1	186
Station efficiency (η_{oe}, %)	28.7	28.2
Relative pump power ($\xi_{p.\ (f.t.)}$, %)	5.4	3.9
Ratio of primary and secondary flows ($G_s/G_{f.t.}$)	1.06	1.74
Improvement with regeneration ($\Delta\eta$, %)	0.5	0

As has already been noted [3], from the point of view of heat balance and mass balance, the operation of a boiling-water reactor is uniquely determined by several parameters: 1) the pressure in the reactor p_0 = idem = = 71 atm, 2) the amount of steam at the reactor output G_s = idem= 637 ton/hr, 3) the number of circulations through the reactor K_r = idem = 18.3, 4) the reactor loading factor β = idem = 0.593. With these parameters the thermal power of the reactor is 658 megawatts.

For simplicity we will carry out the calculation of the cycle only for the case in which a two-stage regenerative water superheater is used (Fig. 1a); the pertinent parameters are as follows: p_1 = 8.5 atm, t_r = 212°C, i_r = = 212 kcal/kg, t_d = 104°C, p_c = 0.085 atm, and p_d = 1.2 atm.

In the heat exchanger, steam is generated at a pressure $p_{h.e.}$ = 36 atm [2]. In calculating the power of the circulating pump the following parameters are assumed: efficiency is 0.72, resistance of the reactor Δp_r = 2 atm,

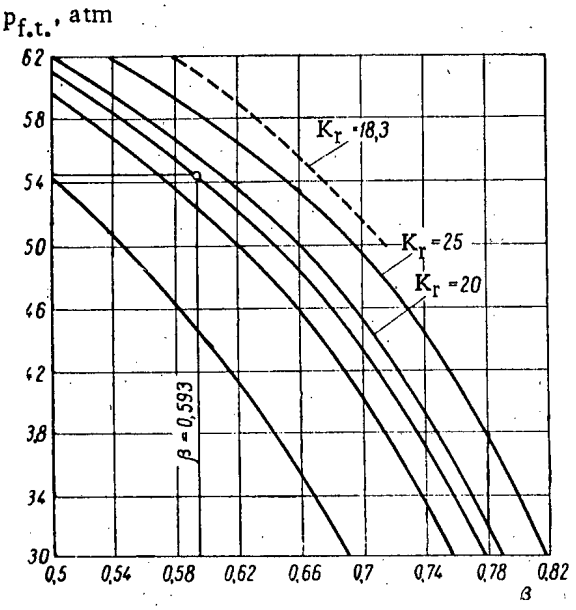

Fig. 2. Flash-tank pressure $p_{f.t.}$ as a function of reactor loading factor β and various numbers of circuits in the reactor K_r and various regeneration temperatures t_r.
The three curves (taken from below) are plotted for K_r equal to 10, 15, and 18.3.
——) t_r = 212°C; – – –) t_r = 104°C.

resistance of the piping Δp_c = 2 atm, resistance of the heat exchanger $\Delta p_{h.e.}$ = 2 atm. The results of a calculation of the heat-exchanger cycle with t_r = 212°C are shown in Table 1.

In the flash-tank cycle (Fig. 1b) the number of circuits through the reactor K_r is connected with the number of circuits through the flash tank $K_{f.t.}$ by the relation

$$K_r = 1 + K_r \frac{G_{f.t.}}{G_s} = 1 + \frac{\Delta i_3}{\Delta i_4}\frac{G_{f.t.}}{G_s}, \qquad (1)$$

where $\Delta i_3 = i''_{f.t.} - i'_{f.t.}$, $\Delta i_4 = i'_0 - i'_{f.t.}$.

The loading factor for the reactor is determined by the equation [3]

$$\beta = \frac{1}{1 + \dfrac{\Delta i_2}{\left(1 + \dfrac{G_{f.t.}}{G_s}\right)\Delta i_1 + \left(\dfrac{\Delta i_3}{\Delta i_4} - 1\right)\dfrac{G_{f.t.}}{G_s}\Delta i_4}}, \qquad (2)$$

where $\Delta i_1 = i'_0 - i_r$, $\Delta i_2 = i''_0 - i'_0$. From Eqs. (1) and (2) we have

$$\beta = \frac{1}{1 + \dfrac{\Delta i_2}{\left[1 + (K_r - 1)\dfrac{\Delta i_4}{\Delta i_3}\right]\Delta i_1 + (K_r - 1)\left(1 - \dfrac{\Delta i_4}{\Delta i_3}\right)\Delta i_4}}. \qquad (3)$$

Assigning the various pressures in the flash tank $p_{f.t.}$, we plot the curve $\beta = f(p_{f.t.})$ shown in Fig. 2. The point on this curve which corresponds to the present value β = 0.593 determines the operation of the flash tank: $p_{f.t.}$ = 54.75 atm ≈ 55 atm. In this case the steam flow rate from the flash tank is $G_{f.t.} = G_w/K_{f.t.}$ = 603 ton/hr.

It should be pointed out that not only is steam of higher quality obtained from the flash tank ($p_{f.t.} > p_{h.e.}$) but also that a greater amount of steam is obtained ($G_{f.t.} > G_{h.e.}$) since the heat of evaporation is reduced as the pressure is increased.

A comparison of these two cycles with t_r = 212°C (cf. Tables 1 and 2) shows that the heat-exchanger cycle, which is more complicated than the flash-tank cycle, has no thermodynamic advantage.

The effect of the number of circuits through the reactor K_r on the change of pressure in the flash tank can be understood by plotting the curves $p_{f.t.} = f(\beta)$ for various values of K_r: 10, 15, 20 and 25. It follows from the curves shown in Fig. 2 that an increase in K_r makes it possible to increase $p_{f.t.}$ and thus to vary the pressure differential in the pump over a wide margin. The increase in the hydraulic resistance of the core under these conditions need not be important since the main pressure differential in the pump is associated with the flash tank.

It is also interesting to consider the effect of the regeneration temperature t_r on the efficiency of the cycle in the case of the heat exchanger and in the case of the flash tank, taking account of the fact that the higher t_r, the more it is necessary to apply step-by-step regeneration and the more complicated the installation must be.

In the flash-tank cycle of a change of t_r with β = idem leads to a change in the parameters of the steam taken from the flash tank. In this case when t_r is reduced, if the temperature of the inlet water is kept constant, it is necessary to increase the water temperature in the flash tank, thereby increasing the steam pressure in the flash tank.

For this reason it is important to understand the way in which the introduction of regeneration changes the efficiency of the cycle. If the improvement in the efficiency due to regeneration is large, the regenerative heater may be limited only by the level which is required for thermal deaeration of the water.

The curve $\beta = f(p_{f.t.})$ for the flash-tank cycle with $t_r = 104°C$, obtained from Eq. (3), is shown in Fig. 2; this curve shows that with no change in the operation of the reactor itself ($\beta = 0.593$), with a reduction in t_r the pressure in the flash tank is increased from $p_{f.t.} = 55$ atm to $p_{f.t.} = 61$ atm for the same $K_r = 18.3$. The data for the flash-tank cycle calculation with $t_r = 104°C$ are shown in Table 2. For the heat-exchanger cycle with $t_r = 104°C$, we have used the same temperature differential at the output and, consequently, the same pressure of the secondary steam $p_{h.e.} = 36$ atm (cf. Table 1).

It is apparent from the Table that the reduction in efficiency due to a reduction in t_r for the flash-tank cycle is considerably smaller than for the heat-exchanger cycle.

SUMMARY

1. Replacing a heat exchanger by a flash tank not only simplifies design but also makes possible certain improvements in efficiency in spite of the fact that the flash-tank cycle means high power consumption for internal requirements and a large pressure differential in the circulation pump.

2. A feature of the flash-tank cycle is the small reduction in efficiency with large reductions in t_r, due to the fact that, with no change in the operation of the reactor, a change in t_r means an increased pressure in the flash tank $p_{f.t.}$. Hence in the flash-tank cycle it is feasible to reduce the temperature of the water regenerative superheater, thus allowing a reduction in the number of regenerator stages and a reduction in the pressure differential in the circulation pump.

Received December 7, 1957

LITERATURE CITED

[1] Proc. Inst. Mech. Engrs. 170, No. 8, 281 (1956).

[2] Problems of Nuclear Power, 1, 34 (1957).

[3] Iu. D. Arsen'ev, Supplement No. 1, J. Atomic Energy (1957) p. 185.*

* Original Russian pagination. See C. B. Translation.

CRITICAL HEAT LOAD FOR LONGITUDINAL WETTING OF A TUBE BUNDLE FOR WATER HEATED TO SATURATION TEMPERATURE

B. A. Zenkevich, V. I. Subbotin, M. F. Troianov

The purpose of this work is to study the critical point in the boiling condition with longitudinal wetting of a tube bundle (one of the possible alternatives for a heat-dissipating element) for water heated to saturation temperature.

The experimental apparatus described in reference [1] was used for the experiments. However the construction of a contact column with the working part consisting of a tube bundle was carried out in conformance with the problem of the present paper.

The tube bundle consisted of 7 or 19 heat elements (the two alternatives were used). The design of the heat-dissipation element is shown in Fig. 1. In both varieties the tube bundle-seen in transverse section, is disposed in triangular array with 6 mm spacing. The upper ends of the copper tubes are passed through a copper current supply cone to which they are brazed (Fig. 2) and below, the ends of the copper rods of the tube bundle, amalgamated with mercury, fit tightly into a stack of eight copper spacers. The working part of the bundle is inserted in sleeves of stainless steel between whose butt joints are placed centering spiders of heat-resistant micanite, protecting the outer tubes of the bundle from bending or warping. The space between the outer tubes of the bundle of the inner wall of the sleeve was 1 mm. In the lower and upper sleeves were windows for entry and outlet of water passing over the outside of the tube bundle (the water moves from bottom to top).

In order to determine the critical condition in the boiling state (the method is the same as that in reference [1]) the central and three peripheral tubes carried chromel-alumel thermocouples, whose hot junctions went through an opening drilled in the walls of the tubes 20 mm below the point where the stainless steel pipe is joined to the copper. The hot junction is arc-welded and is shielded so as not to project above the outer surface of the stainless tube. The lead from the cold junction of the thermocouple passes out of the contact column through a special connector.

The working part, after assembly, is introduced into the contact column (Fig. 2). The copper spacers which make up the lower end of the assembly enter the mercury cup which is tightly enveloped by a copper current supply bus. The copper cone used at the upper end of the assembly is mounted in a tapered hole in the upper current supply bus and tightened with a screw. Thus the tube bundle can freely sustain temperature stresses.

The body of the contact column was electrically insulated from the mercury cup and from the upper current supply bus.

The upper part of the contact column was provided with a gas cap whose internal cavity was insulated from the flow segment of the column by an appropriate gas pressure. Compressed nitrogen at a pressure equal to the pressure in the flow segment of the column was fed into the gas cap from pressure compensators of a B-200 apparatus [1]. Since the inside of the tubes is contiguous with the cavity in the gas cap, the pressure inside and outside the tubes was maintained practically equal, and the tubes were relieved of stresses due to the external pressure of the water. Provision is made in the gas cap for the outlet connector for the thermocouples.

Simulation of heat dissipation in the tube bundle was obtained by passing an electrical current.

In carrying out the experiments, the same basic measurements were made as in [1].

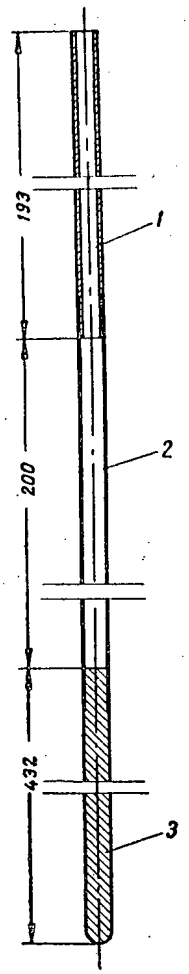

Fig. 1. Heat-dissipating element.
1) Copper current supply tube 5 × 1 mm;
2) heat-dissipating tube 5 × 0.27 mm of stainless steel; 3) copper current supply rod.

The moment of reaching the critical point in the boiling state, marked by a sharp increase in the temperature of the wall of one of the tubes which were provided with thermocouples (in some cases the critical point was noticed simultaneously in two or three tubes), was fixed by indications of the instruments.

The critical heat loading was determined by the electrical power and verified by the heat balance of the water.

At the very beginning of the experiments it was discovered that the first two or three times the critical point was reached in the boiling condition, obtained with one and the same parameters in a new (not having been in use) bank, gave a lowering (of 3 to 4 times) of the value of q_{cr} in comparison with subsequent ones. After several successive occurrences of the critical condition the magnitude of q_{cr} became stable. It was also established that a previous heating by an electrical current of the tube bank in the contact column, at a water pressure

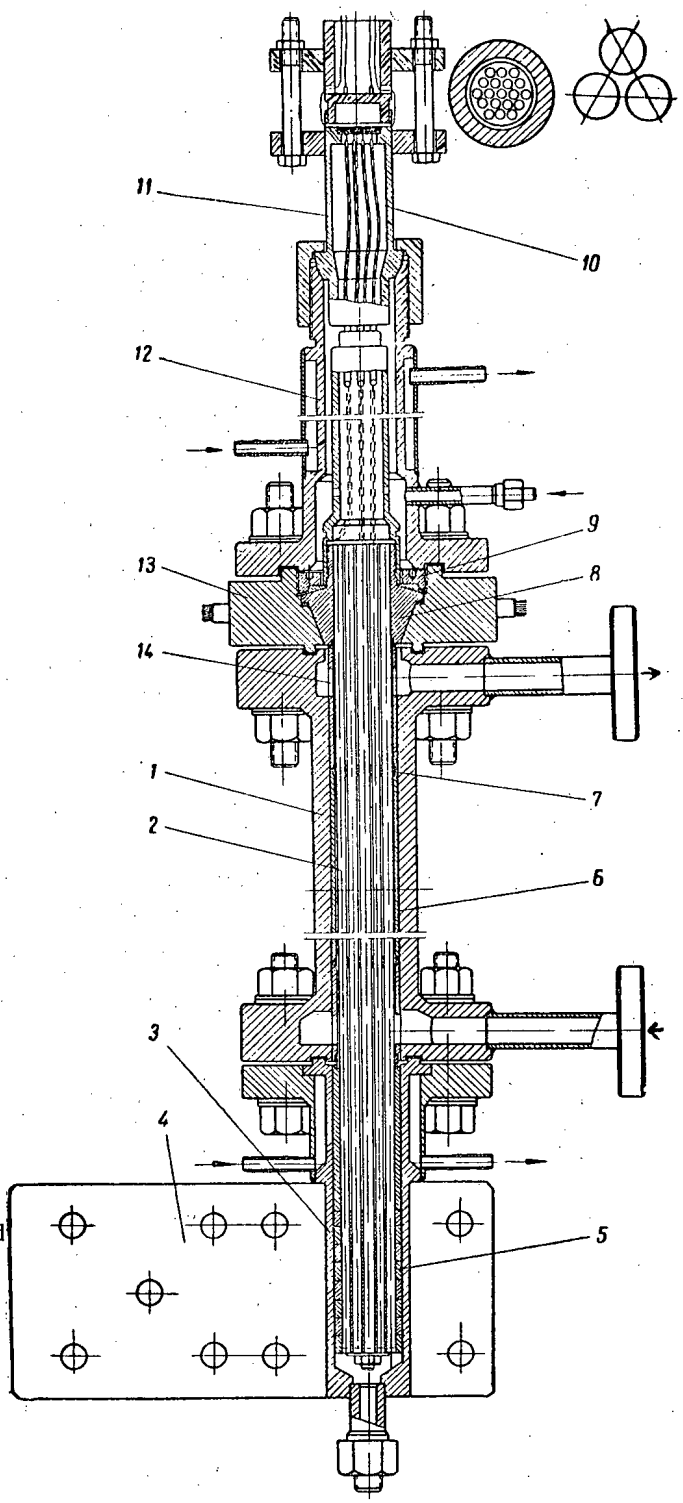

Fig. 2. Contact column with working parts.
1) Body of the contact column; 2) heat-dissipation element of the tube bundle; 3) mercury cup; 4) lower current feed bus; 5) copper spacers; 6) sleeve; 7) centering ring; 8) copper cone; 9) tightening screw; 10) thermocouples; 11) thermocouple outlet assembly; 12) gas cap; 13) upper current feed bus; 14) upper outlet window in the sleeve.

of 220 atmos abs and with tube wall temperatures of 600° to 650°C, also gave at once stable values of q_{cr}. The results given below were obtained on bundles after prior heating.

Experiments for determining the value of q_{cr} were carried out in the pressure range 180 atm to 210 atm and with water velocities of 0.65 to 4.65 m/sec and heated to temperatures less than that of saturation by 10° to 40°C. At a pressure of 220 atm, as was the case in reference [1], a degeneration of the critical point of the boiling state was discovered.

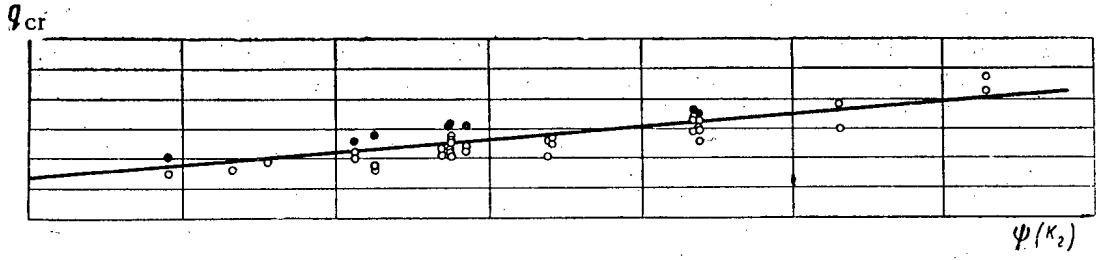

Fig. 3. Experimental data for q_{cr} for tube bundles in dependence on

$$\frac{K}{K_1^{0,65}\left(1+\frac{0,32\cdot 10^6}{R^{1,1+2,6K_1+0,9K_2}}\right)}=\psi(K_2).$$

The straight line corresponds to the theoretical equation; ●) bank of 19 tubes; ○) bank of 7 tubes.

In Fig. 3 are shown the data obtained for q_{cr} for tube bundles in comparison with the theoretical equation (Note: symbolism same as in reference [2]):

$$K=K_1^{0,65}(95+420\,K_2)\left(1+\frac{0,32\cdot 10^6}{R^{1,1+2,6\,K_1+0,9\,K_2}}\right)10^{-5},$$

where

$$K=\frac{q_{cr}}{r}\sqrt{\frac{\nu}{\sigma g W_g}},\quad K_1=\frac{\gamma''}{\gamma_H},\quad K_2=\frac{i_g-i_H}{r},$$

$$R=\frac{W_g\sqrt{\frac{\sigma}{\gamma'-\gamma''}}}{\gamma_H\nu}.$$

As is seen, satisfactory agreement is obtained with the equation, although some deviation of the experimental points is noted, relative to the banks of 7 and 19 tubes. This is probably connected with the differing disparities for both banks between actual determined temperatures of the water and the average temperature of the outflow of the water at the output of the bank, taken as the determined temperature.

Engineer V. I. Krotov took part in carrying out the experiments. Calculations and graph-making were carried out by engineer Z. F. Deriugina and technician N. A. Gushchina.

The authors express their gratitude to Academician A. P. Aleksandrov for setting the problem and Doctor of Phys. and Math. Sciences, A. K. Krasin, for attention and constant interest in the work.

LITERATURE CITED

[1] B. A. Zenkevich, V. I. Subbotin, J. Atomic Energy 3, 149 (1957).*

[2] B. A. Zenkevich, J. Atomic Energy 4, 74 (1958).*

*Original Russian pagination. See C. B. Translation.

NEUTRON DISTRIBUTION IN MEDIA WITH KNOWN PROPERTIES AND PLANE BOUNDARIES

I. I. Tal'ianskii

In formulating a theory of neutron logging, and in certain other cases, one must know the neutron spatial distribution function in media with different neutron properties, which are divided by a given boundary, in the presence of a point source of fast neutrons.

In Ref. [1] this problem has been solved for the case of two media with a cylindrical boundary, corresponding to a well in an infinite stratum.

In the present work we consider a plane boundary between two media; this analysis can be used to study the behavior of a neutron flux in passage from one stratum to another. Just as in Ref. [1] the problem is solved by the two-group method, with the introduction of fictitious sources at the boundary. Thus, let a plane boundary divide an infinite space into two parts, filled with media having different neutron properties (cf. figure on page 490). In what follows these media and all characteristics pertaining to them will be denoted by the subscripts "c" and "r". Further, suppose that in medium c there is a point source of fast neutrons at a distance a from the boundary. Quantities referring to the fast-neutron group and the slow-neutron group (thermal) will be denoted by the subscripts "1" and "2", respectively. We introduce a cylindrical coordinate system with origin coinciding with the point at which the source is located (cf. figure).

The equations for the neutron flux φ for fast and slow neutrons in both media are of the form

$$L^{1c}\varphi_{1c} = -Q\delta(r) - 4\pi\rho^*_{1c}, \tag{1}$$

$$L^{1r}\varphi_{1r} = -4\pi\rho^*_{1r}, \tag{2}$$

$$L^{2c}\varphi_{2c} = -\varkappa^2_{12c}\varphi_{1c} - 4\pi\rho^*_{2c}, \tag{3}$$

$$L^{2r}\varphi_{2r} = -\varkappa^2_{12r}\varphi_{1r} - 4\pi\rho^*_{2r}, \tag{4}$$

where

$$L^{il} = \frac{\partial^2}{\partial r^2} + \frac{1}{r}\frac{\partial}{\partial r} + \frac{\partial^2}{\partial z^2} - \varkappa^2_{il},$$

$$\varkappa^2_{il} = \frac{\Sigma_{il}}{D_{il}}, \quad \varkappa^2_{12l} = \frac{\Sigma_{1l}}{D_{2l}},$$

Σ_{1l} is the macroscopic slowing-down cross section, Σ_{2l} is the macroscopic thermal-neutron absorption cross section, D_{il} is the group diffusion coefficient [2], ρ^*_{il} is the density of fictitious sources at the boundary, $Q = N/D_{1c}$, and N is the number of fast neutrons emitted by the source per unit time ($i = 1,2$; $l = c, r$).

The functions $\rho^*_{il}(r, z)$ are written as follows:

$$\rho^*_{il}(r, z) = a_{il}(r)\,\delta(z - a),$$

where α_{il} is a function of r.

Next $\delta(z-a)$ is expanded in a Fourier integral while $\alpha(r)$ is expanded in a Fourier-Bessel integral:

$$\left.\begin{aligned}\delta(z-a)&=\frac{1}{2\pi}\int_{-\infty}^{\infty}e^{ik(z-a)}\,dk,\\ \alpha_{il}(r)&=\int_0^{\infty}\gamma_{il}(\eta)\,J_0(\eta r)\,\eta d\eta.\end{aligned}\right\}\tag{5}$$

Finally, after carrying out calculations similar to those in [1], we obtain the following expression for the fast-neutron flux:

$$\left.\begin{aligned}\varphi_{1c}(r,z)&=\int_0^{\infty}\frac{1}{\zeta_{1c}}\left[\frac{Q}{4\pi}e^{-\zeta_{1c}|z|}+\right.\\ &\left.+2\pi\gamma_{1c}(\eta)\,e^{-\zeta_{1c}|z-a|}\right]J_0(\eta r)\,\eta\,d\eta,\\ \varphi_{1r}(r,z)&=2\pi\int_0^{\infty}\gamma_{1r}(\eta)\frac{e^{-\zeta_{1r}|z-a|}}{\zeta_{1r}}J_0(\eta r)\,\eta\,d\eta,\end{aligned}\right\}\tag{6}$$

where

$$\left.\begin{aligned}\gamma_{1c}(\eta)&=\frac{Q}{8\pi^2}\frac{D_{1c}\zeta_{1c}-D_{1r}\zeta_{1r}}{D_{1c}\zeta_{1c}+D_{1r}\zeta_{1r}}e^{-\zeta_{1c}a},\\ \gamma_{1r}(\eta)&=\frac{Q}{8\pi^2}\frac{2D_{1c}\zeta_{1r}}{D_{1c}\zeta_{1c}+D_{1r}\zeta_{1r}}e^{-\zeta_{1c}a},\\ \zeta_{il}&=\left|\sqrt{\eta^2+\varkappa_{il}^2}\right|.\end{aligned}\right\}\tag{7}$$

The slow-neutron flux expressions are of the form:

$$\left.\begin{aligned}\varphi_{2c}(r,z)&=\int_0^{\infty}\left\{\frac{\varkappa_{12c}^2}{\varkappa_{2c}^2-\varkappa_{1c}^2}\frac{1}{\zeta_{1c}}\left[\frac{Q}{4\pi}e^{-\zeta_{1c}|z|}+\right.\right.\\ &\left.+2\pi\gamma_{1c}(\eta)\,e^{-\zeta_{1c}|z-a|}\right]+\\ &\left.+2\pi\gamma_{2c}(\eta)\frac{1}{\zeta_{2c}}e^{-\zeta_{2c}|z-a|}\right\}J_0(\eta r)\,\eta\,d\eta,\\ \varphi_{2r}(r,z)&=\int_0^{\infty}\left\{\frac{\varkappa_{12r}^2}{\varkappa_{2r}^2-\varkappa_{1r}^2}\frac{1}{\zeta_{1r}}2\pi\gamma_{1r}(\eta)\,e^{-\zeta_{1r}|z-a|}+\right.\\ &\left.+2\pi\gamma_{2r}(\eta)\frac{1}{\zeta_{2r}}e^{-\zeta_{2r}|z-a|}\right\}J_0(\eta r)\,\eta\,d\eta,\end{aligned}\right\}\tag{8}$$

where

$$\left.\begin{aligned}\gamma_{2c}(\eta)&=\frac{Q}{4\pi^2}\frac{\zeta_{2c}e^{-\zeta_{1c}a}}{(D_{1c}\zeta_{1c}+D_{1r}\zeta_{1r})\,(D_{2c}\zeta_{2c}+D_{2r}\zeta_{2r})}\times\\ &\times\left\{\frac{\varkappa_{12c}^2}{\varkappa_{2c}^2-\varkappa_{1c}^2}(D_{2c}D_{1r}\zeta_{1r}-D_{1c}D_{2r}\zeta_{2r})+\right.\\ &\left.+\frac{\varkappa_{12r}^2}{\varkappa_{2r}^2-\varkappa_{1r}^2}D_{1c}D_{2r}(\zeta_{2r}-\zeta_{1r})\right\},\\ \gamma_{2r}(\eta)&=\frac{Q}{4\pi^2}\frac{\zeta_{2r}e^{-\zeta_{1c}a}}{(D_{1c}\zeta_{1c}+D_{1r}\zeta_{1r})\,(D_{2c}\zeta_{2c}+D_{2r}\zeta_{2r})}\times\\ &\times\left\{\frac{\varkappa_{12c}^2}{\varkappa_{2c}^2-\varkappa_{1c}^2}D_{2c}(D_{1r}\zeta_{1r}+D_{1c}\zeta_{2c})-\right.\\ &\left.-\frac{\varkappa_{12r}^2}{\varkappa_{2r}^2-\varkappa_{1r}^2}D_{1c}(D_{2c}\zeta_{2c}+D_{2r}\zeta_{1r})\right\}.\end{aligned}\right\}\tag{9}$$

Eq. (8), together with Eqs. (7) and (9), yields thermal-neutron distribution over the entire space.

Only one of the integrals which appears in Eq. (8) can be calculated analytically:

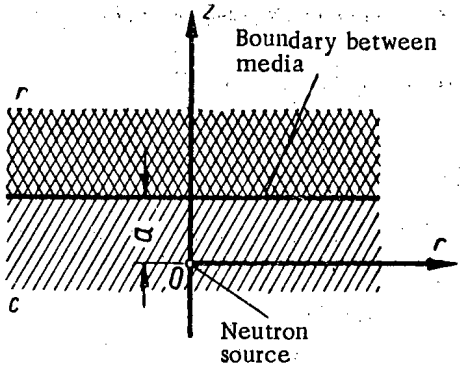

Diagram showing the arrangement of the neutron source and the boundary between the media.

$$\int_0^\infty \frac{e^{-\zeta_{1c}|z|}}{\zeta_{1c}} J_0(\eta r)\,\eta\,d\eta = \frac{1}{\sqrt{r^2+z^2}}\,e^{-\varkappa_{1c}\sqrt{r^2+z^2}}$$

The remaining integrals can be found by numerical methods for each individual case.

The application of these results to the theory of neutron logging will be considered elsewhere.

The authors are indebted to A. E. Glauberman for a discussion of this work.

Received November 21, 1957

LITERATURE CITED

[1] A. E. Glauberman and I. I. Tal'ianskii, J. Atomic Energy 3, 23 (1957).*

[2] Glasstone and Edlund, Fundamentals of Nuclear Reactor Theory (Russian translation) I.L. 1954.

*Original Russian pagination. See C. B. Translation.

MEAN NUMBER OF NEUTRONS EMITTED IN U^{235} FISSION INDUCED BY 14.8-Mev NEUTRONS

A. N. Protopopov and M. V. Blinov

Method

A determination of the mean number ν of prompt neutrons emitted, in a fission event by various isotopes of uranium and plutonium is of considerable interest, both from the point of view of nuclear energy considerations and from that of understanding of the fission process itself. As the energy of the neutrons which induce fission is increased, the measurement of ν becomes more and more complicated. Among the factors which make such measurements difficult are the effect of secondary neutrons in (n, n), (n, 2n) and (n, 3n) reactions and the large background due to primary neutrons.

The use of a coincidence method, in which coincidences are recorded between fragments and neutrons, creates the most favorable conditions for excluding detection of neutrons which do not arise in the fission process itself. Such a method has been developed by Kalashmikov, Lebedev and Spivak [1] for measuring ν in U^{233}, U^{235} and Pu^{239} fission induced by neutrons with energies characteristic of a fission spectrum. The detectors used by the authors in Ref. [1] were several boron counters located in a paraffin block. The resolving time of the coincidence circuit was $2 \cdot 10^{-4}$ sec. In cases in which measurements of ν are made in a fast-neutron flux in which the background is large, it is necessary to reduce the resolving time of the coincidence circuit, and the use of boron counters in paraffin becomes impossible.

In the present paper measurements have been made of ν for U^{235} fission induced by 14.8-Mev neutrons. The neutron detector was insensitive to γ-rays, had almost constant efficiency over the entire fission-neutron spectrum [2], [3], and also could be used with a fast coincidence circuit; this detector was an ionization chamber with a layer of U^{235} applied to the high-voltage electrode. Since this detector has a very low efficiency, it was necessary to keep it as close as possible to the chamber used to detect fission fragments. In practice, both chambers were combined into one double ionization chamber on the high-voltage electrode of which were placed two identical layers of U^{235}. The layers were deposited on discs of thin aluminum foil which were held from the back. Each chamber served as a detector for primary fission events and as a detector for neutrons originating in fission events which took place in the other chamber.

The number of coincidences for fission fragment pulses when the chamber is placed in a neutron flux is given by

$$N_C = N_1 \nu \varepsilon_2 + N_2 \nu \varepsilon_1 = N_1 \nu \varepsilon_2 \left(1 + \frac{N_2}{N_1} \frac{\varepsilon_1}{\varepsilon_2}\right), \quad (1)$$

where N_1 is the number of recorded fission events in the layer in the first chamber; ϵ_2 is the detection efficiency in the second channel for a neutron emitted in fission induced by primary neutrons in the layer in the first chamber; and N_2 and ϵ_1 have corresponding values. The primary neutron flux is the same on both uranium layers, so that $(N_2/N_1)(\epsilon_1/\epsilon_2) = 1$ whence, from Eq. (1) we have

$$\nu = \frac{N_C}{2N_1\varepsilon_2}. \quad (2)$$

The mean number of neutrons emitted in a single U^{235} fission event induced by 14.8-Mev neutrons was measured with respect to the mean number of neutrons emitted in thermal-neutron-induced fission. From Eq. (2) we have

$$\frac{\nu}{\nu^T} = \frac{\frac{N_c}{N_1}}{\frac{N_c^T}{N_1^T}} \frac{\varepsilon_2^T}{\varepsilon_2} \tag{3}$$

(quantities relating to thermal-neutron fission are denoted by the superscript "T").

The chamber was first exposed in a flux to 14.8-Mev neutrons and then in a thermal-neutron flux. In both cases a determination was made of the ratio of the number of coincidences to the number of fission events in one channel. In calculating the ratio ν/ν^T, in addition to the experimentally determined quantities N_c/N_1, one must determine the efficiency ratio. This quantity is not fixed because of the differences in the fragment angular distribution [4], which result in a difference in the fission-neutron distribution. Inasmuch as the ratio ϵ^T/ϵ is very close to unity, it is not necessary to compute the absolute value of the efficiencies and only an estimate of the ratio is sufficient.

Apparatus and Experimental Conditions

In order to increase the fission-neutron detection efficiency the uranium layers were made fairly thick (~ 2 mg/cm^2). The layers were prepared by precipitation from a suspension of U_3O_8 powder in alcohol and were deposited on aluminum foil 0.1 mm thick. The uranium contained 97.5% U^{235}. The diameter of the uranium targets was 20 mm. The distance between the high-voltage electrode and each collector electrode was 2.5 mm. The chamber was filled with a mixture of highly purified argon (97%) and CO_2 (3%) at atmospheric pressure.

TABLE

Results of the Measurements

Neutrons	Number of fragments, N_1	Number of coincidences, N_c	Number of accidental coincidences, N_{ac}	Number of true coincidences, N_{tc}	$\frac{N_{tc}}{N_1} 10^5$	$\frac{N_{tc}}{N_1} : \frac{N_{tc}^T}{N_1^T}$
14.8 Mev	327 059×64	1427	382	1045	5,00	1,83±0,13
Thermal	407 727×64	1137	423	714	2,73	

After amplification and shaping, the pulses, 0.4 microseconds in width, were fed to a coincidence circuit with a resolving time of $1 \pm 0.05) \cdot 10^{-7}$ sec. The resolving time was checked periodically during the course of the experiment. With a counting rate for true coincidences of 10-15 pulses/hour, the background of random coincidences was less than 30-50%.

The neutrons used to irradiate the uranium were obtained from an accelerator, using the T^3 (d, n) He^4 reaction by bombarding a thick tritium-zirconium target with 175-kev deuterons. The total neutron flux was kept at a level of $(1\text{-}2) \cdot 10^9$ neut/sec throughout measurement; this flux corresponds to a counting rate of 3000 to 6000 pulses/sec in the channels.

In making the fast-neutron measurements the chamber was set up along the axis of the deuteron beam in such a way that the uranium layers were perpendicular to the incident beam of 14.8-Mev neutrons at a distance of 5.5 cm from the tritium target. Under these conditions the neutron flux over the area of the uranium layers was uniform within 4%. The chamber was covered by cadmium to provide shielding against thermal neutrons. Under these conditions the background due to fissions caused by scattered neutrons is 3%.

In carrying the thermal-neutron measurements the chamber was placed at a distance of 30 cm from the target. The chamber and target were surrounded by paraffin. The uranium layers were shielded against the fast-

neutrons beam by a lead cylinder 20 cm in length. Using this arrangement the number of fission events caused by supercadmium neutrons was less than 5%.

Results

The results of the measurements are shown in the table. In order to obtain the relative number of neutrons ν/ν^T, in accordance with Eq. (3) it is necessary to multiply the experimental value of the ratio $N_c/N_1 : N_c^T/N_1$ which appears in the last column of the table by the efficiency ratio ϵ^T/ϵ. Taking account of the anisotropy in the distribution of fission fragments in U^{235} fission induced by 14.8-Mev neutrons, the efficiency ratio may be estimated as 1.04 ±0.02. Then we find that ν/ν^T is 1.90 ±0.17. However, certain corrections must be introduced.

First of all account must be taken of the effect of background fission events due to scattered neutrons in the fast-neutron measurements. Using the data reported by Leachman [5], the background due to scattered-neutron fission events increases ν/ν^T by 1.4%. In the thermal-neutron experiments no correction was made for the supercadmium neutrons because of the small change in ν for small increases in neutron energy.

It is also necessary to introduce a correction to take account of the error which has been introduced earlier in Eq. (2) by assuming that $\frac{N_2}{N_1}\frac{\epsilon_1}{\epsilon_2} = 1$. The quantity N_2/N_1 is equal to the efficiency ratio for the chambers for 14.8-Mev neutrons while ϵ_1/ϵ_2 is the efficiency ratio for neutrons characteristic of a fission spectrum. In practice these ratios are not the same, since the channel efficiencies vary in different ways as the neutron energy is varied, because of the thick uranium targets and variations in the channel parameters. This effect leads to a 1.5% reduction in ν/ν^T.

No corrections were introduced to take account of a possible difference in the secondary-neutron spectra. The errors associated with this effect are certainly less than 1%. Also, no correction was introduced to take account of nonuniformities in the thickness of the uranium layers. In view of the uniformity of the thermal-neutron flux and the fast-neutron flux over the surface of the layers, and the fact that only relative measurements were made, this correction should be less than 1%. The effect of any apparatus instability was kept to a minimum by making alternate measurements. No corrections were introduced to take account of apparatus instability.

Taking account of all corrections we find $\nu/\nu^T = 1.90 \pm 0.18$. Using the value $\nu^T = 2.47 \pm 0.03$ [6], we find that ν in U^{235} is 4.7 ± 0.5 for fissions induced by 14.8-Mev neutrons. The error in ν is determined basically by the statistical errors in the measurements.

In Refs. [5, 7 and 8] it has been noted that the experimental values for ν for fast neutrons are in good agreement with the calculations carried out by Fowler (cf. [5]) for a fragment excitation temperature T = 1.4 Mev. If the calculated curves are extrapolated [5] to the value E_n = 15 Mev, as has been done in the survey made by Erozolimski [7], good agreement with the results of the present work and Fowler's calculations is obtained with T = 1 Mev.

In conclusion we wish to express our gratitude to I. A. Baranov and Iu. I. Belianin for operation of the accelerator and to L. I. Radaev for other help.

Received July 8, 1957

LITERATURE CITED

[1] Kalashnikova, Lebedev and Spivak, J. Atomic Energy 2, 18 (1957).*

[2] D. J. Hughes, J. A. Harvey, Neutron Cross Sections, (McGraw-Hill Co., N. Y., 1955).

[3] G. A. Dorofeev and Iu. P. Dobrynin, J. Atomic Energy 2, 10 (1957).*

[4] J. E. Brolley, W. C. Dickinson, R. L. Henkel, Phys. Rev. 99, 159 (1955).

[5] B. B. Leachman, Phys. Rev. 101, 1005 (1956).

[6] D. J. Hughes, R. B. Schwartz, Neutron Cross Sections, BNL-325, Suppl. 1, BNL, 1957.

[7] B. G. Erozolimskii, Supp. No. 1, J. Atomic Energy (1957) p. 74; N. A. Vlasov, J. Atomic Energy 1, 99 (1956).*

[8] P. A. Egelstaff, Atomics and Nuclear Energy 8, No. 1, 21 (1957).

* Original Russian pagination. See C. B. Translation.

PREPARATION OF STABLE LAYERS OF URANIUM, NEPTUNIUM, PLUTONIUM AND AMERICIUM BY ELECTROLYTIC DEPOSITION

G. I. Khlebnikov and E. P. Dergunov

A number of investigations in nuclear physics, in cyclotrons and other equipment, require relatively thin (from 0.1 to 0.4 mg/cm^2) layers (targets) of various chemical elements, among them uranium, neptunium, plutonium and americium. Besides mechanical stability, these targets must withstand long periods of bombardment with intense beams of heavy charged particles (N^{14}, C^{12}, $O^{16, 18}$) as well as sharp changes in the temperature: from room to 500-700°C.

There are several methods known for preparing thin layers: electrolytic, cathode sputtering, deposition with organic bonding agents, etc. The electrolytic method is the most widely used in practice.

A substantial difficulty in the electrolytic preparation of stable layers of uranium and transuranium elements is that the elements are deposited on the cathode in the form of a hydroxide of complex composition and not as the metal.

The conditions described in the literature for preparing electrolytic deposits have a series of disadvantages. They do not ensure a quantitative yield of the element [1]-[3], [5], [7] or do not form sufficiently stable layers [4], [6].

The preparation of the starting compounds – anhydrous chlorides ($PuCl_3$, etc.) [3] – is a complicated problem.

In this work we chose the best electrolysis conditions for obtaining high yields of the elements in very stable thin layers. The electrodeposition can be carried out from nitric acid and hydrochloric acid solutions of the element in any valence state.

This article gives practical details for preparing the layers.

As is known, in electrolysis from aqueous solutions, the most stable layers are obtained by adding complexing agents to the electrolyte [5], [7]. We used ammonium oxalate dissolved in water (0.05-0.07 M) and, in some experiments, formic acid as the complexing agents. The electrolyzers used in the work were similar to those described in the literature [5], [6].

To prepare 0.5 × 1.2 cm targets with a layer thickness of 0.15-0.25 mg/cm^2, an ammonium oxalate solution (1.5-2.0 cc) was placed in an electrolysis vessel in which the distance between the electrodes was equal to 1.5-2.0 cm. Then a nitric acid or hydrochloric acid solution (~0.2 cc) with the element to be electrolyzed (U^{+6}, Np^{+4}, Pu^{+4}) was added with careful stirring, in a sufficient amount to give the required layer. The pH of the solution was brought to 8-9 with several drops of concentrated NH_4OH.

The electrolysis was carried out at room temperature and a cathode current density of 100-150 ma/cm^2. Changes in the current density within this range did not affect the yield of the element or the quality of the layer. With higher current densities the hydroxide layer became very uneven and friable. With lower current densities the yield of the element became low even after prolonged electrolysis. Regardless of the initial amount of element (calculated for a layer not greater than 0.4 mg/cm^2), after 2-2.5 hours about 50% of it separated on the cathode and after 5-6 hours it had deposited quantitatively (95-98%).

Numerous experiments showed that an increase in the electrolysis time to 12-14 hours resulted in the formation of a dense, stable layer and a fuller yield of the element (99-99.5%).

There was intense gas evolution at the given cathode current density so that a revolving anode or special mixing of the electrolyte was unnecessary.

After the experiment the electrolyte was removed with a pipette, the target washed twice with distilled water (free from CO_2) with ammonia added, and dried in air at room temperature for 2-3 hours. This stage of prolonged drying was especially important for the preservation and strengthening of the layer. Then the target was dried in a drying cupboard at 80°C or in a desiccator. If the material of the backing was suitable, the target could be fired to produce the oxides of the corresponding elements.

The stability of the target was tested by rubbing the layer with a dry cotton pad. With a layer thickness of about 0.2 mg/cm^2, the decrease in weight was 5-10%.

The yield of material on the cathode was found by weighing the target and by measuring the α-activity of the electrolyte layer and the wash water. Nickel, platinum, aluminum and copper alloys in the form of a foil of 2.5 μ to 1 mm thickness were used as cathode materials. The cathodes of aluminum and copper and its alloys were found to be unstable in the electrolyte used (pH 8-9). A thick foil had to be used, the pH lowered to ~7, and the electrolysis time reduced to 2-3 hours, without attempting to reach complete deposition, when using aluminum or copper cathodes.

The anodes were made of platinum, graphite and nickel. Under the conditions developed by us for the electrolysis, the graphite crumbled due to the oxidizing process that occurred at the anode. A diaphragm, made of No. 3 glass filter, had to be used in experiments with a graphite anode.

Before the electrolysis the cathode, anode and electrolyzer were degreased with alcohol, benzene or trichlorethylene; this considerably improved the quality of the layer (increased the evenness, stability and yield of element).

An oxalate electrolyte could not be used in preparing thin americium layers due to the formation of insoluble americium oxalate. We therefore used an electrolyte consisting of a hydrochloric or nitric acid solution of americium in 0.2 M formic acid and 0.2 M ammonium formate [8].

The electrolysis was carried out for 3.5 hours with the initial medium pH equal to 3, the cathode current density 100-150 ma/cm^2, and t = 20°C. The materials used for the electrodes were platinum (anode) and nickel and platinum (cathode). The conditions of treatment of the cathode deposit were similar to those described for the oxalate electrolyte. The experiments showed that in the use of an electrolyte containing formic acid, a considerably more stable layer was formed than that obtained from an alcohol–acetone mixture [4].

From the formic acid electrolyte in addition to americium, we obtained quite good layers of plutonium and neptunium hydroxides with the conditions described above.

We should note that for uranium, neptunium, plutonium and americium, the stable layers obtained in one stage were not thicker than 0.4 mg/cm^2. Quantitative deposition was attained if the starting concentration of the element was such that the layer thickness would not exceed 0.4 mg/cm^2. This was established in numerous experiments with different starting concentrations of the elements examined.

Received November 27, 1957

LITERATURE CITED

[1] L. Koch, J. Nucl. Energy, No. 2, 110 (1955).

[2] H. Diamand, P. R. Fields, J. Mech, M. G. Inghram, D. C. Hess, Phys. Rev. 92, 1490 (1953).

[3] A. Glass, Studies in the Nuclear Chemistry of Plutonium, Americium and Curium and the Masses of the Heaviest Elements, Univers. Calif. Res. Labor. 1954, p. 25.

[4] V. B. Dedov, V. N. Kosiakov, Investigations in the Fields of Geology, Chemistry and Metallurgy (Reports of the Soviet Delegation at the International Conference on Peaceful Uses of Atomic Energy) (Acad. Sci. USSR Press, 1955) p. 250.

[5] D. L. Hufford, B. F. Scott, The Transuranium Elements, Ed. by G. Seaborg, part II (1949) p. 1149.

[6] G. N. Iakovlev, P. M. Chulkov, V. B. Dedov, V. N. Koslakov, Iu. P. Sobolev, Atomic Energy I, 5, 131 (1956).*

[7] K. Kasto, Analytical Chemistry of Uranium and Thorium, (For. Lit. Press, 1956) p. 327 [Russian translation].

[8] Roy Ko, Nucleonics 14, No. 7, 74 (1956).

* Original Russian pagination. See C.B. Translation.

THE NUMBER OF ISOTOPIC MOLECULES IN SIMPLE AND COMPLEX SUBSTANCES AND THEIR CONCENTRATIONS

I. G. Petrenko

In the study of various physical and chemical processes using stable isotopes and in exact and rapid analyses of complex gas mixtures, various types of mass spectrometers are used very frequently and their main operating principle is based on the separation of the components of the gas mixture by their molecular weight. In connection with this it seemed very interesting to develop a method of calculating the number of isotopic molecules and their concentrations (without considering the isotope effect) in simple and complex chemical substances.

A study of the molecular isotopic composition of simple and complex substances is valuable both theoretically and practically, for example in mass-spectrometric investigations, molecular spectroscopy, problems of isotope separation etc. However, the literature does not give any methods for calculating the molecular isotopic composition of various substances.

The basic principles of mathematical statistics may be used for solving the problem of the number of isotopic molecules in the composition of any simple or complex substance.

Investigations showed that the total number of isotopic molecules N_i of any simple substance may be established using the method of combinations [1]:

$$N_i = \frac{(n+m-1)!}{n!\,(m-1)!}. \tag{1}$$

The number of isotopic molecules of complex organic and inorganic compounds may be determined using the equation

$$N_i = \frac{(n_1+m_1-1)!}{n_1!\,(m_1-1)!}\,\frac{(n_2+m_2-1)!}{n_2!\,(m_2-1)!}\cdots\frac{(n_i+m_i-1)!}{n_i!\,(m_i-1)!}\cdots$$
$$\cdots=\prod_i \frac{(n_i+m_i-1)!}{n_i!\,(m_i-1)!}, \tag{2}$$

where n is the number of atoms of the given element in the composition of a molecule, m is the number of isotopes in the composition of the given element.

The number of terms in Equation (2) is limited by the number of elements in the molecular composition of the substances being studied.

The stable isotope content of elements varies from one to ten, but is not greater than four for most of the elements. The number of atoms of different elements in the composition of an inorganic compound is also relatively small and usually does not exceed ten. Organic molecules may consist of a large number of carbon and hydrogen atoms, but these elements have only two stable isotopes each.

Equation (2) may be simplified considerably for calculating the number of isotopic molecules in separate classes of complex compounds. Thus, for example, Equation (2) would become

$$N_i=(n_1+1)\,(n_2+1) \tag{3}$$

TABLE 1

The Number of Isotopic Molecules in Some Simple and Complex Substances

Substance	H_2	O_2	CO	CO_2	H_2O	SO_2	SO_3	CH_4	C_2H_6	C_6H_6	C_2H_6O	H_2SO_4
Number of isotopic molecules	3	6	6	12	9	24	40	10	21	49	63	180

TABLE 2

Isotopic Molecules of Carbon Monoxide and Dioxide and Their Concentrations

CO \ A	28	29	30	31	Σn_2	Σc_2, %
$C^{13}O$	$C^{12}O^{16}$ 98,654	$C^{12}O^{17}$ $3,659 \cdot 10^{-2}$	$C^{12}O^{18}$ $2,017 \cdot 10^{-1}$		3	98,892
$C^{13}O$		$C^{13}O^{16}$ 1,105	$C^{13}O^{17}$ $4,099 \cdot 10^{-4}$	$C^{13}O^{18}$ $2,26 \cdot 10^{-3}$	3	1,108
Σn_1	1	2	2	1	6	
Σc_1, %	98,654	1,142	$2,021 \cdot 10^{-1}$	$2,26 \cdot 10^{-3}$		100,000

CO_2 \ A	44	45	46	47	48	49	Σn_2	Σc_2, %
$C^{12}O_2$	$C^{12}O_2^{16}$ 98,416	$C^{12}O^{16}O^{17}$ $7,3 \cdot 10^{-2}$	$C^{12}O^{16}O^{18}$ $4,025 \cdot 10^{-1}$ $C^{12}O_2^{17}$ $1,354 \cdot 10^{-5}$	$C^{12}O^{17}O^{18}$ $1,493 \cdot 10^{-4}$	$C^{12}O_2^{18}$ $4,115 \cdot 10^{-4}$		6	98,892
$C^{13}O_2$		$C^{13}O_2{}^{16}$ 1,103	$C^{13}O^{16}O^{17}$ $8,179 \cdot 10^{-4}$	$C^{13}O^{16}O^{18}$ $4,509 \cdot 10^{-3}$ $C^{13}O_2^{17}$ $1,517 \cdot 10^{-7}$	$C^{13}O^{17}O^{18}$ $1,673 \cdot 10^{-6}$	$C^{13}O_2{}^{18}$ $4,611 \cdot 10^{-6}$	6	1,108
Σn_1	1	2	3	3	2	1	12	
Σc_1, %	98,416	1,176	$4,034 \cdot 10^{-1}$	$4,658 \cdot 10^{-3}$	$4,132 \cdot 10^{-4}$	$4,611 \cdot 10^{-6}$		100,000

for a large number of aliphatic and aromatic compounds with the general formula of $C_{n_1}H_{n_2}$.

Thus, in using Equation (2) practically no supplementary calculation methods are required, as it is simplified due to the fact that the values of n and m are usually limited to the first ten natural numbers and that these terms are reduced to numerators and denominators.

As an example, Table 1 gives the number of isotopic molecules of simple and complex substances.

The mass numbers of the isotopic molecules of complex substances vary over a much smaller range. Therefore, isotopic molecules form isotopic groups, whose number is determined by the limit within which the mass

TABLE 3

Isotopic Molecules of Methane and Their Concentrations

CH_4 \ A	16	17	18	19	20	21	Σn_2	Σc_2, %
$C^{12}H_4$	$C^{12}H_4^1$ 98,835	$C^{12}H_3^1H^2$ $5,733 \cdot 10^{-2}$	$C^{12}H_2^1H_2^2$ $1,247 \cdot 10^{-5}$	$C^{12}H^1H_3^2$ $1,206 \cdot 10^{-9}$	$C^{12}H_4^2$ $4,371 \cdot 10^{-14}$		5	98,892
$C^{13}H_4$		$C^{13}H_4^1$ 1,107	$C^{13}H_3^1H^2$ $6,424 \cdot 10^{-4}$	$C^{13}H_2^1H_2^2$ $1,397 \cdot 10^{-7}$	$C^{13}H^1H_3^2$ $1,351 \cdot 10^{-11}$	$C^{13}H_4^2$ $4,898 \cdot 10^{-16}$	5	1,108
Σn_1	1	2	2	2	2	1	10	
Σc_1, %	98,835	1,164	$6,549 \cdot 10^{-4}$	$1,409 \cdot 10^{-7}$	$1,355 \cdot 10^{-11}$	$4,898 \cdot 10^{-16}$		100,000

numbers of isotopic molecules of the given substance vary and is established by the use of the simple equation

$$N = \sum_i (A_n - A_1)_i \, n_i + 1, \tag{4}$$

where A_n and A_1 are the mass numbers of the limiting isotopes of the given element in the composition of a complex substance's molecule.

This equation is applicable to a large number of cases.

It is also very important to be able to establish by calculation the concentration of the isotopic molecules of simple and complex compounds. In order to establish the concentration of the isotopic molecules of any simple substance by calculation (without considering the isotope effect), the following equation of polynomial analysis may be used [2]:

$$(\theta_1 + \theta_2 + \ldots + \theta_m)^n. \tag{5}$$

In order to calculate the concentration of isotopic molecules of complex inorganic and organic substances, the following equation is used:

$$(\theta_{11} + \theta_{12} + \ldots + \theta_{1m})^{n_1} (\theta_{21} + \theta_{22} + \ldots + \theta_{2m})^{n_2} \ldots \ldots (\theta_{i1} + \theta_{i2} + \ldots + \theta_{im})^{n_i} \ldots = \prod_i (\theta_{i1} + \theta_{i2} + \ldots + \theta_{im})^{n_i}, \tag{6}$$

where n is the number of atoms of the element in the composition of the molecule, θ is the concentration of isotopes of the given element in the composition of the molecule, expressed in fractions, i.e., $\theta_{i1} + \theta_{i2} + \ldots + \theta_{im} = 1$. The number of factors in Equation (6) corresponds to the number of elements in the composition of the given compound and the number of integrated terms in each factor corresponds to the number of isotopes of the given element.

On solving the polynomials (5) and (6), we obtain magnitudes which characterize the concentrations of isotopic molecules, expressed as fractions of unity.

The calculations are based on the latest data [3] on the concentration of isotopes in chemical elements. As examples, Tables 2 and 3 give the isotopic molecules of carbon monoxide and dioxide and of methane and their concentrations; the isotopic molecules are divided into groups (vertical columns) and classes (horizontal columns). The isotopic groups include all the isotopic molecules which have equal mass numbers (A), while the classes include all the isotopic molecules which have the same elemental isotope. The tables also give the concentrations of isotopic molecules (without considering the isotope effect), the number of isotopic molecules by groups and by classes (Σn), and their total concentration (Σc).

If the molecule of the complex compound being investigated includes only one atom of one of the elements, then the total concentrations of the isotopic molecules of each class (Σc_2) will correspond exactly with the concentrations of the isotopes of the given element. This may be seen in the tables given.

When complex substances are formed under natural conditions at a very low temperature, they become enriched in one of the isotopes due to the influence of the isotope effect. It seems to us that the calculated value for the concentration of isotopic molecules, obtained for the balanced stationary distribution of isotopes, could be the basis for characterizing the enrichment of a complex substance with one or another isotope.

Received June 26, 1957

LITERATURE CITED

[1] J. Meyer and M. Heppert-Meyer, Statistical Mechanics, (Foreign Lit. Press, 1952) [Russian translation].

[2] A. Khaĭd,* Mathematical Statistics with a Technical Application, (Foreign Lit. Press, 1956) [Russian translation].

[3] G. Seaborg, I. Perlman and J. Hollender. Table of the Isotopes, (Foreign Lit. Press, 1956) [Russian translation].

*Transliteration of Russian— Publisher's note.

APPLICATION OF RADIOACTIVE INDICATORS TO THE SOLUTION OF THE PROBLEM OF INTERNAL ADSORPTION IN SOLIDS

V. I. Arkharov, S. M. Klotsman and A. N. Timofeev

One of the most important factors affecting the physical properties of technical materials is the internal adsorption of certain impurities at various structural inhomogeneities [1-3]. The excess energies of these latter (as compared with regions of the undistorted crystal lattice) are partially lowered by the production at these places of nonuniform concentrations of certain soluble impurities. This effect appears most strongly for sufficiently large differences of the orientations of crystallites meeting each other at joints (boundaries) between crystallites. The enrichment of the transition zones between the crystallites with soluble adsorption-active ("horophilous") impurities has important consequences, particularly in cases in which, because of temperature changes that are not sufficiently gradual, the concentration of the horophilous impurities in the adsorption zones does not have time to follow these changes, and a local supersaturation of the solid solution occurs in the adsorption zones. The local disintegration that occurs on this account causes a situation in which the polycrystalline alloy has running through it very thin interstitial layers which lie along the grain boundaries and have decidedly altered properties. This evidently provides the explanation of many cases of the appearance of intercrystallite brittleness of alloys [4-6].

For practical purposes it is important to make detailed studies of the phenomenon of internal adsorption. The zones of altered concentration, however, are very thin (according to indirect estimates their maximum thickness is some hundreds of Angstroms), and it is very hard to study them.

It is natural to use the method of marked atoms for the solution of this problem. Direct observation of the effect of intercrystallite internal adsorption by the method of autoradiography does not, however, turn out to be very easy, since the thicknesses of the enriched layers are so small.

As is shown by qualitative considerations and special calculations [7], the detection of the effect requires the existence of definite relations between the increase of concentration of the active constituent in the adsorption zones and the scattering of its radiation, which depends on the energy of the radiation and the properties of the main constituents of the alloy. When these conditions are unfavorable, the effect "washes out" and will not be detected. For example, in the optimal case of the adsorption of Po^{210} (which emits α-particles of energy about 5 Mev) in an alloy based on lead, the maximum width of the blackened region is 43 μ [8].

Therefore, the first work done in our laboratory had as its purpose not the direct detection of adsorption irregularities in the distribution of "marked" impurities in polycrystalline alloys, but the study of internal adsorption through a secondary effect – its influence on the degree of abruptness of the intercrystallite diffusion of the indicator constituent in the alloy. In carrying out such studies by ordinary metallographic methods it was noted, for example, that the diffusion of silver into copper with small amounts of admixed antimony gives an irregular front with salients reaching far into the copper along the boundaries between the crystallites [9-12]. Since it was also found that in solid solutions of antimony in copper with large concentrations of antimony the volume diffusion of silver is considerably more rapid than for silver diffusing into pure copper, it was assumed that the metallographic pattern found for the diffusion front of silver in an alloy of copper with a small amount of antimony is due to adsorption of the antimony between the crystallites.

When an autoradiographic study was made [13], it confirmed the results previously obtained by the metallographic method: when a small amount of antimony is present in the copper the diffusion of silver from the outside into such an alloy gives a front which reaches far into the copper along the grain boundaries, with intrusions much more sharply marked than in the diffusion of silver into pure copper.

It must be remembered, however, that the autoradiographic picture of the diffusion (like that obtained by metallography) does not reproduce in its pure form the effects arising from the joints between the crystallites (the transition zones), since it is complicated by the effect of "lateral" diffusion into the grains, in directions normal to the zones between the crystallites, which gives a broadening of the wedge-shaped intrusions on the diffusion front. If the diffusion along the actual boundaries between the crystallites run definitely ahead of the volume diffusion front (i.e., the diffusion through the volume of each grain), then the wedges detected in autoradiographic or metallographic studies are formed through both true intercrystallite diffusion and also lateral diffusion, which is essentially a volume effect, the same as goes on on the main parts of the front, which pass through the interiors of grains. Furthermore, the first of these contributing effects, that associated with the narrow boundary between grains, is not accessible to direct observation by autoradiographic or metallographic methods, and is not manifested separately from the second effect.

The possibility of autoradiographic detection of salients on the diffusion front depends on the ratio of the coefficients of volume and intercrystallite diffusion.

A more detailed study of the effect of internal adsorption on intercrystallite diffusion can be made by calculations based on a model proposed by Fisher [14]. The basic quantity which must be obtained from experiment is the total amount of the diffusing component with the radioactive indicator which penetrates during a given time of diffusion to a depth y from the surface of the specimen. This quantity is proportional to the specific radioactivity i, measured at different depths by grinding off successive layers from the specimen.

In the case in which intercrystallite diffusion predominates, as compared with volume diffusion, $\ln i$ is a linear function of y, and the slope of the straight line $\ln i = ky$ gives the quantity $D_{vol}^{1/2}/\delta D_{gr}$, where D_{vol} is the coefficient of volume diffusion, D_{gr} is that of intercrystallite diffusion, and δ is the effective thickness of the transition zone between two neighboring crystallites.

Radiometric studies [15, 16] have shown that in the diffusion of Ag^{110} into pure copper or into copper containing a small amount of antimony or beryllium there is a linear relation between $\ln i$ and y. Control experiments with single crystals of copper and of an alloy of copper with 0.4% antimony showed that there is little difference between the coefficients of volume diffusion in the two cases (because of the small concentration of antimony). From this it follows that admixture of antimony or beryllium causes considerable changes of the diffusion permeability of the zones between crystallites (δD_{gr}), which indicates the presence of an effect of internal adsorption of the impurity. Here an important fact was brought to light: addition of antimony decreases the value of δD_{gr} in copper. At first sight such a result is in contradiction with the metallographic and autoradiographic data. One must, however, remember the complex origin of the metallographic and radiographic pictures of the diffusion front, in which the actual penetration of the diffusing element along the true intercrystallite zone escapes observation (because of the extremely small value of δ).

According to metallographic data, large concentrations of beryllium slow down the volume diffusion of silver into copper. According to the radiometric data, an admixture of 0.1% beryllium considerably alters the value of δD_{gr} in copper, which indicates that the beryllium is internally adsorbed at the joints between crystallites. Also, there is an increase of the rate of intercrystallite diffusion of silver.

It must be remarked that although the model taken as the basis for Fisher's method gives an improved approximation for the separate estimates of the diffusion in the joints between crystallites and that through the actual grains themselves (in the regular lattice), it still uses a very simplified concept of the intercrystallite zone as a layer of definite thickness, sharply distinguished from the grains themselves and differing discontinuously from them in its value of D. Actually, however, this zone merges continuously with the two grains between which it lies, and in it there is a smooth transverse gradient of the lattice distortions, and also of the value of D and the concentration of the adsorbed impurity. Therefore, the speed of diffusion in the intercrystallite zone can change in a complicated way under the influence of adsorption of an impurity; in the central, most distorted part of the zone the effect is different from that in the parts located nearer to the undistorted lattices of the adjoining crystallites, i.e., it varies across the transverse section of the intercrystallite zone. The result found by the radiometric method gives a value of the diffusion averaged through the entire cross section of the intercrystallite region. Nevertheless, this result gives a more detailed account of the effect than the results obtained by the metallographic or autoradiographic methods.

It has also been found [16] that the change of the value of δD_{gr} in the alloy Cu + 0.1% Be depends on the temperature of the preliminary annealing. This indicates that the effect of internal adsorption of beryllium in copper depends on the temperature. Regarding these results as preliminary evidence, we can conclude that the method of radioactive indicators will make it possible to obtain more accurate ideas about the mechanism of intercrystallite diffusion.

Received January 9, 1958

LITERATURE CITED

[1] V. I. Arkharov, Trudy IFM UFAN SSSR* No. 8, 54 (1946).

[2] V. I. Arkharov, Trudy IFM UFAN SSSR,* No. 14, 16 (1954).

[3] V. I. Arkharov, Trudy IFM UFAN SSSR,* No. 20 (1958).

[4] V. I. Arkharov, Doklady Akad. Nauk SSSR 50, 293 (1945).

[5] V. I. Arkharov and T. Iu. Gol'dshtein, Trudy IFM UFAN SSSR,* No. 11, 114 (1950).

[6] V. I. Arkharov, S. I. Ivanovskaia, N. M. Kolesnikova and T. A. Fofanova Fizika Metallov i Metallovedenie 2, 57 (1956).

[7] V. I. Arkharov, V. S. Galishev, S. M. Klotsman and A. N. Timofeev, Studies on Heat-Stable Alloys (in Russian), Vol. III (AN SSSR Press 1958).

[8] R. G. Ward, Acta Metal. 5, 681 (1957).

[9] V. I. Arkharov and T. Iu. Gol'dshtein, Doklady Akad. Nauk SSSR 66, 1113 (1949).

[10] V. I. Arkharov and T. Iu. Gol'dshtein, Trudy IFM UFAN SSSR,* No. 11, 81 (1950).

[11] V. I. Arkharov, S. I. Ivanovskaia and N. N. Skorniakov, Trudy IFM UFAN SSSR, No. 16, 69 (1955).

[12] V. I. Arkharov and A. A. Pen'tina, Fizika Metallov i Metallovedenie 5, No. 1 (1957) (Sverdlovsk 1958).

[13] V. I. Arkharov, S. M. Klotsman and A. N. Timofeev, Fizika Metallov i Metallovedenie 5, No. 2 (1957) (Sverdlovsk 1958).

[14] J. C. Fisher, J. Appl. Phys. 22, 74 (1951).

[15] V. I. Arkharov, S. M. Klotsman, A. N. Timofeev and I. I. Rusakov, Studies on Heat-Stable Alloys (in Russian), Vol. III (AN SSSR Press 1958).

[16] V. I. Arkharov, S. M. Klotsman and A. N. Timofeev, Fizika Metallov i Metallovedenie (in press) (Sverdlovsk, 1958).

*Institute of the Physics of Metals, Ural Branch, Academy of Sciences, USSR.

A CHARGING DEVICE WITH AN ATOMIC BATTERY

G. D. Gorlovoi and E. G. Kardash

One of the most convenient individual dosimeters used in work with radioactive materials is the pocket direct-reading dosimeter DK-0.2. Dosimeters of this type are charged from a charging device fed by a battery.

The main disadvantage of this instrument is the necessity of frequent changes of the battery. In the Central Scientific Research Laboratory of the State Inspectorate of Mining Technology of the U.S.S.R. there has been developed a charging device for dosimeters of this type which uses as its source of voltage an atomic battery, or, speaking more precisely, an atomic cell.

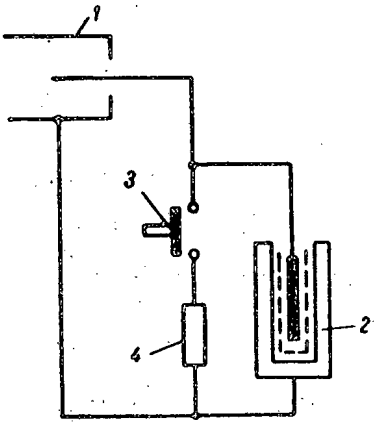

Fig. 1. Outline sketch of the charging device.
1) Charging jack; 2) atomic cell; 3) discharging button; 4) discharging resistance.

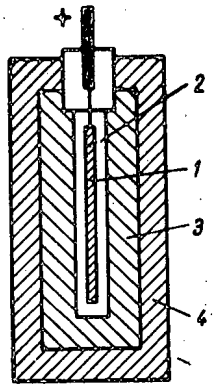

Fig. 2. Diagram of the construction of the atomic cell.
1) Plane β-ray emitter; 2) insulator; 3) collector; 4) lead cover.

An outline sketch of the charging device is shown in Fig. 1. The atomic cell 2 is connected to the charging jack 1. The sleeve of the charging jack is connected to the negative electrode of the cell and the case of the charging device. The dosimeter to be charged is inserted in jack 1. The capacity of the cell is larger than that of the charging jack and dosimeter. Since the potential across the electrodes of the cell is somewhat larger than needed to charge the dosimeter DK-0.2, at the first moment the dosimeter filament goes off scale to the left. To set the filament at zero one presses the button 3, so that the charge leaks off through the resistance 4 and the filament moves slowly to the right. When the filament reaches the zero one releases the button and removes the dosimeter from the jack. With this procedure less than 15 seconds are required to charge the dosimeter. If the atomic cell has been discharged, the time for charging a dosimeter depends on the capacity of the cell. In this case a full displacement of the filament across the scale requires about 30 sec, i.e., about the same time as with the use of the ordinary charging device. The charging device described here makes it possible to charge practically any number of dosimeters at intervals of not more than 1 minute.

To observe the position of the filament during charging and to determine the dose that has been received the instrument is held with its window to the light, and the use of ordinary batteries can be completely dispensed with.

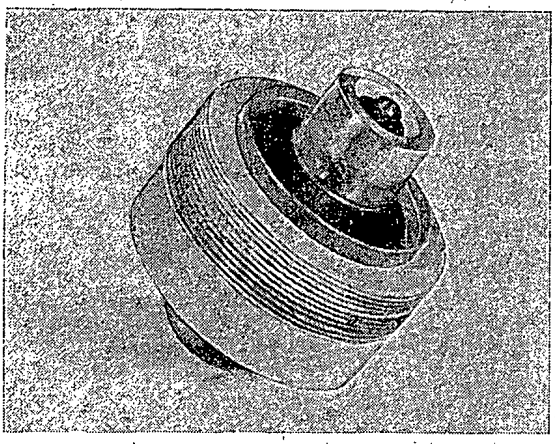

Fig. 3. Outside view of the atomic cell.

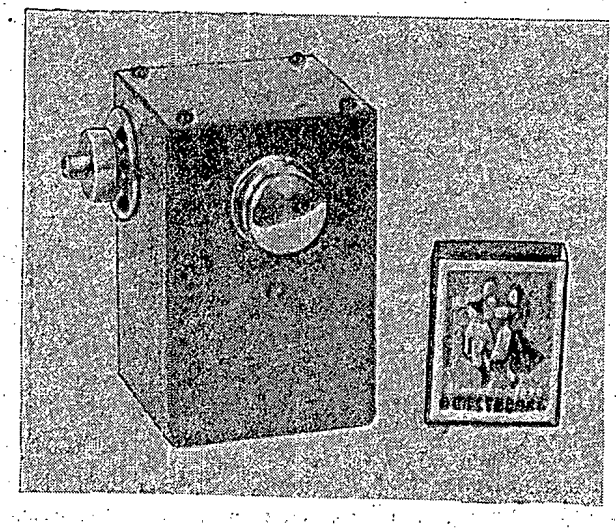

Fig. 4. Outside view of the charging device.

A diagram of the construction of the atomic cell which we have developed for the charging device is shown in Fig. 2.

In our first models we used Sr^{90} and Tl^{204} for the β-ray emitter 1, although in general one can use any long-lived β-active isotope. It would be preferable to use a radioactive material consisting of elements of small atomic number emitting β-particles of low energies, since it is desirable that the energy and intensity of the secondary bremsstrahlung radiation be at minimum values. On these considerations the isotopes Pm^{147}, H^3, Er^{164} would be preferable, and studies are now being made with them. The thickness of the β-ray emitter is chosen so as to minimize self-absorption.

The insulator 2 between the radiator and the collector is a polyethylene film of thickness 15 μ and high electric resistance. For the collector 3 in which the stopping of the β-particles occurs, the material used is magnesium, one of the lightest metals. The thickness of the collector is made approximately equal to the maximum range of the β-particles in the collector metal; for example, when Sr^{90} is used, the thickness of the magnesium collector is 4 mm.

To cut down the intensity of the x-rays produced by the stopping of the β-particles in the collector, the cell is inclosed in the lead cover 4 of thickness 3 mm. As was found by measurements, a layer of lead of this thickness weakens the bremsstrahlung radiation by a factor of about 500. The intensity of the bremsstrahlung at the surface of a charging device with a cell without the lead shield is less than 2 μr per sec. In order to eliminate the possibility of dispersal of the radioactive material, the lead cover is made airtight. The current strength from an atomic cell with a radiator (Sr^{90}) of activity 10 mC is found by measurements to be about 10^{-10} amp at voltage 300 v; the capacity of the element is about 100 $\mu\mu f$.

Outside views of the atomic cell and the charging device are shown in Figs. 3 and 4.

The charging device that has been described is considerably smaller in size than the usual charging device; it is essentially a pocket apparatus. The charging device is convenient to use, has no parts that can fail or get out of order (tubes, batteries), and has a long service life – twice or three times the half-value period of the isotope used. The advantages of the charging device with the atomic cell will show up most clearly in work under actual field conditions.

Received December 25, 1957

VOLTAGE-CURRENT CHARACTERISTICS OF BORON IONIZATION CHAMBERS

A. B. Dmitriev

The voltage-current characteristics of chambers of types KNT-49, KNT-50, and KNT-52 have been determined with the chambers under irradiation by slow neutrons in a reactor channel.

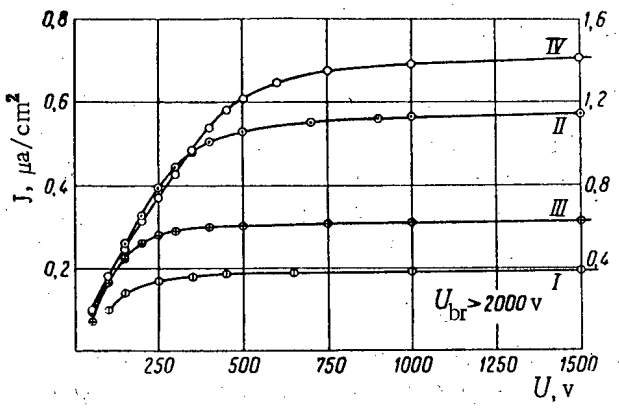

Fig. 1. Voltage-current characteristics of chamber KNT-49. Working gas; air under pressure 600 mm Hg (curves I and II) and 400 mm Hg (curves III and IV). The values of the current density for curves I, II, and III are shown on the left-hand scale, and for curve IV on the right-hand scale.

The electrode system of chamber KNT-49 consists of two coaxial cylinders of diameters 30 and 40 mm. The central electrode is coated with boron carbide. The chamber was connected by a dural tube 3.5 m long to a vacuum system, so that the chamber could be pumped out to pressure 10^{-2} mm Hg and filled with various gases. The intensity of the neutron flux was varied by stepped changes of the reactor power.

The electrode system of chamber KNT-50 consists of three coaxial cylinders of diameters 12, 24, and 36 mm. The largest and smallest cylinders make up the high-voltage electrode, and the middle cylinder is the collector. The outer surfaces of the cylinders of diameters 12 and 24 mm are coated with boron carbide.

The electrode system of chamber KNT-52 is a set of plates of diameter 43 mm, coated with boron carbide, and with the odd-numbered ones forming one electrode and the even-numbered ones the other.

In the experiments with the chambers KNT-50 and KNT-52 the intensity of the irradiation was varied by displacing the chambers along the channel while the reactor power remained constant.

The voltage-current characteristics of the chambers are shown in Figs. 1-3. The values of the ionization current per unit area of the collecting electrode are plotted as ordinates; U_{br} is the breakdown voltage of the space between the electrodes.

TABLE

Comparative Characteristics of Boron Ionization Chambers

Type of chamber	d, mm	Working gas	Pressure p	U_{sat}, v	i_{sat}, $\mu a/cm^2$	$i_{sat\ 500}$, $\mu a/cm^2$
KNT-49	5	Air	660 mm Hg	1000	0,20	0,05
			410 mm Hg	1000	0,30	0,07
		Neon	at 3 atmos	400	0,20	0,31
			3 atmos	300	0,10	0,28
		Argon	2 atmos	750	0,16	0,07
			600 mm Hg	500	0,15	0,15
			320 mm Hg	250	0,06	0,28
			320 mm Hg	300	0,11	0,30
KNT-50	6	Argon	600 mm Hg	350	0,16	0,33
KNT-52 (1st sample)	1,6	Argon	6 atmos	300	0,46	1,3
				450	0,92	1,2
				550	1,6	1,3
KNT-52 (2nd sample)	1,6	Argon	6 atmos	800	5,4	2,1
				300	0,76	2,2

Remarks: U_{sat} is the experimental value of the saturation voltage; i_{sat} is the experimental value of the saturation current density; $i_{sat\ 500}$ is the value of the saturation current density at voltage 500 v; d is the gap between electrodes; and p is the pressure of the working gas.

The neon and argon used to fill the chambers were of high purity (impurity content less than 0.001%).

In the comparison of the electrode systems the most interesting quantity is the maximum saturation current at a potential of 500 v (the voltage at which these chambers are used). This quantity was computed from the relation $U_{sat} \approx i_{sat}^{1/2}$. A comparison of the characteristics of the chambers is given in the table on this page.

As can be seen from the table, the chamber KNT-52, which has a small interelectrode distance and is filled to a high pressure, has decidedly higher values of $i_{sat\ 500}$ than the other chambers. When the chamber is filled with neon, saturation is attained at lower voltages; this is due to the larger mobility of Ne^+ ions (4.4 $cm^2/v \cdot sec$) as compared with that of A^+ ions (1.6 $cm^2/v \cdot sec$). Because of the small breakdown voltage of the discharge gap the possibilities for using neon are limited.

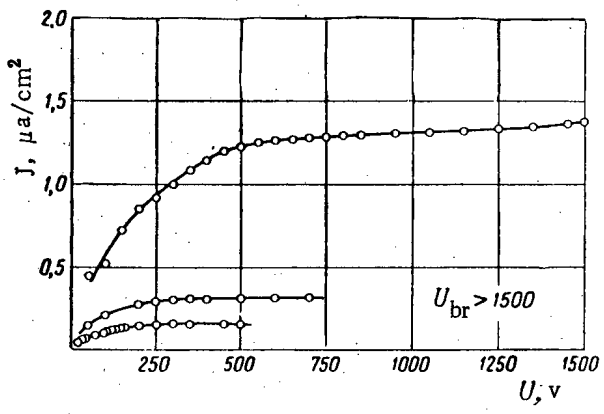

Fig. 2. Voltage-current characteristics of chamber KNT-50. Working gas: argon at pressure 600 mm Hg.

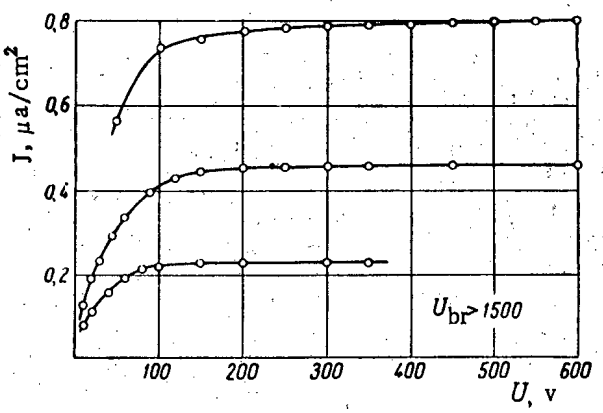

Fig. 3. Voltage-current characteristics of chamber KNT-52 (1st sample). Working gas: argon at pressure 6 atmos.

The smaller value of $i_{sat\ 500}$ for the chamber KNT-49 filled with argon to pressure 600 mm Hg, as compared with the chamber KNT-50, is explained by contamination of the argon during the filling of the chamber. The KNT-49 chamber was pumped out to the pressure $1 \cdot 10^{-2}$ mm Hg before filling, whereas the chambers KNT-50 and KNT-52 were pumped to pressures $1 \cdot 10^{-5}$ to $1 \cdot 10^{-6}$ mm Hg during prolonged baking-out.

In conclusion the writer expresses his gratitude to L. G. Kosmarskaia, M. G. Vorob'ev, and the reactor operating crew for aid in performing the experiments.

Received May 21, 1957

LITERATURE CITED

[1] K. K. Aglintsev, J. Tech. Phys. (U.S.S.R.) 16, 1121 (1946).

[2] A. C. Lapsey, Rev. Sci. Instr. 24, 8, 602 (1953).

[3] J. W. Boag, T. Wilson, Brit. J. Appl. Phys. 3, 7, 222 (1952).

[4] A. Engel' and M. Shtenbek, Physics and Technology of Electric Discharges in Gases (in Russian) Vol. 1, p. 320 (ONTI 1936).

REMARKS ON THE TWO-COMPONENT NEUTRINO THEORY OF LEE AND YANG

A. A. Sokolov

In the construction of their new theory of the neutrino, Lee and Yang have used a two-component formulism [1] (cf. also the papers of Landau [2] and Salam [3]). As we have already shown [4], a new theory of the neutrino ($k_0 = 0$) can also be constructed by using the Dirac equation with oriented spin [5]. The present paper gives a comparison of the results obtained with the two theories.

In the theory of Dirac particles with oriented spin, the wave function ψ obeys not only the Dirac equation

$$\left(-\frac{\hbar}{i}\frac{\partial}{\partial t}-c\frac{\hbar}{i}(\alpha\nabla)-\rho_3 k_0\hbar c\right)\psi=0 \tag{1}$$

but also the supplementary equation

$$\left(s-\frac{(\sigma\nabla)}{i\sqrt{-\nabla^2}}\right)\psi=0, \tag{2}$$

where the quantity $s = \pm 1$ characterizes the doubled value of the spin component in the direction of motion.

In this case in calculating the matrix elements of the spinor functions one must use not the Casimir formula, in which the states are separated only according to the sign of the energy ($\epsilon = \pm 1$) and there is an averaging with respect to the spin states, but a formula in which there is an explicit separation of the states both according to the sign of the energy ($\epsilon = \pm 1$) and according to the sign of the spin component ($s = \pm 1$). As has been shown in reference [4], this formula, as applied to particles with different masses ($k_0 \neq k_0'$) takes the form

$$\langle\gamma', \gamma\rangle=\frac{1}{16}\ \mathrm{Tr}\ \gamma'\left(1+\rho_1\varepsilon's'\frac{k'}{K'}+\rho_3\varepsilon'\frac{k_0'}{K'}\right)\left(1+s'\frac{(\sigma k')}{(k')}\right)\gamma\left(1+\rho_1\varepsilon s\frac{k}{K}+\rho_3\varepsilon\frac{k_0}{K}\right)\left(1+s\frac{(\sigma k)}{k}\right), \tag{3}$$

where the quantity $\epsilon c\hbar K = \epsilon c\hbar\sqrt{k^2+k_0^2}$ gives the energy of the particle, and $\epsilon = \pm 1$ the sign of the energy. As has been shown in reference [5], the momentum $\epsilon\hbar k$ of the particle depends on the value of the quantity ϵ, so that in the theory of Dirac particles with oriented spin we choose for the neutrino $\epsilon s = 1$ and for the antineutrino $\epsilon s = -1$.* From here on we shall use unprimed quantities for the neutrino. In order to obtain the Casimir formula from Eq. (3), we must carry out a summation over the spin states s and s'.

The matrices γ and γ' that determine the character of the interaction can conveniently be taken in the form (21.13) of reference [5] (from now on we shall use the notations of that paper).

*If the mass of the particle is zero ($k_0 = 0$), then the value of the matrix element (3) will depend only on the product ϵs. The results of Lee and Yang can be obtained from Eq. (3) if we assume that for arbitrary $\epsilon = \pm 1$ one has for the neutrino $s = 1$ (right-hand screw) and for the antineutrino $s = -1$ (left-hand screw).

As can be seen from Eq. (21.17) of reference [5], in the nonrelativistic case with the scalar ($\gamma^S = \rho_3$), tensor ($\gamma^T = \rho_3\sigma$), vector ($\gamma^V = I$), and pseudovector ($\gamma^A = \sigma$) interactions, the coefficients characterizing the polarization properties of the electrons emitted in β-decay will be proportional, respectively, to the quantities ($\epsilon' = 1$)

$$\left.\begin{matrix} R^{S,T}_{\varepsilon's'} \\ R^{V,A}_{\varepsilon's'} \end{matrix}\right\} = \left.\begin{matrix} \rho_{33} \\ \rho_{44} \end{matrix}\right\} = 1 \mp \varepsilon s \varepsilon' s' \frac{v}{c} \tag{4}$$

(quantities relating to the electron are distinguished by primes; the mass of the neutrino $k_0(\hbar/c)$ is taken to be zero; $\frac{k'}{K'} = \frac{v}{c}$). From this we find for the longitudinal polarization the expression

$$P^{S,T} = -P^{V,A} = \frac{R_1 - R_{-1}}{R_1 + R_{-1}} = -\varepsilon s \frac{v}{c}. \tag{5}$$

Since according to the experimental data [6] $P = -\frac{v}{c}$, we conclude that in our theory in the case of S, T-interactions a neutrino ($\epsilon s = 1$) must be emitted along with an electron, and in the case of V, A-interactions an antineutrino ($\epsilon s = -1$).

On the other hand, in the theory of Lee and Yang (see Eq. (13) of reference [1]) it is the other way around; for electron emission S, T-interactions are associated with the antineutrino, and V, A-interactions with the neutrino.

Furthermore, to describe the polar asymmetry of emission of the electrons from the spontaneous decay of neutrons, using Eqs. (21.17) and (21.18) of reference [5] we can get the following expression, in the case of a pure interaction type:

$$R = 1 + \varepsilon s a \frac{v}{c} \cos\theta,$$

where θ is the angle between the directions of the spin of the neutron and the momentum of the electron. In this last formula we must put

$$a^S = a^V = 0, \quad a^A = -a^T = \frac{2}{3}.$$

The experimental data [7], however, give for the coefficient in question the value $\epsilon s a = -0.37$. Therefore, in the case in which an antineutrino is emitted along with the electron ($\epsilon s = -1$) it is best to take the combination of the V and A interactions, which is in agreement with the polarization experiments [6], whereas for the case of a neutrino one takes the combination of S and T interactions.

Finally, in the decay of a stationary spinless π-meson into a μ-meson and a neutrino (or antineutrino), the interaction must be the pseudoscalar one ($\gamma^P = \rho_2$), and therefore the corresponding spin part of the matrix element will be proportional to the expression

$$R = \rho_{22}\sigma_{44} = \left(1 - \varepsilon s \varepsilon' s' \frac{k'}{K'}\right)\left(1 + ss' \frac{(kk')}{kk'}\right), \tag{6}$$

where $k_0 = 0$ and the primed quantities refer to the μ-meson. Taking into account the law of conservation of momentum ($\epsilon k = -\epsilon' k'$, we find that

$$R = \left(1 - \varepsilon s \varepsilon' s' \frac{k'}{K'}\right)(1 - \varepsilon s \varepsilon' s'),$$

i.e., if the spin of one particle is directed along its momentum (ϵ 's' = 1), then the spin and momentum of the other particle must be in opposite directions (ϵ 's' = −1).

Thus, if from the decay of a charged π-meson a μ-meson is produced with its spin parallel to its momentum ($\epsilon s = 1$), then according to our theory an antineutrino ($\epsilon s = -1$) is emitted along with it.

It is interesting to note that if in one system of coordinates the doubled component of the spin of a neutrino along the direction of motion is equal to unity ($s = 1$), then in any other coordinate system (including a Lorentz transformation which can change the direction of motion) the quantity $\underline{s}$ for a free particle will also be equal to unity. Therefore, for the neutrino ($k_0 = 0$) we can regard this component as prescribed in any system of coordinates.

If, for the antineutrino, experiment reveals the opposite picture of violation of symmetry, then we shall have every reason to suppose that the asymmetry of our world as a whole is due to the overwhelming predominance of the number of nucleons over the number of antinucleons.

Received January 16, 1958

LITERATURE CITED*

[1] T. D. Lee and C. N. Yang, Phys. Rev. 105, 1671 (1957).

[2] L. D. Landau, J. Exptl.-Theoret. Phys. (U.S.S.R.) 32, 405 (1957).

[3] A. Salam, Nuovo Cimento 5, 299 (1957).

[4] A. A. Sokolov, J. Exptl. - Theoret. Phys. (U.S.S.R.) 33, 794 (1957).

[5] A. A. Sokolov and D. D. Ivanenko, Quantum Theory of Fields (in Russian), Secs. 21, 23. (Gostekhizdat, Moscow-Leningrad 1952); A. Sokolov, Quantenelectrodynamik (Akademie-Verlag, Berlin 1957).

[6] H. Frauenfelder, R. Bobone, E. Von Goeler, N. Levine, H. R. Lewis, R. N. Peacock, A. Rossi, G. DePasquali, Phys. Rev. 106, 386 (1957).

[7] M. T. Burgy, R. J. Epstein, V. E. Krohn, T. B. Novey, S. Raboy, G. R. Ringo, V. L. Telegdi, Phys. Rev. 107, 1731 (1957).

*Russian translations of papers [1, 3, and 6] are contained in the collection "New Symmetry Properties of Elementary Particles," IL 1957.

SCIENTIFIC AND TECHNICAL NEWS

OPENING OF THE ATOMIC POWER STATION AT SHIPPINGPORT, PENNSYLVANIA

On December 22, 1957, an atomic power station, in which a pressurized-water reactor (PWR) is used, was put into operation at Shippingport (Pennsylvania, USA). It was originally intended to complete construction in July 1957. This is the third operating power reactor of five which are planned under a five-year program of the United States Atomic Energy Commission.

There are now five nuclear reactors in the world which are producing electrical power: the reactor at the first atomic power station (USSR, 1954), the reactor at the Calder Hall station (England, 1956), the experimental boiling-water reactor at Argonne National Laboratory (USA, February, 1957), the experimental sodium-graphite reactor at Los Alamos (USA, April, 1957) and finally, the reactor at Shippingport.

According to various estimates, the cost of the Shippingport power station varies from 70 to 110 million dollars [1], [2], considerably exceeding the original estimated cost (48 million dollars).

The heat source of the atomic power station is a reactor, the core of which is a right cylinder [3-7] consisting of two parts: a part with enriched uranium, in the form of slabs which are covered by a layer of zircalloy-2, and a breeding zone, the fuel elements of which are zircalloy tubes (10.5 mm in diameter and 0.7 mm wall thickness) containing dioxide of natural uranium. Each fuel assembly consists of 100 tubes. The slabs with enriched uranium are also installed in assemblies. In the initial operation of the reactor the enriched-uranium zone will generate about 40% of the heat and, as the plutonium accumulates, the heat generated in the breeding zone will increase. In order to make maximum use of the fuel in the breeding zone it is intended to recharge the enriched uranium zone about twice as frequently as the breeding zone.

The problem of controlling the reactor is simplified considerably because of the negative temperature coefficient -3.6×10^{-4} deg^{-1}. In order to reduce the number of control rods, the slabs containing enriched uranium contain an absorber (boron), the poisoning effect of which will be reduced gradually as a result of neutron capture during the operating of the reactor. The control rods are made from crystalline graphite.

The coolant-moderator is ordinary water of high purity, at a pressure of 140 atm. The water enters the reactor through the base; 90% of the water flows upward through the fuel slabs and control rods, while the remainder cools the walls of the reactor frame and the heat shield. The heat obtained by the water in the core of the reactor is transferred in heat exchangers to the water in the secondary circuit and wet steam is produced; the steam is then fed to a separator. The dry saturated steam from the separator is then used to drive the turbine. Three of the circulation loops are in constant use, while the fourth is kept in reserve.

The core is enclosed in a steel cylindrical frame with a hemispherical bottom and a removable hemispherical top. The reactor frame, in turn, is placed in a spherical steel shell (diameter 11.6 m) which has a cylindrical housing in its upper part (5.5 m in height) in which the driving mechanisms for the control rods are located. Two other cylindrical steel shells (diameter 15 m, length 30 m) are located around the first shell and are used for the circulation loops, with two loops in each shell. The fourth shell (diameter 15 m, length 45 m), contains the auxiliary equipment. All four shells are mainly below ground level and are surrounded by concrete. With this arrangement it should be possible to contain radioactive fission products in the event of an accident at the reactor (failure of the primary cooling system and melting of the core, with the subsequent loss of fission products).

According to a preliminary estimate, the personnel at the station will amount to 130 people, approximately twice the number of people required at an ordinary electrical power station of the same capacity.

Characteristics of the PWR Reactor

Thermal power	264 megawatts
Electrical power	68 megawatts
Internal power requirements	8 megawatts
Core height	180 cm
Core diameter	180 cm
Enriched uranium charge	52 kg
Natural uranium dioxide charge	12 tons
Number of control rods	24
Core water pressure	140 atm
Water flow through the core	2.84 m^3/sec
Water temperature at core inlet	265°C
Water temperature at core outlet	283°C
Velocity of cooling water in enriched-uranium zone	6.6 m/sec
Velocity of cooling water in breeding zone	3.3 m/sec
Pressure of dry saturated steam at input to steam turbine	42 atm
Temperature of dry saturated steam at input to steam turbine	255°C
Height of frame	10 m
Internal diameter of frame	2.7 m
Frame thickness	216 mm
Roof thickness	250 mm
Base thickness	150 cm

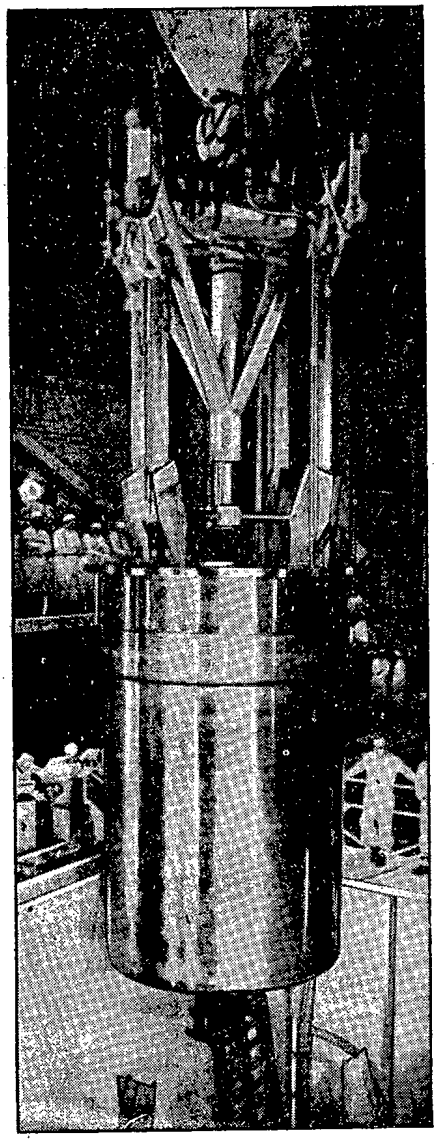

Fig. 1. The core being placed into the rector frame.

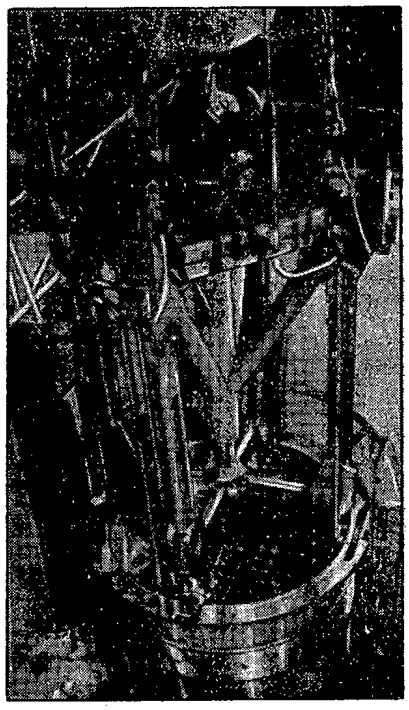

Fig. 2. View of the core from above.

The actual start-up of the reactor, on December 2, 1957, marked the fifteenth anniversary of the first nuclear chain reaction in the world.

At start-up the reactor was run at a level of 25 kw (thermal) [8]. During this time numerous experimental tests were made to determine the nuclear properties of the core and to test the operation of the individual elements of the system.

A picture of the 58-ton core being loaded into the 10 m frame of the reactor is shown in Fig. 1; Fig. 2 shows the assembly

of the upper lattice which contains the fuel elements and the graphite control rods.

On December 22 the Shippingport atomic power station first supplied current to the electrical power network of the Duquesne Light Company.

LITERATURE CITED

[1] Nucl. Power 3, 21, 3 (1958).

[2] Nucleonics 14, 12, 27 (1957).

[3] A. Radkovskii and S. Krasik, Physical Problems in a Pressurized Water Reactor (PWR), Atomic Power (Reports of Foreign Members to the International Conference on the Peaceful Use of Atomic Energy, Geneva 1955) (State Power Press, Moscow 1956) p. 347.*

[4] A. Radkovskii and S. Krasik, Critical Experiments in a Reactor Cooled by Pressurized Water, ibid, p. 375.*

[5] Simpson et al., Atomic Power Station With Pressurized Water Reactor, ibid, p. 401.*

[6] Ch. F. Bonilla, Nuclear Engineering (McGraw-Hill Book Co., Inc. New York, Toronto, London, 1957).

[7] S. Glasstone, Principles of Nuclear Reactor Engineering (Van Nostrand Company, 1955).

[8] Engineering 184, 4790, 827 (1957).

*In Russian.

ATOMIC AIRPLANES*

Unlimited flight duration, the presence of radiation and concentration of weight: these are the principal specific features of an airplane powered by atomic energy.

The two latter factors lead to considerable design difficulty, but are more than compensated for by the tremendous advantages of the first factor. For instance, an atomic airplane may be used as an automatic television relay station, remaining in the air for long periods of time without any operating personnel. In England plans are being made for creation of an atomic seaplane as an aerial tug [1].

In the opinion of a group of American specialists, a civilian atomic airplane can be realized in 15 to 20 years, although "the perspective for creation of a military atomic airplane is good"** [2].

The more complicated design problems for an atomic airplane originate from the presence of radiation emanating from the reactor. Crew shielding will require between 0.8 and 8 kg of shielding materials for each cubic decimeter of crew compartment. It is possible to achieve a decreased crew compartment volume; however, this will restrict motion of the pilots and will make emergency ejection from the compartment more difficult. Shielding also restricts visibility, as the radiation scattered by the air forces the placing of shields around the forward side of the crew compartment. Even the windshield must be made of some transparent shielding material of considerable thickness. Residual radiation from the reactor complicates maintenance of the airplane on the ground, particularly when a divided shield is used. Remote handling mechanisms may do away with the danger to maintenance personnel. However, the length of time required for maintenance increases by five to ten times, even when direct visual observation of the operation is possible. Because of this, several plans for a "disassembly" airplane [3] have been advanced; this airplane's reactor, together with its biological shielding, is removed from the airframe at the airport, thus creating favorable conditions for servicing the rest of the airplane's equipment, but consideration must still be given to induced radioactivity. It is also necessary to consider the effects of radiation damage on the structural materials. It is also possible that the air about the airplane, ionized by the radiation, will interfere with propagation of radio signals [4]. However the level of ionization that would affect radio transmission is not known. At the present time studies are being conducted in the U.S.A. on the behavior of various electronic equipment under conditions of high temperature and intense radiation [5].

The concentration of weight is a result of the heavy biological shielding required in the airplane. Figure 1 shows the weight of an aircraft reactor as a function of its thermal power; the curve was obtained on the assumption that the shield is made of ideal materials without consideration of their cost [6]. It is possible to obtain a considerable weight saving by utilizing the divided shield concept; it is not necessary in this case to shield the reactor equally on all sides. However it is possible to predict beforehand that the weight of the reactor, of the shields, and of the engines will add up to more than half the weight of the fully equipped airplane minus the crew. Because of its great weight, the reactor must be located near the center of gravity of the airplane. The engines must be located near to the reactor in order to minimize the flow path of hot gases. Any jettisionable weight must also be located near to the center of gravity, in order to minimize center-of-gravity shift. In contrast to a conventional airplane which has a low landing weight and a high takeoff weight (because of the chemical fuel), the atomic airplane will have virtually constant weight, and this will require stronger structure. The atomic airplane does have some design advantages which consist of low center-of-gravity shift in flight and a decreased effect of increases in useful load. An increase in useful load or in equipment of one kg will increase the design weight and weight of fuel by 1.5 to 4 kg in contrast to 3 to 10 kg for a conventional airplane.

---

*See "Atomic Energy" I, No. 5, 157 (1956) [Original Russian pagination].

**Translated from the Russian – Publisher.

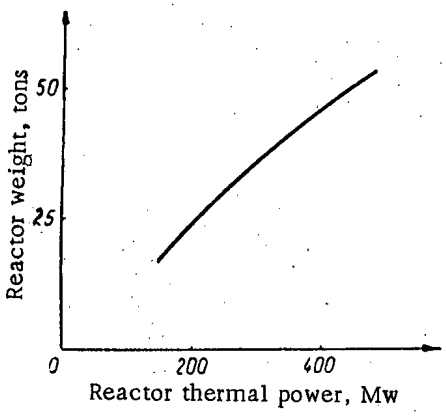

Fig. 1. Aircraft reactor weight as a function of power.

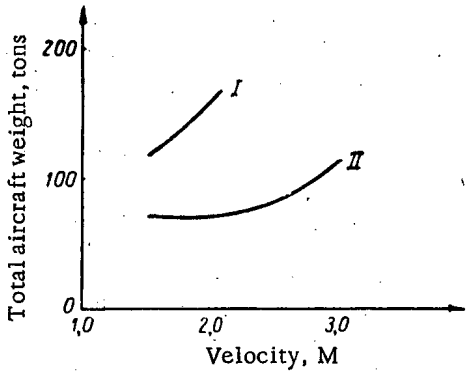

Fig. 2. Total atomic airplane weight with turbojet engine,as a function of its design flight speed (in Mach numbers).
I) At working fluid (air) temperature of 600°C;
II) at working fluid (air) temperature of 800°C.

It is presupposed that the first atomic airplanes will use turbojet engines. The calculated weight of such an airplane for various temperatures of the working fluid and various flight speeds are shown in Fig. 2 [6].

Work on an atomic airplane has been done with the greatest intensity in the U.S.A. The United States Department of Defense recently created a new program for development of an atomic airplane [7]. Details of the program have not been made public, but according to some reports, first flight of the airplane is planned for the mid 1960's.

Over fifteen organizations and private firms are participating in the atomic airplane program.

A number of companies in cooperation with the Atomic Energy Commission and the U. S. Dept. of Defense are operating and equipping research laboratories having experimental reactors.

At Oak Ridge (November, 1954) an aircraft shield test reactor went critical for the first time [8]. The fuel was enriched uranium tetrafluoride. Height of the reactor is 91.5 cm, diameter is 84 cm; design power is 1.5 Mw, but the reactor has already operated at a power of 2.5 Mw.

Three reactors are being operated at Fort Worth. One of these reactors was installed in an airplane [9], but was not used as a propulsion power plant.

The General Electric Co. has decided to build a new laboratory at Danville, California, dedicated to design of atomic power installations for aircraft and guided missiles [10]. This company has conducted ground tests with a conventional turbojet engine driven by a reactor [11, 12].

At Dawsonville, Georgia, a new experimental facility is being set up, consisting of two reactors of 10 Mw each [13], [14]. Another facility including a zero-power reactor is being set up at Palo Alto, California [15]. In the reactor hall, located 4.4 m underground, variations of reactor core and reflector design will be investigated. In one case the core will contain uranium foil (85% enrichment) that will be installed between two layers of metallic beryllium and will be divided into two cylinders of variable height. The reactivity of the system will depend on the distance between these two cylinders. Control rods are located along the cylindrical axis.

Towards the middle of 1958, construction is scheduled to be completed on a large nuclear facility at Wright-Patterson air base; this installation, costing 12 million dollars, was designated for engineering tests in the general area of atomic aircraft construction [16]. This facility has a 10 Mw reactor for testing the equipment for an atomic airplane. It will be equipped with chambers in which conditions of flight at great altitudes will be reproduced. The construction of another large laboratory for aviation atomic power plants is under completion at Middletown, Conn. [17]. In 1960 completion is scheduled for a reactor of Sandusky, Ohio [18]. Highly enriched uranium will be used for fuel in the reactor. Cost of construction of this reactor is five million dollars. Investigations associated with development of new types of rubber and rubber devices that possess satisfactory properties even under irradiation, including tires and other rubber parts for atomic aircraft, are being conducted in radiation laboratories in Akron [19].

A special group of experts is studying the possibility of construction of atomic seaplanes [20]. The possibility of installing an atomic power plant on the Seamaster-type seaplane or on one of its versions is not excluded. The possibility of using nuclear power plants on helicopters is being investigated [21]. The research program includes work aimed toward creation of a helicopter of 450 tons gross weight. A longer range program is studying the possibilities of utilizing ionic propulsion power plants in interplanetary rockets [22]. It is proposed to install in a rocket weighing 1.5 tons an atomic power plant that will create an electric field by means of which ions at a speed of up to 197 km/sec will be expelled from the tail of the rocket.

In England the best possibility for atomic aircraft is considered to be offered by a fast reactor [23]. It is proposed to use liquid sodium as coolant, circulating the sodium through a plate-type heat exchanger located directly within the "combustion chamber." Liquid sodium temperature at exit from the reactor must be 750 to 800°C, thus ensuring a high reactor efficiency with low reactor size,resulting in a decreased frontal aerodynamic resistance. In France it is proposed to begin operation during 1960 of a high-temperature reactor that will utilize 20% enriched uranium as the fuel and beryllium as the moderator, while the coolant will be air [24]. Air temperature at exit must be no lower than 600°C. This reactor may be the prototype for an aviation power plant.

V. Artamkin

LITERATURE CITED

[1] Science News Letter 71, No. 14, 214 (1957).

[2] Amer. Aviat. Daily 106, No. 7, 74 (1956).

[3] SAE Journal 65, No. 3, 61 (1957).

[4] Aviat. Week 66, No. 26 (1957).

[5] Amer. Aviat. Daily 106, No. 19, 189 (1956).

[6] Aeroplane 91, No. 2363, 905 (1956); No. 2364, 938 (1956).

[7] Atomic Energy Reporter No. 98, 127 (1957).

[8] Nucl. Engng. 2, No. 16, 298 (1957).

[9] Amer. Aviat. 20, No. 26, 28 (1957).

[10] Amer. Aviat. Daily 106, No. 31, 313 (1956).

[11] Jet Propulsion 26, No. 11, 994 (1956).

[12] Atomic Energy Guidletter No. 108, 6 (1957).

[13] Financial Times, April 12, 1957, p. 11.

[14] Chem. Eng. 63, No. 7, 373 (1956).

[15] Engineering 184, No. 4768, 124 (1957).

[16] Amer. Aviat. Daily 107, No. 13, 135 (1956).

[17] Interavia Air Letter No. 3680, 2 (1957).

[18] Atomic Energy Guidletter No. 104, 107 (1956).

[19] Amer. Aviat. Daily 107, No. 25, 235 (1956).

[20] Aviat. Week 65, No. 13, 34 (1956).

[21] Atomic Energy Clearing House 2, No. 52, 10 (1957).

[22] New York Times, April 6, 1957, p. 5.

[23] Flight 70, No. 2494, 771 (1956).

[24] L'age Nucleare No. 5, 27 (1957).

THE FUEL ELEMENT OF THE FR-2 RESEARCH REACTOR AT KARLSRUHE

Recently there has been made public considerable detailed information [1] on the heavy-water research reactor FR-2. The core of the reactor consists of 158 fuel elements (5.0 tons of uranium) whose centers (diameter 32 mm, length 2160 mm) are made of alloyed, heat-treated uranium. The top and bottom of this fuel rod has a special shape which minimizes resistance to coolant flow (D_2O). The design of the fuel element (FE) [2] is shown in Fig. 1. The FE is made in the experimental shops of the Dehusse Company [3] which has made use of Swedish experience in reactor building. To improve heat transfer the uranium rod is clad with a special non-neutron-absorbing aluminum cover 1 mm thick which is soldered to the fuel rod. The ends of the aluminum cover are welded shut with an argon shielded arc. To increase corrosion resistance of the cladding in the presence of D_2O, its surface was subjected to a special electrochemical treatment. The solder is corrosion resistant, and in case of damage to the cladding it reduces the corrosion of the uranium rod. The surface of the uranium is also treated (oxidized) to decrease corrosion in case of damage to the cladding. The water (t = 35°C) enters the cooling channels at a velocity of 2.5—10 m^3/hr, depending on the position of the FE within the core. The velocity of the water is measured by a Voltman rotometer through an electromagnetic recorder. The flow is regulated so that the exit

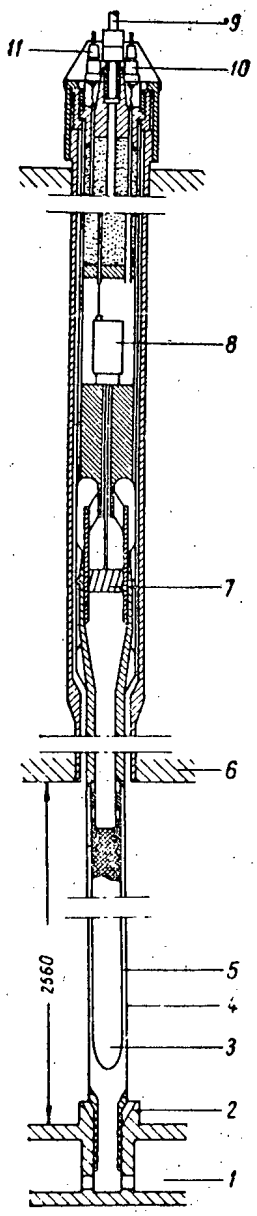

Fig. 1. Fuel element.
1) Coolant plenum chamber; 2) fuel element locating hole in grid plate; 3) uranium rod; 4) coolant channel; 5) circular gap for coolant flow in channel; 6) reactor cover plate; 7) Voltman rotometer; 8) recorder of rotometer signals; 9) D_2O sampling tube for control of damaged cladding 10) fitting for temperature measurement; 11) fitting for measurement of coolant flow.

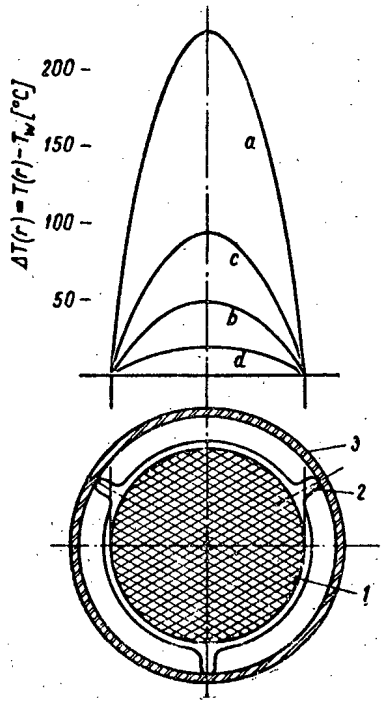

Fig. 2. Temperature distribution in the uranium rod for various positions of the FE within the core.
1) Uranium rod; 2) cladding with locating projections; 3) coolant channel.

water temperature, measured by a chromel-alumel thermocouple within an MgO sheath, is equal to 45°C (no higher than 60°C). Samples for determination of radioactivity are automatically taken from the exit water; any appearance of radioactivity means damage to the aluminum cladding and the introduction of fission products into the coolant.

Figure 2 shows temperature distribution along the cross section of the uranium rod. At a reactor power of 12 Mw the maximum temperature within the FE uranium, located at the center of the core, is 350°C (when exterior temperature is about 100°C). The average temperature of the cladding is 80°C, and the maximum power density is 90 watts per cm^2. At a reactor power of 24 Mw maximum temperature at the center of the uranium rod reaches 550°C.

G. Z.

LITERATURE CITED

[1] K. Wirtz, Atomwirtschaft II, 403 (1957).

[2] K. Engel, Atomwirtschaft II, 406 (1957).

[3] H. E. Schimmelbusch und H. Hardung-Hardung, Atomwirtschaft II, 421 (1957).

THE REBATRON – A RESONANT ELECTRON ACCELERATOR WITH IMPROVED LONGITUDINAL BUNCHING*

The principles of operation of the rebatron are similar to those of the klystron.

The rebatron consists of two cavities A and B (see Fig. 1). In the first cavity (low-voltage) we have preliminary weak bunching of the electron beam; in the second cavity the electron beam is accelerated to 1-3 Mev and becomes highly bunched.

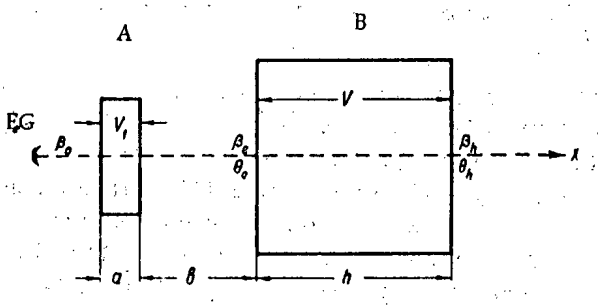

Fig. 1. Diagram of the rebatron; A and B) cavities; EG) electron gun.

After moving through a distance h the phase of an electron θ_h is

$$\theta_h = \theta_e + \omega \int_0^h \frac{dx}{v},$$

where θ_e is the electron phase on entering the cavity B ($x = 0$), ω is the angular frequency, x is the distance and v is the electron velocity. If the following condition is satisfied for all θ_e,

$$\theta_h = \text{const}, \qquad v(h, \theta_e) = \text{const}, \tag{1}$$

at the point at which electrons leave cavity B the time dependence of the current and the velocity distribution in the beam are described by δ-functions.

The problem of designing a rebatron is essentially that of finding a relation between the parameters θ_e, θ_h, β_e, β_h, V and h, such that the relations in (1) are satisfied. We may note that β_e and β_h are the relative values of the electron velocity ($\beta = \frac{v}{c}$, where c is the velocity of light) while V is the peak voltage across cavity B.

The equation of motion of an electron along the axis of a cavity which is excited in the fundamental TM_{010} mode ($E_x = E_0 \sin\theta$) is

$$\omega \frac{dmv}{d\theta} \approx cE_0 \sin\theta = e\frac{V}{h}\sin\theta, \tag{2}$$

where m and e are the mass and charge of the electron.

Finally we can write

$$\frac{2\pi h}{\lambda} = \int_{\theta_e}^{\theta_h} f(\theta, V)\, d\theta, \tag{3}$$

*P. D. Coleman, J. Appl. Phys. 28, 9, 927 (1957).

where $f(\theta, V)$ is the solution of Eq. (2). The solution of Eq. (3) consists of finding the upper limit of integration θ_h for a given set of values of V, $\underline{h}$, θ_e and β_e. It should be noted that at certain values of the parameters Eq. (3) cannot be solved.

The energy of the electrons at exit from the acceleration cavity is given by the usual formula

$$W_h = m_0 c^2 \left[\frac{1}{\sqrt{1-\beta_h^2}} - 1 \right]. \tag{4}$$

From Eq. (3) it is possible to find a number of relations between θ_h and the input phase θ_e while Eq. (4) allows us to obtain the electron energy as a function of θ_e for various values of β_e and $\underline{h}$. An analysis of these relations indicates that close to $\theta_e = 0$ there is a region of θ_e for which θ_h and β_h vary over small ranges.

We may consider the following example. Let β_0 be the relative velocity of the injected electrons, V_1 the voltage across cavity A, $\underline{a}$ the length of cavity A, $\underline{b}$ the distance between the cavities, $\Delta\theta_h$ the spread in phase.

If $\beta_0 = 0.272$, $\frac{eV_1}{m_0c^2} = 0.0124$, $\frac{2\pi a}{\lambda} = 0.185$, $\frac{2\pi b}{\lambda} = 2.222$, $\frac{eV}{m_0c^2} = 4.282$, $\frac{2\pi h}{\lambda} = 2.332$, we have β_h = = 0.9687 ± 0.07%, while $\Delta\theta_h$ = 0.004 rad.

Good bunching can be achieved simultaneously with acceleration only when the accelerated particles become relativistic. It is only in this case that the solution of Eq. (2) satisfies the requirements imposed in this problem.

It can be shown that the rebatron is relatively insensitive to small changes in the radio-frequency power supplied to cavity B (allowable variation is ±20%) and the voltage V_1 (up to ± 5 %). The uncertainty in the value of β_0 is compensated by a change in phase shift of the oscillations between cavities A and B. The highest accuracy is required in the phasing system between the oscillations in these cavities. The phase shift must be maintained with an accuracy of $0.002\,\lambda_p/2\pi$, where λ_p is the wavelength associated with the oscillations in cavity B. Typical parameters for an existing rebatron are as follows: Injection voltage in the electron gun 20-25 kv, injection current 0.3 amp, beam radius at injection, 0.5 mm, modulation amplitude in cavity A 5 kv, radio-frequency power required for the accelerating cavity, 0.8 megawatts, wavelength for the accelerating field 10.75 cm, length of cavity B 4 cm, radius of cavity B 4.115 cm. Using these parameters, electrons have been accelerated to 1 Mev and a current of 0.035 amp has been obtained. The experimental results are found in agreement with the theory.

G. I. Zhileiko

USE OF LINEAR ELECTRON ACCELERATORS FOR GENERATING MILLIMETER RADIOWAVES

One of the problems which faces present-day radio physics is the generation of electromagnetic waves in the wavelength region 5-1 mm and below. The use of millimeter waves would make it possible to increase the number of messages which could be transmitted simultaneously over transmission systems, would increase the resolving power of radar systems and would yield new information about extra-terrestrial radiation. Methods of generating and amplifying millimeter waves have not yet been developed and the use of centimeter-wave generators and amplifiers (klystron, traveling-wave tube, backward-wave tube, magnetron) is not feasible at wavelengths shorter than 3-4 mm [1]. The most promising approach would seem to be in the radiation obtained from electrons which move with accelerated motion. This radiation is found in synchrotrons, betatrons and microtrons and is often called the "radiating electron" effect. However the use of a cyclical accelerator for generating millimeter waves is not as convenient as the use of linear accelerators. Ginzburg [2] has shown the theoretical basis for the possibility of generating millimeter radiowaves by a beam of fast electrons which are subject to magnetic or electric fields which act in a direction perpendicular to the direction of motion of the beam.

In a system consisting of periodic magnetic or electric fields, which is called the undulator, the electron trajectories are periodic curves somewhat reminiscent of sinusoids. Because of acceleration the electrons emit an electromagnetic spectrum which is predominantly at the fundamental frequency.

Because of the Doppler effect, the wavelength λ at the fundamental radiated frequency, observed in the direction of motion of the electrons, can be shown to be [1], [3]

$$\lambda = d\left(\frac{c}{v} - 1\right),$$

where d is the period of the transverse electric or magnetic field, c is the velocity of light and v is the velocity of the electron. It is apparent from this expression that higher values of v mean shorter radiated wavelengths. The radiated energy is a maximum when all the electrons radiate coherently and is observed when the electrons form bunches whose linear dimensions are smaller than a half wavelength of the radiated wave (the radiated power is proportional to the square of the number of electrons in a bunch). This method of generating electromagnetic radiation has been realized by Motz and his co-workers [3] [5].

Using a linear accelerator with an electron energy of 100 Mev-these investigators were able to obtain radiation in the visible region. Electrons of relatively low energy, approximately 2-5 Mev, are sufficient for generating millimeter and sub-millimeter waves. The buncher of the 630-Mev Stanford University accelerator (Mark III) was used for this purpose. After bunching the electron energy was 4-5 Mev while the length of a bunch (in angle) was approximately 20° (linear dimensions 5.5 mm). Using this buncher, millimeter and sub-millimeter waves were obtained at a power level of 1 watt.

An accelerator designed for x-ray research has also been used (electron energy 2-3 Mev). Because the electron bunching in this accelerator was not satisfactory, a special pre-bunching system was used; this pre-buncher consists of two low-voltage resonators which bunch the electrons and a single high-voltage resonator which accelerates the electrons to v = 0.5 c. The pre-buncher compresses the electrons into a bunch with an angular duration of 30° and the accelerator compresses this bunch to a few degrees. This system consisting of the pre-buncher and accelerator has been used to investigate the generation of millimeter and sub-millimeter waves.

The theoretical and experimental work indicate that in order to increase the radiated power it will be necessary to reduce the bunch dimensions and to increase the number of electrons in a bunch, i.e., to increase the current of accelerated particles.

G. I. Zhileiko

LITERATURE CITED

[1] G. I. Zhileiko, Electrosviaz' 12, 27 (1956).

[2] V. L. Ginzburg, Izv. Akad. Nauk SSSR, Ser. Fiz. 9, 165 (1947).

[3] H. Motz, J. Appl. Phys. 22, 527 (1951).

[4] H. Motz, J. Appl. Phys. 24, 826 (1953).

[5] H. Motz, Trans. IRE AP-4, No. 3, 374 (1956).

THE PREPARATION OF NEW ELEMENTS

In addition to the 88 elements found in nature, at the present time 14 elements have been prepared artificially. Of these, four – 43 (technetium), 61 (promethium), 85 (astatine) and 87 (francium) – fill vacancies in the appropriate groups in the periodic system. The remaining ten (over 80 isotopes) are transuranic and were prepared exclusively by man, though it was discovered that extremely small trace amounts of neptunium and plutonium are formed as a result of the action of scattered neutrons on uranium.

It is well known that the synthesis of new transuranic elements is possible in accelerators giving beams of charged ions of high energy, in nuclear reactors – intense sources of neutrons – and in the explosion process of a hydrogen bomb [1], which is a short-lived, but extremely intense source of neutrons.

The first transuranic elements, neptunium and plutonium, were prepared by bombarding uranium with α-particles in a cyclotron. Later they were prepared by the irradiation of uranium in a reactor (Fig. 1,a). Combining irradiation in a reactor with bombardment of the heavy elements obtained with α-particles made it possible to prepare successively all the new transuranic elements up to fernium (element 100). It was also shown that elements 99 and 100 were obtained during the explosion of a hydrogen bomb, due to rapid and successive neutron captures by U^{238} (Fig. 1,b).

However, the possibility of further preparations of new transuranic elements in nuclear reactors is exhausted, as close to element 100 in the table such short-lived α-emitters appear that these elements decay during the formation process and the chain is broken. Irradiation with α-particles leads to a jump through one atomic number. Thus in the reaction $Es^{253}(\alpha, n)Md^{256}$ element 101 (mendelevium) was obtained [3]. Bombardment with heavier ions (of carbon, nitrogen and oxygen) gives more hope of success. In this case it is possible to effect a jump through several atomic numbers, equivalent to a reaction chain occurring during neutron irradiation. Thus, in the bombardment of Cm^{244} with C^{13} ions, the last new element, 102 (nobelium) [4], was obtained (Fig. 1,c, curve 1). We must bear in mind the fact that actually the jump which occurs is more complicated. For example, in the bombardment of U^{238} with C^{12} ions (Fig. 1,c, curve 2) there is first formed the excited compound nucleus Cf^{250}, which ejects several neutrons and is converted into a lighter isotope of californium. The whole process proceeds so rapidly that it can be considered as one jump. The difficulty of realizing this procedure consists of choosing the direction of the jump. It is always such that it proceeds (the longer it is, the more so) somewhat to the left of the region of the most stable nuclei, which form a diagonal band in Fig. 1, a, b, c. Therefore, for the irradiation the heaviest stable isotope lying in the stability region as far as possible to the right should be chosen. The direction of the jump may be controlled to a small degree by selecting a heavier ion, for example C^{13}, and even C^{14}, instead of C^{12}.

In the next few years one may expect the accumulation of Cm^{246}, of heavier curium isotopes, and Cf^{252} in nuclear reactors, and the use of heavy ions up to neon for bombardment. Under these conditions, the possibility of obtaining new elements will depend on the rates of radioactive decay (α-, β-, electron capture etc.) and especially the rate of their spontaneous fission, which increases rapidly with an increase in atomic numbers over 100. Nevertheless, it will probably be possible [2] to synthesize another six or so elements from eka-lutecium and eka-hafnium (elements 103 and 104) to eka-osmium (element 108), before instantaneous radioactive decay will impose a limitation on further preparations of new elements.

G. Z.

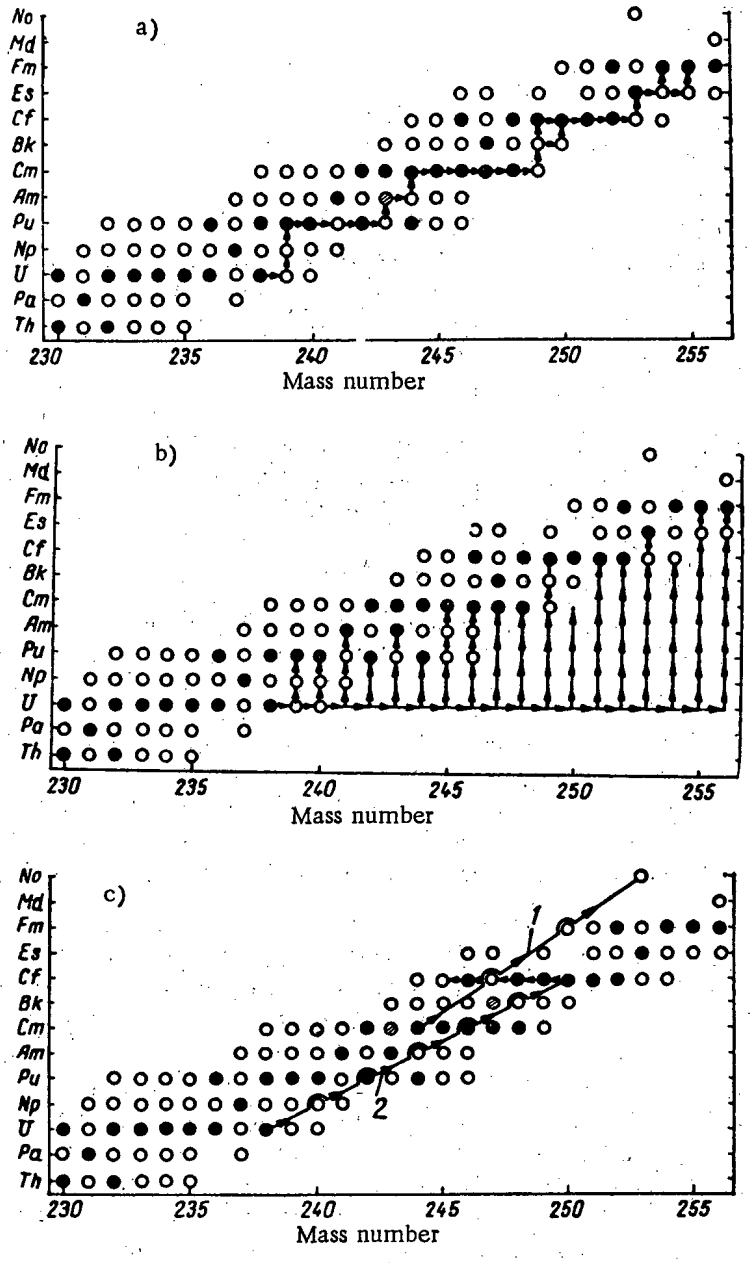

Fig. 1. Scheme of nuclear processes in the preparation of transuranic elements.

a) Irradiation of U^{238} with neutrons, b) reactions in a thermonuclear explosion, c) bombardment with heavy ions.

1) Reaction for preparing nobelium; 2) reaction for preparing californium; ●) isotopes stable against β-decay; ○) β-active isotopes; ⊘) no reliable data; →) neutron capture; ↑) β-decay.

LITERATURE CITED

[1] P. R. Fields et al., A. Giorso et al., Phys. Rev. 102, 180 (1956).

[2] H. A. C. McKay, Nature 180, 4594, 1010 (1957).

[3] A. Giorso et al., Phys. Rev. 98, 1518 (1955).

[4] P. R. Fields, A. M. Friedman, J. Nilsted et al., Phys. Rev. 107, 1460 (1957).

SEPARATION OF THORIUM FROM RARE EARTH ELEMENTS IN A NITRIC ACID MEDIUM BY AN ANION EXCHANGE METHOD*

The distribution of Th^{234} and rare earths was investigated on a column with a charge cross section of 1 cm^2 and 5 cm high. The anion exchanger used was Dowex-1 with 8% divinylbenzene and a grain size of 50-100 mesh.

In the first stage of the experiments, the distribution of indicator amounts of Th (IV) and Pr (III) was examined. Onto the column was placed about 2 ml of a solution of Th^{234} and Pr^{143} in 5 M HNO_3. The elution was carried out with acid of the same molarity at a flow rate of 0.4 ml/min. The Pr^{143} was completely removed from the resin with a volume of acid equal to three times the volume of the column. This did not desorb the Th^{234}. This element was washed from the column with 2.4 M HCl.

In the separation of milligram amounts of Th (IV) from microgram amounts of Sm (III), the latter was removed from the column with 7.3 M HNO_3. The thorium was desorbed with 2.4 M HCl.

Experiments with La (III), Nd (III), Eu (III) and Y (III) showed that these metals were readily removed from the column with 5-8 M HNO_3 and, consequently, could be separated from Th (IV).

A complete separation of Th (IV) from Ce (IV) in nitric acid could not be achieved in one stage. The addition of hydrogen peroxide to the nitric acid lowered the absorbtivity of cerium and facilitated its separation into the filtrate.

V. P.

*J. Danon, J. Inorg. Nucl. Chem. 5, 3, 237 (1958).

DATA ON THE Sr^{90} CONTENT OF BIOLOGICAL SAMPLES (ENGLAND, 1956)*

Due to the very immediate importance of problems related to the pollution of the earth's surface with the radioactive products of test explosions, the data given below on the radio-strontium content of soil, grass, milk and the inhabitants' bones in England in 1956 is of great interest.

Due to the chemical similarity and identical behavior in biological processes of strontium and calcium, the strontium content of biosubstrata is referred to in so-called "strontium units" (s.u.). This unit is equal to 10^{-12} curie of Sr^{90} per 1 g of calcium.

The data obtained in 1956 from 13 points in England give the following Sr^{90} contents of soil, grass and sheep bones (see Table 1).

TABLE 1

Sr^{90} Content of Soil, Grass and Sheep Bones

Sample	Sr^{90} content	
	Minimum	Maximum
Soil (a 10 mm layer):		
absolute values	1.9 mC/km^2	10.0 mC/km^2
relative values	0.15 s.u.	8000 s.u.
Grass	26.0 s.u.	2100 s.u.
Sheep bones	8.7 s.u.	160 s.u.

TABLE 2

Sr^{90} Content of Biological Samples in 1956

Sample	Location from which the material was collected	Sr^{90} content, s.u.		
		maximum	minimum	average
Grass	Acid soils on hills	2100	91	130
	Normal soils	77	11	37
Sheep bones	Hilly pasture	170	24	57
	Level pasture	15.6	7.8	13.7
Milk	Somerset county	5.7	2.9	4.4
	Other regions	10.3	3.9	6.7
Human bones:				
Up to 5 years		1.55	0.15	0.70
From 5 to 20 years		0.38	0.15	0.26
Over 20 years		0.13	0.06	The average values are not given as only two samples were investigated

*F. J. Bryant, A. C. Chamberlain, A. Morgan, G. S. Spicer, J. Nucl. Energy 6, 1/2, 22 (1957).

A detailed analysis of the data given indicates a regular decrease in the relative Sr^{90} content with increasing pH of the soil. The maximum value for Sr^{90} content in soil, grass and sheep bones was found in acid soils with pH = 4.3-5.6,and the minimum value was found at a pH of the soil equal to 6.8-8.0. The Sr^{90} content of sheep bones varied with the nature of the pasture. On level pastures it varied over the range 7.8-15.6 s.u. (average 14 s.u.), in hilly pastures over the range 24-160 s.u. (average 57 s.u.).

A comparison of the Sr^{90} content of sheep bones and of grass gave a coefficient of transfer of Sr^{90} from the food to the bones of the sheep, equal to 0.23 on the average, with fluctuations from 0.09 to 0.42. An investigation of the relative content of stable strontium gave close values: 0.24 (0.15-0.31).

The Sr^{90} content of cow's milk was higher in the northern than in the southern sections of the British Isles and reached 10 s.u., which is due to the large amount of precipitation in the northern regions.

Milk is the main source from which the inhabitants of England acquire Sr^{90} in their organism. Calculations show that only 0.002 s.u. of Sr^{90} penetrates the organism by inhalation and is deposited in the bones. The amount of Sr^{90} absorbed through the drinking water is likewise negligible. The amount entering with vegetables is also relatively little,as the external, mechanical pollution of the vegetables is removed to a great degree during culinary treatment.

Investigation of the Sr^{90} content of human bones showed that the maximum amount was contained in the bones of children up to 5 years old (0.15-1.55 s.u.,with an average value of 0.7 s.u.) and the highest Sr^{90} content was found in the bones of children from the northern and north-eastern regions of the country.

Table 2 illustrates the above in a summary form.

The amounts of Sr^{90} reported in children's bones indicate an irradiation of the organism with a dose of 2-4 mr per year, which is about 1/30 of the level received from natural sources.

The highest Sr^{90} content of children's bones (1.55 s.u.) corresponds to a level which is 1/60 of the level permissible for the whole human race according to the recommendations of the Medical Investigation Committee, and is only 1/6 of the level above which immediate measures are required to limit the penetration of radioactive material into the human organism, according to the same recommendations.

S. L.

ENGLISH AND AMERICAN WORK ON CONTROLLED THERMONUCLEAR REACTIONS*

Seven papers by English and American authors which describe the results of research into the possibility of realizing a controlled thermonuclear reaction in a high-current discharge in deuterium gas [1-7] were published in January, 1958, in the journal "Nature." The possibility of thermalizing a plasma and heating it to a temperature sufficient for thermonuclear reactions in straight discharge chambers had been investigated in papers published earlier [8-15]. In this work it was established that the contraction of a discharge in deuterium by virtue of the self-magnetic field is characterized by heating to temperatures greater than one million degrees and that the emitted neutrons are formed as a result of the D + D reaction. However, an analysis of the results shows that the pinch is not stable and that the neutron radiation is not due to thermal heating of the plasma but rather to some ion acceleration mechanism which is connected with the instability.

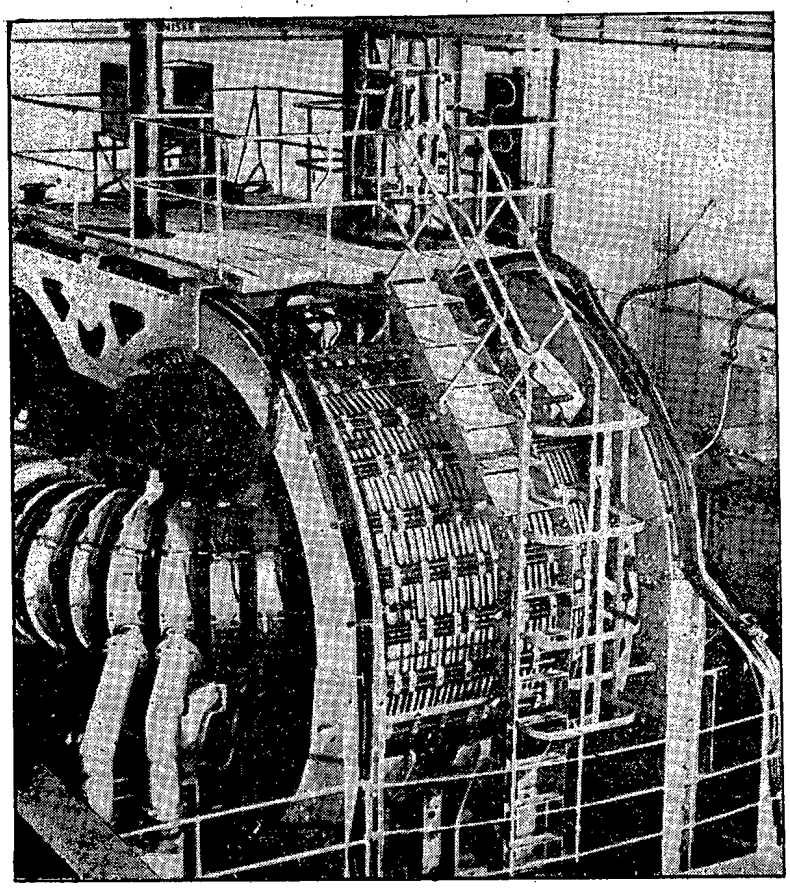

Photograph of "ZETA."

*This report is a short survey of papers published in the January 25th, 1958, edition of the English journal "Nature." A complete translation of these papers has been published in the journal "Foreign Nuclear Technology" No. 2 and No. 4, 1958.

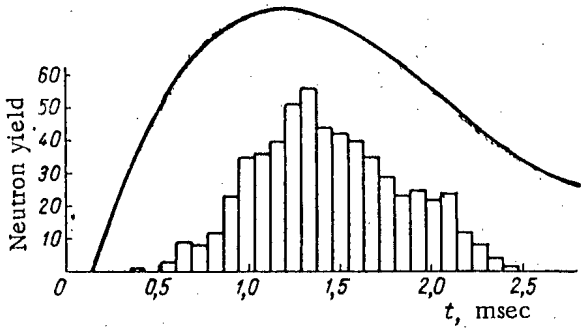

Fig. 2. Neutron yield as a function of discharge current development.
Condenser bank voltage 17 kv, peak discharge current 120 ka.

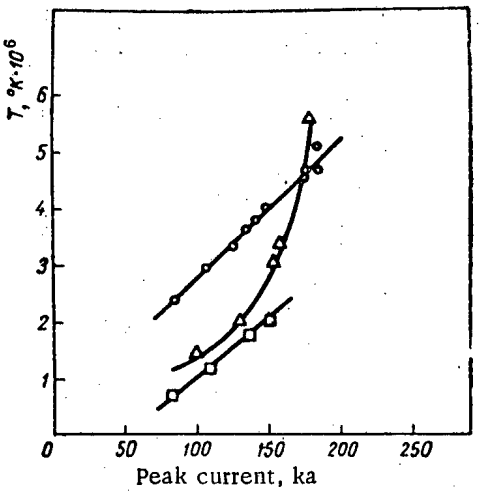

Fig. 3. Ion temperature as a function of peak discharge current.
O) Denotes the neutron yield; Δ) obtained from the Doppler broadening of the oxygen line (O V); □) obtained from the Doppler broadening of the nitrogen line (N IV).

There are two possible means of circumventing the difficulties which arise as a result of the instability of the pinch. The first approach is to achieve the required temperature in a time shorter than the time required for the instability to develop. Attempts along this line have been carried out by American workers and the results obtained in this work are presented below. The second approach lies in increasing the stability of the pinch by means of a longitudinal magnetic field which is set up in the chamber before the discharge is initiated. A discharge of this type has been studied in Ref. [16]; a theoretical analysis of the stability of a discharge in a magnetic field has been carried out in Refs. [17] and [18]. Another method of increasing the stability of the discharge is the use of a chamber with highly conducting walls: when the discharge pinch deviates from the axis of such a chamber, eddy currents are set up in the walls, and these currents produce a magnetic field which forces the pinch to return to its initial position [18].

By using both methods of stabilization simultaneously it has been possible to achieve a relatively long-lived discharge in a toroidal chamber; this work is described in two papers by English authors [1], [3]. The results obtained by these English investigators are extremely interesting and indicate that significant progress has been made in this work.

A large machine has been built at the Atomic Energy Research Establishment at Harwell by Thonemann, Fry, Thomson, et al. and is called the Zero Energy Thermonuclear Apparatus (ZETA). This machine consists of a toroidal aluminum chamber with a mean diameter of 3 m and a cross sectional diameter of 1 m. The gas in the chamber, which is at a pressure of approximately 10^{-4} mm Hg is ionized by a radio-frequency discharge and becomes highly conducting. The cold plasma which is thus produced becomes the secondary winding of a large pulse transformer; the primary of the transformer is connected to a bank of condensers. On discharge this bank can furnish an energy of $5 \cdot 10^5$ joules. The bank can be discharged every ten seconds and provides a maximum discharge current of 200 ka in the toroid. The discharge lasts for several milliseconds. In order to increase the stability of the discharge, a constant magnetic field in the direction of the circular axis of the toroid is set up by coils which are mounted on the apparatus. The strength of this field can be varied from 0 to 400 gauss. A general view of the machine is shown in Fig. 1. Measurements made with magnetic probes, Langmuir probes, and photographs of the discharge, taken through a window in the chamber wall, show that the current channel is quasi-stable and stays away from the walls of the chamber for the greater part of the discharge (2-3 microseconds); at maximum current the diameter of this channel is 20-40 cm. Microwave measurements show that the electron density is greater than $6 \cdot 10^{13}$ cm^{-3}, thereby verifying the assumption of a completely ionized plasma. Using scintillation counters, it has been established that neutrons are emitted during the discharge. The neutron yield as a function of maximum current in a discharge in a mixture of deuterium was 5% nitrogen (pressure $1.2 \cdot 10^{-4}$ mm Hg, stabilizing field 160 gauss) is shown in the table; in Fig. 2 is shown the dependence of neutron yield on discharge current. In the third column of the table are shown the temperatures of ions in the

plasma computed under the assumption that all the neutrons are produced as a result of a thermonuclear reaction and are emitted uniformly for one microsecond from a current channel 20 cm in diameter. The ion temperature was also determined spectroscopically from the Doppler broadening of the nitrogen and oxygen spectral lines. A comparison of the ion temperatures obtained by both methods is shown in Fig. 3. The mean ion energy is estimated as 300 ev at an ion density of 10^{13}-10^{14} cm^{-3}. The maximum ion temperature in ZETA is approximately five million degrees K.

TABLE

Total Neutron Yield and Plasma Temperature as a Function of Peak Discharge Current

Current, ka	Total neutron yield per pulse	T, °K·10⁶ (calculated)
84	$0{,}4 \cdot 10^4$	2,4
117	3,1	2,9
126	9,2	3,3
135	14,2	3,6
141	26,5	3,8
150	41,6	4,0
177	108	4,5
178	125	4,6
187	134	4,65

It should be pointed out that the use of the term temperature in this case requires special explanation. In the ordinary sense a temperature characterizes the mean energy of the chaotic motion of particles with a Maxwellian velocity distribution. In attempts to determine the temperature of a plasma from the neutron yield or from the Doppler broadening of spectral lines the physicist obtains information on the kinetic energy of particles; on the other hand, it cannot be maintained that there are no collisions between parallel currents of particles which are produced by virtue of instabilities and possible accelerating mechanisms in the plasma.

The American physicist Spitzer, who is in charge of thermonuclear work at Princeton University, has analyzed the results obtained with ZETA and indicates [2] that the observed velocity associated with the heating of the ions cannot be explained by an electron-ion collision mechanism; to explain the rate of increase of the temperature and the degree of thermalization of the plasma it is necessary to invoke other, as yet almost entirely uninvestigated, mechanisms to explain the heating of the plasma (oscillation, shock waves, hydromagnetic turbulence, etc).

Hence, in order to show that the observed neutrons are of thermonuclear origin it is necessary to investigate the relation between neutron energy and emission direction over the entire plasma (cf. below the results obtained with the American machine "Columbine II"). However, because of the small intensity of the neutron flux it is impossible to carry out such measurements with ZETA at the present time. Nonetheless, it should be noted that the observed neutron yield is compatible with the assumption that these neutrons are of thermonuclear origin.

The machine called "Sceptre III" built at the research laboratories of the Associated Electrical Industry in Aldermaston under the direction of Allibone and Ware is similar to ZETA but is smaller in size and is characterized by the following parameters: 1) energy in the condenser bank, 40,000 joules; 2) mean diameter of the toroid, 115 cm; diameter of the tube, 30 cm; 3) maximum axial magnetic field, 1,000 gauss; 4) maximum pulse current 200 ka; chamber pressure $9 \cdot 10^{-4}$-$7 \cdot 10^{-3}$ mm Hg. The results obtained in this work lead to the following conclusions. The current channel is isolated from the walls throughout almost the entire discharge, which lasts for approximately 400 microseconds. The neutron yield is a maximum ($8 \cdot 10^3$ neutrons per discharge) at a pressure of $2 \cdot 10^{-3}$ mm Hg and an axial field of 500 gauss. The maximum kinetic temperature obtained with this system is four million degrees K.

Several papers by American authors were published simultaneously with the English work; these papers report on the results of investigations of very fast discharges at Los Alamos.

In a paper by Honsaker, Karr, Osher, Phillips and Tuck [7] results are reported of experiments carried out with a quartz toroidal chamber "Perhapsatron S-3" (mean diameter 32.4 cm, tube diameter 5.3 cm, axial magnetic

field up to 5,000 gauss, discharge current 200 ka , duration of the discharge 600 microseconds) built in the middle of 1957. The first neutrons detected with this apparatus were found in December of 1957. The neutrons (approximately 10^6 per discharge) appear in the form of a pulse approximately two or three microseconds after breakdown. A considerably smaller neutron pulse was detected after ten-fifteen microseconds at the tail of the neutron distribution. The observed neutron yield corresponds to a temperature of six million degrees K. No measurements were made to determine whether or not these neutrons were of thermonuclear origin.

In a paper by Hagerman and Mather a description is given of a straight ceramic chamber "Columbine II" [5] (started up in the summer of 1957) which yields $3 \cdot 10^8$ neutrons per discharge at a maximum discharge current of 800,000 amp , which is reached in two microseconds. The neutron yield is reduced by 55% in an axial stabilizing field of 125 gauss and is increased by a factor of 2.3 when the pressure is changed from 0.07 to 0.2 mm Hg, and by a factor of two when the voltage is increased from 40 to 50 kv. In order to verify the degree of thermalization of the plasma, photographic plates were exposed at the ends and along the walls of the chamber. An analysis of the plates showed that the spectrum of neutrons emitted in the direction of the cathode is shifted toward higher energy by 170 kev compared with the spectrum for neutrons emitted in the direction of the anode. Furthermore, the number of neutrons emitted in the cathode direction is considerably greater. These findings show that there is a directed deuteron motion characterized by an energy of approximately 12 kev in the direction of the cathode; this motion arises as a result of some unknown acceleration mechanism. Within the limits of accuracy of the experiment the neutron yield in the radial direction is uniform along the axis of the chamber, with the exception of a narrow region (approximately 5 cm) near the anode.

A paper by Burkhardt and Lovberg is devoted to an investigation of a discharge in a straight discharge chamber "Columbine S-4" which differs from "Columbine II" only in size and the capacity of the condenser bank [6].

In a apaper by Burkhardt, Lovberg and Phillips [4] reports are given of an investigation of the time dependence of the radial current distribution in the "Columbine" discharge chamber described earlier in Ref. [15]. The measurements were made by means of small magnetic probes (coils consisting of 40 turns wound on a form 1 mm in diameter).

It may be noted that the papers reported by the American investigators contain no new theoretical knowledge which has not been presented in the results published by Soviet physicists in 1956. Hence greatest interest attaches to the work carried out by English workers who were successful in isolating a plasma with a particle density of 10^{13}-10^{14} cm^{-3} at a temperature of several million degrees from the walls of the chamber for several milliseconds. These workers were successful in maintaining a completely ionized plasma for a time sufficient for the investigation of the complicated and little-known mechanisms which are characteristic of high-temperature plasmas. Although it has not been conclusively demonstrated that the observed neutrons are of thermonuclear origin, the results of this work represent a step forward on the path toward realizing a controlled thermonuclear reaction. However, it is well worth pointing out that there are still many difficulties to be overcome before this goal is reached. To build a reactor with a positive energy balance it is necessary to initiate and maintain a plasma at a temperature of the order of four hundred million degrees for a time of several seconds. The energy evolved as a result of the D + D reaction in ZETA is smaller than this energy by a factor of 10^{12}.

Nevertheless, the diversity of approaches to the problem of controlled thermonuclear reactions and the results which are presently available all indicate that the idea of using the energy evolved in the formation of helium nuclei from nitrogen as a means of obtaining electrical power will be realized in the not too distant future.

G. B.

LITERATURE CITED

[1] P. C. Thonemann, E. P. Butt, R. Carruthers, A. N. Dellis, D. W. Fry, A. Gibson, G. N. Harding, D. J. Lees, R. W. P. McWhirter, R. S. Pease, S. A. Ramsden and S. Ward, Nature 181, 217 (1958).

[2] L. Spitzer, Nature 181, 221 (1958).

[3] N. L. Allen, T. E. Allibone, D. R. Chick, R. F. Hemmings, T. P. Hughes, S. Kaufman, B. S. Liley, J. G. Mack, H. T. Miles, R. M. Payne, J. E. Read, A. A. Ware, J. A. Wesson and R. V. Williams, Nature 181, 222 (1958).

[4] L. C. Burkhardt, R. H. Lovberg and J. A. Phillips, Nature 181, 224 (1958).

[5] D. C. Hagerman and J. W. Mather, Nature, 181, 226 (1958).

[6] L. C. Burkhardt and R. H. Lovberg, Nature 181, 228 (1958).

[7] J. Honsaker, H. Karr, J. Osher, A. Phillips and J. L. Tuck, Nature 181, 231 (1958).

[8] I. V. Kurchatov, J. Atomic Energy I, No. 3, 65 (1956)*

[9] Artsimovich et al., J. Atomic Energy, 1, 3, 76 (1956).*

[10] M. A. Leontovich and S. M. Osovets, J. Atomic Energy 1, 3, 81 (1956).*

[11] Artsimovich et al., J. Atomic Energy 1, 3, 84 (1956).*

[12] S. Iu. Luk'ianov, and V. I. Sinitsyn, J. Atomic Energy 1, 3, 88 (1956).*

[13] S. Iu. Luk'ianov and I. M. Podgornyi, J. Atomic Energy 1, 3, 97 (1956).*

[14] Anderson et al., Problemy Sovremennoi Fiziki 1, 116 (1958).

[15] L. Burkhardt, R. Dunaway, J. Mather, J. Phillips, G. Sawyer, T. Stratton, E. Stovall and J. Tuck, J. Appl. Phys. 28, 519 (1957); Problemy Sovremennoi Fiziki 1, 141 (1958).

[16] Bezbatchenko et al., J. Atomic Energy 1, 5, 26 (1956).*

[17] V. D. Shafranov, J. Atomic Energy 1, 5, 38 (1956).*

[18] M. N. Rosenbluth, Proc. 3rd Inter. Conf. on Ionization Phenomena in Gases, Venice, 903 (1957).

*Original Russian pagination. See C. B. Translation.

BRIEF COMMUNICATIONS

USSR. The Committee on Lenin Prizes in the field of science and engineering at the Council of Ministers of the USSR announced that the following papers have been submitted on atomic energy in the competition for the 1958 Lenin Prize:

1. L. A. Artsimovich, A. M. Andrianov, O. A. Bazilevskaia, S. I. Braginskii, I. N. Golovin, M. A. Leontovich, S. Iu. Luk'ianov, S. M. Osovets, I. M. Podgornyi, V. I. Sinitsyn, N. V. Filippov, N. A. Iavlinskii "Investigation of Powder Discharge in a Gas for Obtaining High-Temperature Plasma." (Presented by the Atomic Energy Institute of the Academy of Sciences of the USSR).

2. V. I. Veksler, V. A. Petukhov, M. S. Rabinovich, L. P. Zinov'ev, D. V. Efremov, E. G. Komar, N. A. Monoszon, A. M. Stolov, A. L. Mints, S. M. Rubchinskii, G. M. Drabkin, F. A. Vodop'ianov "A 10-Mev Synchrophasotron." (Presented by Academician D. V. Skobel'tsyn and the Atomic Energy Institute of the Academy of Sciences of the USSR).

USSR. In February, 1958, a working conference was held at the Consolidated Institute for Nuclear Research on the spectroscopy of neutron-deficient nuclei and on the application of radiochemical techniques to the study of nuclear reactions. 5 review articles and over 20 scientific communications were reported out.

USSR. A nuclear research reactor is being installed at Sverdlovsk for the Ural branch of the Academy of Sciences of the USSR.

Australia. 244 tons of U_3O_8 were produced during the year 1957 at the Rum Jungle site in the Northern Territory.

Britain. At Harwell construction and repair work has been started on the "ZETA" thermonuclear installation. In the course of the reconstruction work, the transformer winding will be improved upon and a more powerful condenser battery will be set up. The English scientist J. Cockcroft announced that the increase in the power of the condenser battery will make it possible to obtain plasma at temperatures of 15 million °K.

Britain. Harwell will be host during June, 1958, to a conference on nuclear reactor technology, at which the attendance of about 200 representatives of British industry is anticipated.

Venezuela. The research reactor being designed for Venezuela in the USA has a special shielding device which, on receiving radio signals reporting the beginnings of earthquake tremors from seismographic stations serving the reactor, will immediately scram the reactor.

Denmark. The first research reactor in the country, DZEF, reached its critical state. This homogeneous reactor employs as fuel a solution of uranyl sulfate (uranium enrichment of 20%). The reactor power, with the coolant loop shut off, is 5 watts, and reaches 500 watts with the coolant loop turned on.

Italy. The USA has delivered 7000 kg of U^{235} (in a mixture with U^{238}) to Italy for two atomic-powered electric power stations with American PWR-type reactors of 136 and 130 Mw thermal power, and also about 6 kg of uranium, 90% enrichment, for research reactors. In addition, Italy will receive the blueprints and designs for five research reactors of different power levels, which will be set up in Milano (two of them), Pisa, Frascati and Cagliari.

Canada. The Canadian branch of the Westinghouse Corp. has proposed a design for a heavy water-moderated HPTR reactor (a pressurized reactor with horizontal piping). It is suggested that, with an electric power delivery of 311 Mw, it will be able to provide electric power costing from 1.2 to 0.65 cents per kilowatt-hour, and, with subsequent technological refinements, less than 0.65 cents per kilowatt-hour. The high savings will be secured due to the high fuel burn-up, using natural uranium moving in horizontal piping against other flows of fuel, so that the low reactivity on account of the spent fuel will be compensated for by the high reactivity on the part of the fresh fuel.

Canada. According to the evaluation of a commission responsible for a study of economic perspectives in Canada, need is seen, towards the end of the seventies or the start of the eighties, for no less than 50 atomic-fuel

electric power plants for the country, each power plant delivering 100 Mw. The bulk of the power stations will be needed in the southern portion of Ontario province, the remainder in the Maritime Provinces and possible in southern Manitoba.

Norway. A group of scientists headed up by E. Jansen and S. Rosseland at the Norwegian Institute of Atomic Energy and the Astrophysical Institute has worked out a plan for work in the field of controlled thermonuclear processes. The plan calls for the construction of a "ZETA" type installation.

USA. At Princeton University, under the direction of L. Spitzer, Jr., a large "Stellarator" thermonuclear installation costing $25 million is under construction, with temperatures of 50 million °K aimed at. Construction will be completed in 1960. Thermonuclear work will also be carried out in other scientific institutions under the leadership of J. Tuck (Los Alamos laboratory), S. Colgate and R. Post (University of California), E. Shipley (Oak Ridge Laboratory), N. Rosenblatt (Institute of General Mechanics in San Diego), E. Teller (Livermore laboratory).

USA. Construction is proposed for an experimental atomic power installation at Hanford with a reactor using a slurry of plutonium-enriched uranium in heavy water as fuel. The projected output of the plant will be 84.5 tons of steam per hour. At the Oak Ridge and Los Alamos laboratories, different investigations are in progress on the applications of plutonium; in particular, the Los Alamos laboratory is doing development work on equipment using tantalum capable of standing up to the corrosive effects of fused plutonium.

USA. Three American firms have designed a high-temperature power reactor of 188 Mw thermal power with gaseous heat exchanges. The temperature of the gas (He) at the reactor outlet will be 815°C. Channels running through the graphite moderator section of the reactor are filled with spherical fuel elements (measuring 25 mm in diameter), made from a homogeneous mixture of enriched-uranium carbide and graphite. A reactor of a similar type is being planned in West Germany.

USA. At Fort Greeley (96 km south of Fairbanks, Alaska), installation work has been proposed on an APPR-2 (Army Packaged Power Reactor) delivering 1700 kw electric power. This reactor is similar to the APPR-1 reactor set up at Fort Belvoir, Virginia.

USA. Lockheed Aircraft, by agreement with the Atomic Energy Commission, has begun a study of the effect of earthquakes on the following reactor types: pressurized-water, boiling-water, sodium graphite, fast-neutron breeders, gas-cooled and homogeneous. Recommendations will be made after the investigations are completed.

USA. The atomic submarine "Sea Wolf" will be remodeled in 1958. The intermediate-neutron sodium-cooled reactor will be replaced by a pressurized-water reactor.

USA. The firms "United States Industries," "Columbia National" and "Carborundum Chemical" propose the production, in 1958, of 900, 360 and 680 tons, respectively, of reactor-grade zirconium sponge.

USA. The AEC announced that, for 1957, the yield of U_3O_8 amounted to 8,640 tons, of which 146 tons were produced as a by-product in the processing of Florida and Illinois phosphate rocks, and also from euxenite ores. U_3O_8 imports for 1957 amounted to 11,826 tons.

USA. The Atomic Energy Commission for the first time issued a license to one of the industrial research laboraries for the use of four spent fuel elements from the MTR reactor. 3, 9, and 300 days following their withdrawal from the reactor, these fuel elements will provide a dosage rate of the order of 2,500,000, 800,000, and 216,000 r/hr, respectively.

USA. At the Inland laboratory, Morton Grove, Illinois, a cobalt emitter of 62,100 curie activity, obtained from Canada, was installed. The unit, intended mainly for verifying the radiation stability of lubricants may be used used for other purposes as well. In the chamber, measuring 4.8 × 4.8 × 4.6 meters, there are also other openings for admission and withdrawal of air, an observation window, manipulators and an overhead crane.

France. At the Saclay atomic research center, under the supervision of P. Yvon, thermonuclear units with linear and doughnut chambers, in which temperatures of 1 million °K have been obtained, have been set up. A linear discharge chamber is under construction in another French research center located in the vicinity of Châtillon (in Fontaine-aux-Roses).

France. The International Conference on Nuclear Physics will be held in Paris, from July 7 to July 12, 1958, on the theme "Low-Energy Nuclear Interactions and Structure of the Nucleus." The draft program of the Conference

contains three sections: 1) nuclear reactions, 2) models of the nuclei, 3) weak interactions. Each section of the program has scheduled the reading of several review papers embracing all the original material relating to the question under discussion which will have been presented at the Conference. The proceeding of the Conference will be published. Reports and discussions will be published in French, English and Russian. The address of the Conference Organizing Committee is Paris, rue P. Curie 11, Radium Institute (Comité d'Organisation du Congrès International de Physique Nucleaire, Institut du Radium, 11, rue Pierre Curie, Paris 5^{e}).

West Germany. L. Bierman of the Max Planck Institute of Physics has announced the commencement of work on thermonuclear processes. The work is being conducted by Kiel, Aachen and Bonn universities. The work will be under the supervision of W. Fuchs, G. Ecker, S. Weizsäcker, A. Schlüter, L. Bierman and W. Lochte-Holtgreven.

West Germany. The Commission on Atomic Energy has approved an eight-year program for atomic power development in the country. The realization of this program will require an appropriation of 2.2 to 2.4 billion mark.

Switzerland. From June 30 to July 5, 1958, the annual International Conference on the Physics of High-Energy Particles will be convened at Geneva. The organizing committee of the Conference will be headed up by the General Director of CERN, S. J. Becker. The following problems will come under discussion at the Conference: structure of nucleons; collisions between nucleons and π-mesons, photons, nucleons and antinucleons; fundamental theories of particles; formation and interactions of strange particles; principles of invariance and selection rule; weak interactions.

The agenda of the Conference will undergo a change this year. One or two reporters will report out all of the material referable to a given problem that is presented at the Conference. Time will then be made available for discussion and additional communications. The materials should be presented to Geneva no later than June 1.

Sweden. K. Ziegbahn has announced that a large doughnut chamber unit similar to the English "ZETA" unit has been build at Uppsala University, and that a unit twice the size of the "ZETA" will be installed in the spring of 1958. K. Ziegbahn is heading up thermonuclear work at the university. Work is also going on at the Royal Technical College in Stockholm, under the supervision of H. Alfvén.

Sweden. The Atomic Energy Corporation (atomenergiaktiebolaget) has announced the development of an economic technique for uranium extraction from Swedish shale deposits. The firm has two uranium ore processing plants: one is located in central Sweden for the production of uranium concentrates of from ~10% uranium up, from schists containing 0.02-0.03% uranium; another in Stockholm, for the production of metallic uranium. Sweden's total uranium needs by 1960 are anticipated at 20 tons, and, for 1970, upwards of 200 tons.

Japan. A group of physicists, headed by I. Arata, announced that they achieved a temperature of 1 million °K in a discharge in a linear chamber, with 10^{6} neutrons per discharge observed. The research unit was built at Osaka University, and the experiments were conducted under the supervision of M. Okada.

Japan. A consortium of 56 firms has been organized to coordinate the efforts of various industrial groupings for the construction, in the immediate future, of a small experimental vessel powered by an atomic engine. The plan of the Ministry of Transportation for the construction of a large atomic-powered ship during a 10-year period (starting from 1956) has not met with full approval. A pressurized-water reactor imported by the Japanese Atomic Energy Commission is being suggested for the experiments.

BIBLIOGRAPHY

NEW LITERATURE

Books and Symposia

K. K. Aglintsev. Dosimetry of Ionizing Radiations. 2nd edition. Gostekhizdat, 1957, 504 pp, 18 rubles, 60 kopeks.

The second edition of this monograph is considerably expanded and rounded out (the first edition was published in 1950). Chapters devoted to scintillation, chemical and calorimetric techniques of dosimetry are introduced, as well as chapters on radiochemical methods used in counting radiations. A description is provided of techniques for measuring the activity of radioactive preparations. The monograph is intended for scientific workers and engineers working in the field of dosimetry.

Transactions of the Fourth Session of the Commission on the Determination of the Absolute Age of Geological Formations. Publ. by the Academy of Sciences of the USSR, 1957, 297 pp, 13 rubles, 85 kopeks.

The symposium contains reports throwing light on the results of the determination of the absolute age of rock strata. Part of the reports is devoted to the techniques used in determining absolute age (radiochemical, mass-spectrometric, and other research techniques). The symposium is intended for scientific workers: geologists, radiogeologists, radiochemists and geochemists.

Radiometry Handbook. For geophysicists and geologists. Edited by V. I. Baranov. Gosgeoltekhizdat, 1957, 199 pp, 9 rubles, 40 kopeks.

The handbook compiles information relating to radioactive decay and to the properties of radioactive radiations. Tabular and numerical material is checked by reference to the latest published sources. Brief information is supplied on radiometric equipment, radiometry techniques, methods for determining absolute geological age, abundance of radioactive elements in the earth's core. The handbook is written for engineer-geophysicists, geologists and students in the corresponding special fields.

Uranium in South Africa, 1946-1956. A two-volume symposium. Vol. 1, 546 pp with illustrations; vol. 2, 483 pp with illustrations. Publ. by the South African Institute of Mining and Metallurgy. Johannesburg (in English).

Articles in the Periodical Literature

Akchurin I. A., Development of the Physics of Antiparticles, Voprosy filosofii No. 6 (1957).

Arifov U. A. et al., Water-shielding Unit for Gamma Radiation Research Using a Co^{60} Source With Activity up to 1000 C, Doklady Akad. Nauk of the Uzbek SSR, No. 10 (1957).

Belikov I. F., The Technique of Labeled Atoms in Scientific Research (studies of the biology of agricultural plants) Sov. Primor'e, No. 23 (1957).

Bogoiavlenskii A. F. and Vedernikov A. P., Use of Radioactive Isotopes in Studies of the Kinetics of Accumulation of Electrolyte Ions ($SO_4^{=}$) in an Al_2O_3 Anode Film (brief communication), Zhur. prikladnoi khim. vol. XXX, No. 12 (1957).

Bromlei N. V., On the Use of Radiophosphor Isotope in Protein Synthesis and Turnover Studies, Trudy Mosk. vet. akad., vol. 21 (1957).

Burov B. M. et al., Neutron-Neutron Logging Technique in Studies on the Geological Cross Section of Drillings, Geologiia nefti No. 12 (1957).

Vdovenko V. M., Use of Radioactive Methods in Analytical Chemistry, Vestniki Leningradsk. Universiteta, Seriia fiziki i khimii, No. 4 (1957).

Vedenov A. A., On Some Solutions for Equations of Plasma Hydrodynamics (letter to the editor), ZhETF, vol. 33, No. 12 (1957).*

Voikovskii B. A. et al., Photometric Traces of Charged Particles in a Photoemulsion, Pribory i Tekh. Eksp. No. 6 (1957).

Volod'ko L. V., Electron Spectra of Uranyl Salt Solutions, Trudy Instituta fiziki i matematiki, Academy of Sciences of Beilorussian SSR, No. 2 (1957).

Wolfgang R., Use of Nuclear Recoil for Segregating Uranium From Fission Products, Khimiia i khim. tekhnol. (Special translations from the foreign periodical literature), No. 12 (1957).

Golitsyn G. S., Staniukovich K. P., Some Questions of Magneto-Gas Dynamics Taking into Account Finite Conductivity, ZhETF, vol. 33, No. 12 (1957).*

Grigor'ev E. P. et al., Ho^{160} Conversion Spectrum, Doklady Akad. Nauk SSSR, vol. 117, No. 1 (1957).

Zhuk E. G., Observation on the State of Higher Nervous Activity in Persons Working Under Conditions of Radioactive Exposure, Voenno-meditsinskii zhurnal, No. 11 (1957).

Kazarnovskii M. V., Space-energy Distribution of Neutrons in a Heavy Gaseous Moderator, ZhETF, vol. 33, No. 12 (1957).*

Kalita A. P., On the Composition of Obruchevite in a Hydrated Uranium-Yttrium-bearing Variety of Pyrochloride, Doklady Akad. Nauk SSSR, vol. 117, No. 1 (1957).

Mandzhavidze Z. Sh., Chikovani G. E., Rectangular Double Cloud Chamber for Observations of Unstable Heavy Particles, Pribory i Tekh., Eksp. No. 6 (1957).

Ostroumov V. I., Filov R. A., On Angular Correlation Between Fragments and Charged Particles Emitted upon Fission of Uranium Nuclei, ZhETF, vol. 33, No. 12 (1957).*

Portnoi K. I. and Samsonov G. V., A Property of Ternary Alloys of Titanium, Chromium and Zirconium Diborides, Doklady Akad. Nauk SSSR, vol. 116, No. 6 (1957).

Pushkarev V. V. et al., Protection of Water Reservoirs Against Contamination by Radioactive Substances, Gigiena i sanitariia, No. 11 (1957).

Sergeev S. N., Effect of Physical Training on the Development of Compensatory and Adaptive Reactions on the Part of the Organism (to Radiation Sickness), Voen.-med. zhur., No. 11 (1957).

Stepanov B. A., Desorption of Some Fragmentary Radioelements from Certain Deposits, Gigiena i sanitariia, No. 11 (1957).

Tret'iakov E. F. et al., Toroidal Beta Spectrometer For Investigating Conversion Radiation Accompanied by Alpha Decay, Pribory i Tekh. Eksp., No. 6 (1957).

Finkel'shtein Ia. B. et al., Experiment in Using Tritium as an Indicator in Studies on the Dynamics of Underground Waters, Doklady Akad. Nauk SSSR, vol. 116, No. 4 (1957).

Fioletova A. F., On an Express Luminescent Determination of Uranium in Solutions, Zhur. analit. khimii, vol. 12, No. 6 (1957).

Shcherbina V. V., Behavior of Uranium and Thorium Under Conditions of Sulfate-Carbonate and Phosphate Media of Hypergenesis Zone, Geokhimiia No. 6 (1957).

Eig L. S., Chaikovskii V. G., On the Lifetime of Argon-Methylal-filled Radiation Counters, Pribory i Tekh. Eksp., No. 6 (1957).

* J. Exptl.-Theoret. Phys. (USSR).

From Foreign Periodicals*

Aten A. H. W. Jr., Beers M. J. and de Groot D. C., J. Inorg. and Nucl. Chem. 5, 3, 159 (1958). The Szilard-Chalmers Reactions and Associated Processes in Oxides-I. Chemical State of U^{239} in U_3O_8, Exposed to Neutron Irradiation.

Aten A. H. W. Jr., Schenck P. A. and Ohm H., J. Inorg. and Nucl. Chem. 5, 3, 161 (1958). Szilard-Chalmers Reactions and Associated Processes in Oxides-II. Chemical State of Neutron-Irradiated Metastable Pb^{204} in Pb_3O_4.

Danon J., J. Inorg. and Nucl. Chem. 5, 3, 237 (1958). Separation of Thorium and Rare Earth Elements in a Nitrate Medium Using the Anion Exchange Method.

Engineer 205, 5319, 5 (1958). Atomic Energy in 1957.

Engineer 205, 5319, 8 (1958). Critical Review of Nuclear Power Installations.

Francois C. A., Analyt. Chem. 30, 1, 50 (1958). Rapid Spectrophotometric Method for Determining Milligram Quantities of Uranium.

Fried S., Westrum E. F., Baumbach H. L. and Kirk P. L., J. Inorg. and Nucl. Chem. 5, 3, 182 (1958). Micrometallurgy of Plutonium and Production of the Metal on a Micro Scale.

Hellstrand E., J. Appl. Phys. 28, 12, 1493 (1958). Measurements of Effective Resonance Integral of Metallic Uranium and Uranium Oxide for Different Geometric Conditions.

Hurotoshi Sano and Reiko Shiomi., J. Inorg. and Nucl. Chem. 5, 3, 251 (1958). Niobium and Zirconium Separation Process Using Cation Exchange.

Klemm A., Angewandte Chemie No. 1, 21 (1958). Lithium in Nucleonics.

Willoughby R. M., Burton A., Nuclear Power 3, 21, 30 (1958). On Possibilities of Working with Miniature Cyclones.

* The titles of these papers have been retranslated from the Russian. For this reason the wording may vary from the original – Publisher.

SIGNIFICANCE OF ABBREVIATIONS MOST FREQUENTLY ENCOUNTERED IN SOVIET PHYSICS PERIODICALS

AN SSSR	*Academy of Sciences, USSR*
FIAN	*Physics Institute, Academy of Sciences USSR*
GITI	*State Scientific and Technical Press*
GITTL	*State Press for Technical and Theoretical Literature*
GOI	*State Optical Institute*
GONTI	*State United Scientific and Technical Press*
Gosenergoizdat	*State Power Press*
Gosfizkhimizdat	*State Physical Chemistry Press*
Gozkhimizdat	*State Chemistry Press*
GOST	*All-Union State Standard*
Goztekhizdat	*State Technical Press*
GTTI	*State Technical and Theoretical Press*
GUPIAE	*State Office for Utilization of Atomic Energy*
IF KhI	*Institute of Physical Chemistry Research*
IFP	*Institute of Physical Problems*
IL	*Foreign Literature Press*
IPF	*Institute of Applied Physics*
IPM	*Institute of Applied Mathematics*
IREA	*Institute of Chemical Reagents*
ISN (Izd. Sov. Nauk)	*Soviet Science Press*
I YaP	*Institute of Nuclear Studies*
Izd	*Press (publishing house)*
KISO	*Solar Research Commission*
LETI	*Leningrad Electrotechnical Institute*
LFTI	*Leningrad Institute of Physics and Technology*
LIM	*Leningrad Institute of Metals*
LITMiO	*Leningrad Institute of Precision Instruments and Optics*
Mashgiz	*State Scientific-Technical Press for Machine Construction Literature*
MATI	*Moscow Aviation Technology Institute*
MGU	*Moscow State University*
Metallurgizdat	*Metallurgy Press*
MOPI	*Moscow Regional Institute of Physics*
NIAFIZ	*Scientific Research Association for Physics*
NIFI	*Scientific Research Institute of Physics*
NIIMM	*Scientific Research Institute of Mathematics and Mechanics*
NII ZVUKSZAPIOI	*Scientific Research Institute of Sound Recording*
NIKFI	*Scientific Institute of Motion Picture Photography*
OIYaI	*Joint Institute of Nuclear Studies*
ONTI	*United Scientific and Technical Press*
OTI	*Division of Technical Information*
OTN	*Division of Technical Science*
RIAN	*Radium Institute, Academy of Sciences of the USSR*
SPB	*All-Union Special Planning Office*
Stroiizdat	*Construction Press*
URALFTI	*Ural Institute of Physics and Technology*

NOTE: Abbreviations not on this list and not explained in the translation have been transliterated, no further information about their significance being available to us.—*Publisher.*

Just published in complete translation from Russian,

THE GEOLOGY OF URANIUM

TODAY, WORLDWIDE INTEREST in fissionable material has focused more attention than ever on uranium—*the origin of its deposits, its mineralogy, and methods of investigation.* As a result, the Soviet *Journal of Atomic Energy* devoted an entire supplement (No. 6) to current problems on the geology of uranium, which was published December, 1957 in Russian.

Now this collection of twelve important papers by leading Soviet specialists is available, in English, for those Western scientists who must keep abreast of the latest developments in the field by their Russian counterparts. Here, in well written and concise style, are graphic expositions of the main problems encountered in current investigations, with attention directed mainly toward *the study of uranium deposits which formed contemporaneously with sedimentary rocks.* The important role of *diagenesis* and of subsequent *epigenetic and metamorphic* phenomena, which have produced redistribution and concentration of uranium under favorable geological conditions, is clearly illustrated by actual occurrences; processes which lead to formation of epigenetic infiltration uranium deposits in coal basins are keenly analyzed; and various hypotheses, reported in Soviet and foreign literature, on the origin of such deposits are discussed in detail.

Additionally, this new work covers *a comprehensive survey of aerial geophysical methods* in various countries; *methods for radiometric study of uranium in three-component ore containing radioactive elements of the uranium and thorium series;* a description of several *new* minerals (including recent data on *nenadkevite,* described earlier in the journal *Atomic Energy*); and the results of *thermal investigations* conducted on a number of uranium minerals, which, on the whole, open the door to the possibility of determining other minerals difficult to analyze. In short, this richly-authoritative volume not only reveals the most up-to-date Soviet progress, but also adds *new* knowledge to our growing storehouse of information and stimulates incentive for further investigation into THE GEOLOGY OF URANIUM.

CONTENTS

Case-Bound, 124 Pages, Profusely Illustrated, $6.00

CONSULTANTS BUREAU, INC.
227 W. 17th St., NEW YORK 11, N. Y.